Liquid Phase Desulfurization of Hydrocarbon Fuels under Ambient Conditions using Regenerable Mixed Oxide Supported Silver Adsorbents

by

A. H. M. Shahadat Hussain

A dissertation submitted to the Graduate Faculty of
Auburn University
in partial fulfillment of the
requirements for the Degree of
Doctor of Philosophy

Auburn, Alabama
May 04, 2014

[Desulfurization, Silver adsorbent, Titania, Alumina, Hydrocarbon fuels, Infrared, Density functional theory]

Approved by

Bruce J. Tatarchuk, Chair, Professor of Chemical Engineering
Yoon Y. Lee, Professor of Chemical Engineering
W. Robert Ashurst, Associate Professor of Chemical Engineering
Michael L. McKee, Professor of Chemistry and Biochemistry

Abstract

Sulfur derivatives are major contaminants in hydrocarbon fuels. Sulfur emission from fuel is a major environmental concern and many countries around the world are enacting laws to limit it. In addition, the development of fuel cell systems is restricted because of the demand of ultra low sulfur fuels as pre-reformate streams. Therefore the removal of sulfur from hydrocarbon feed streams is essential. Conventional hydrodesulfurization (HDS) process in the refinery is efficient in removing most of the sulfur from crude oils. However, the process becomes expensive for producing ultra low sulfur fuels. Among several alternative processes, adsorptive desulfurization has shown to be a promising process for the intended applications. This dissertation discusses the aspects of liquid fuel desulfurization using regenerable oxide adsorbents at ambient conditions.

In this work, the development of an adsorptive desulfurization process using mixed oxide supported silver oxides along with the corresponding characterization analyses and the mechanisms involved have been presented. The TiO_2–Al_2O_3 and TiO_2–SiO_2 mixed oxides were formulated by dispersing titanium precursor on high surface area Al_2O_3 and SiO_2 supports. The mixed oxides were subsequently impregnated with $AgNO_3$ followed by calcination. The resulting formulation yielded highly dispersed titania and silver oxide phases that had promising sulfur adsorption capacities (~10 mg S/g adsorbent) and lowered exit sulfur threshold (<75 ppbw). The adsorbents were effective

toward a wide variety of commercial (off-road and ultra low sulfur diesels) and logistic (JP5 and JP8 jet fuels) fuels. The mixed oxides also provided seats for more silver loading (up to ~12 wt% Ag on TiO_2–Al_2O_3), consequently increasing sulfur adsorption capacities. The adsorbent retained its capacity after multiple cycles of regeneration in air. The variations in sulfur adsorption capacities for different fuel blends were also established. The presence of thiophenic molecules with methyl groups created steric hindrances for sulfur adsorption. The adsorbent formulation, performance, regeneration and variations of sulfur species are discussed in chapter III.

The promising performance of mixed oxide supported silver adsorbents called for a detailed analysis regarding the active sites involved and the effect of surface acidity. The Ag/TiO_2–Al_2O_3 adsorbent was characterized via fixed bed continuous adsorption (breakthrough) experiments, N_2 physisorption, X-ray diffraction (XRD), UV-vis spectroscopy, Raman spectroscopy, O_2 chemisorption, NH_3 adsorption, and infrared (IR) spectroscopy (chapter IV). The mesoporous adsorbent demonstrated enhanced capacity through higher surface area, greater TiO_2 (<4 nm) and Ag dispersions (~23% for 10 wt% Ag loading on TiO_2–Al_2O_3). TiO_2 and Ag dispersion resulted in 89% (compared to TiO_2) and 91% (compared to TiO_2–Al_2O_3) increase in sulfur capacity, respectively. Anatase TiO_2 dispersion on Al_2O_3 also allowed increase in adsorbent activity (3.27 eV band gap). The synergistic effect of TiO_2–Al_2O_3 resulted in higher surface acidity (~14 cc/g NH_3 uptake at P = 800 mm). Infrared spectra of the adsorbent samples treated with probe molecules (Ammonia, 2-lutidine, trimethyl chlorosilane, and thiophene) revealed the presence of surface acid sites. These acid sites were primarily responsible for silver incorporation (Lewis acid sites) and sulfur adsorption (surface hydroxyl groups).

Having established the active surface sites, the adsorption mechanisms for aliphatic and aromatic sulfur compounds onto $Ag/TiO_2–Al_2O_3$ adsorbents were investigated via complimentary breakthrough experiments and IR spectroscopy (chapter V). The mesoporous mixed oxide supported silver adsorbent demonstrated effective adsorption capacities for different organosulfur compounds. However, the selectivity varied for different sulfur species as well as non-sulfur aromatics. The adsorbent had higher breakthrough capacities for sulfur aliphatics than sulfur aromatics. The presence of non-sulfur aromatics negatively affected the sulfur adsorption capacities (~18% loss in capacity for $Ag/TiO_2–Al_2O_3$). Infrared spectra of adsorbent samples treated with different sulfur molecules were acquired and investigated. Organosulfur adsorption on $Ag/TiO_2–Al_2O_3$ was primarily attributed to the surface hydroxyl groups (via hydrogen/σ bonding) and the surface bound silver oxides (via π bonding). The presence of non-sulfur aromatics (benzene) reduced the sulfur adsorption capacity by occupying the π interaction sites.

Finally, a density functional theory (DFT) study was carried out to estimate the adsorption selectivity toward different sulfur and non sulfur species. For the cluster model, a silver atom was placed on a titania (anatase) matrix. A hybrid DFT method (B3LYP) was applied for geometry optimization, frequency analysis, and single point energy calculations using LANL2DZ and 6-31G(d)+SDD basis sets. The organosulfur compounds (thiophene, benzothiophene, dibenzothiophene, 4,6-dimethyldibenzopthiophene) and non-sulfur aromatics (quinoline, benzofuran, benzene, naphthalene) species were adsorbed on $Ag–TiO_2$ clusters. The adsorption on $Ag–TiO_2$ demonstrated higher adsorption energies; and the adsorption orientation was π-preferred. Attached benzene rings in the sulfur heterocycles increased adsorption energies. The

adsorbent affinity toward heterocycles with different functional groups followed the order: quinoline>benzothiophene>benzofuran. The computational calculations were in good agreement with the experimental results.

Acknowledgments

I would like to express my sincerest gratitude to my advisor Dr. Bruce Tatarchuk for all his guidance and encouragement during my studies and also providing me the opportunity for pursuing my graduate studies. I would also like to thank my committee members: Dr. Yoon Lee, Dr. Bob Ashurst, and Dr. Michael McKee for their time in serving on my committee and their advices regarding my research work. I also acknowledge the suggestions from Dr. Curtis Shannon as the external reader for this dissertation.

I am grateful to my wife, Sabrina Wahid for being by my side all throughout my PhD studies. In the area of adsorptive desulfurization, I had received ample encouragement and helpful ideas from Dr. Hongyun Yang (Intramicron Inc.). Acknowledgement goes to Dr. Sachin Nair, Achintya Sujan, and Xueni Sun from the adsorption group for their help and suggestions in my research. My heartfelt appreciation goes to Dr. Ram Gupta and Ms. Shaima Nahreen from the Chemical Engineering department and Dr. Shannon Curtis and Ms. Sanghapi Ndzesse from the Chemistry and Biochemistry department for their help with Infrared spectroscopy and Raman spectroscopy, respectively. I am thankful to Mr. Brian Schwieker (chemical engineering shop) and Mr. Matt Montgomery (Auburn glass shop, chemistry and biochemistry) for helping me in building my experimental setup. Financial support from the US Army (TARDEC) is greatly acknowledged.

This dissertation is a result of unbound support from my colleagues at the Center for Microfibrous Materials Manufacturing (CM3). Among them, special thanks go to Dwight Cahela, Dr. Donald Cahela, Dr. Wenhua Zhu, Kimberly Dennis, Megan Schumacher, Dr. Amogh Karwa, Dr. Priyanka Dhage, Dr. Shirish Punde, Dr. Min Sheng, Robert Henderson, Dr. Abhijeet Phalle, Zenda Davis, Pengfei Zhao, and Peng Cheng among many others. I am also thankful to Mr. Troy Barron and Dr. Paul Dimick from Intramicron Inc. I would like to acknowledge the efforts from Dr. Mario Eden and Dr. Christopher Roberts in making the chemical engineering department and the program great for graduate students. Thanks to Sue Ellen Abner and Karen Cochran for their administrative support throughout my time at Auburn.

This dissertation would not have been possible without the unwarranted love and support of my parent. I am indebted to my sister Safina Hussain for all her guidance and selfless acts throughout my life. I am grateful to my friends at Auburn for making my stay enjoyable and eventful. Finally I would like to thank the Almighty Allah for making all these happen.

Table of Contents

List of Tables

List of Figures

List of Abbreviations

PEM	Proton Exchange Membrane
SOFC	Solid Oxide Fuel Cells
EPA	Environmental Protection Agency
HDS	Hydrodesulfurization
PPMW	Parts Per Million by Weight
PPBW	Parts Per Billion by Weight
FCC	Fluid Catalytic Cracking
ODS	Oxidative Desulfurization
MOF	Metal Organic Framework
CM3	Center for Microfibrous Materials Manufacturing
ESR	Electron Spin Resonance
XPS	X-ray Photoelectron Spectroscopy
IW	Incipient Wetness
CP	Co-precipitation
ULSD	Ultra Low Sulfur Diesel
ORD	Off-Road Diesel
MF	Model Fuel
T	Thiophene
BT	Benzothiophene

MBT	Methylbenzothiophene
TMBT	Trimethylbenzothiophene
DBT	Dibenzothiophene
MDBT	Methyldibenzothiophene
DMDBT	Dimethyldibenzothiophene
1-C4T	1-Butanethiol
DES	Diethyl Sulfide
WHSV	Weight Hourly Space Velocity
LHSV	Liquid Hourly Space Velocity
TSA	Total Sulfur Analyzer
GC	Gas Chromatograph
PFPD	Pulsed Flame Photometric Detector
BET	Brunauer-Emmett-Teller
XRD	X-ray Diffraction
SEM	Scanning Electron Microscope/Microscopy
UV-DRS	Ultraviolet-Diffuse Reflectance Spectroscopy
IR	Infrared
TMCS	Trimethyl Chlorosilane
CUS	Coordinatively Unsaturated Sites
DFT	Density Functional Theory
ECP	Effective Core Potential
C6	Benzene
C10	Naphthalene

EXAFS	X-ray Absorption Spectroscopy
RH	Relative Humidity
SDD	Stuttgart Effective Core Potentials

I. Introduction and Literature Review

I.1. Introduction

Sulfur and its derivatives are major contaminants in hydrocarbon fuels. Airborne sulfur compounds are one of the primary health hazards present in the environment. Sulfur compounds produces sulfur dioxide, which is a chief source of acid rain, smog, and dry deposition. Increase in sulfur concentration in the atmosphere is a major concern from an environment point of view. In 2005, the emission of SO_2 in the USA was 15 million tons per year, and most of the SO_2 emissions have been produced from petroleum fuels [5]. As a result, the policy for maximum sulfur levels in fuel in the USA is getting more stringent in every decade. For example, the maximum sulfur concentration in highway diesel fuel in the USA has been limited to 15 ppmw from 2006, down from 500 ppmw [6-8]. Other transportation fuels are also being regulated to reduce the sulfur content. The maximum allowable sulfur concentrations in transportation fuels are shown in Table I.1. Many countries around the world are also enacting laws for limiting maximum sulfur emission from transportation fuels. Besides the USA, the European Union has limited the maximum sulfur content of diesel to 10 ppmw by 2009 [9]. Japan has also limited sulfur to 10 ppmw for diesel in 2007 [9]. The ever increasing environmental regulations have created an impetus on sulfur removal processes.

Table I.1 Environmental policy for maximum sulfur levels among commercial fuels in the USA [5]

Fuel	S level (ppmw)	Enforcing year
Gasoline	30–80	2006
On road Diesel	<15	2006
Non-road Diesel	<15	2010
Marine and Locomotive Diesel	<15	2012

In addition, desulfurization has gained importance after the advent of fuel cell technologies and the introduction of the hydrogen economy concept. The use of hydrogen as the primary energy source has the edge over conventional energy sources from an environmental point of view [10]. Transportation fuels such as gasoline and diesel are ideal for producing hydrogen in on-board fuel cell systems for higher energy density, availability, and operational safety factors. High hydrogen yield can be achieved from the fuel reformer (<30%) at >800–900°C, that makes hydrogen vehicles more efficient than current hydrocarbon fuel based vehicles. Fuel cell systems are also environmental friendly as compared to Internal Combustion (IC) engines. However, the development of fuel cell systems is restricted due to the demand of ultra low sulfur feeds in their reformation systems [11]. Sulfur poisons precious metal electrodes in fuel cells and reforming catalysts, therefore only fuels with less than 0.1 ppmw sulfur content are allowable in fuel cell systems such as Proton Exchange Membrane (PEM) fuel cells [6, 12]. Even for high temperature Solid Oxide Fuel Cells (SOFC), the sulfur concentration

of the feedstock has to be less than 30 ppm before it can enter the reforming process [13]. As a result, desulfurization of transportation fuels is critical for application in these systems. Among other hydrocarbon fuels, jet fuels contain higher sulfur concentrations since these are not regulated by the EPA [14]. Sulfur removal from logistic fuels is also necessary for fuel cell applications in appropriate fields such as the military vehicles [12]. All these issues point to the need of developing a highly efficient and cost effective process for deep desulfurizing hydrocarbon fuels.

Due to both environmental concerns and fuel cell requirements, the demand for ultra clean fuel is increasing. However, refineries have to deal with crude oil containing large amounts of sulfur concentrations. In recent years, refineries are seeing higher amounts of sulfurous crude oil due to diminishing sweet crude oil. With the ever increasing energy demand, there is also a growing impetus on extracting commercial fuels from heavier fractions of refinery streams at the distillation columns. For example, the processing of heavy petroleum feeds from the vast deposits of north american bitumen, oil sands, and shale oil is a major challenge because of the high sulfur content [14]. As a result, the desulfurization cost in the fuel refineries is increasing (Figure I.1) [15]. For example, the cost of desulfurization catalysts accounted for around 36% of the total catalyst cost in the refineries in 2005, as compared to only 12% in 1992 [6]. The increased consumption of energy also adds to the cost. Therefore, the development of cost effective deep desulfurization technologies is essential and currently an actively pursued goal.

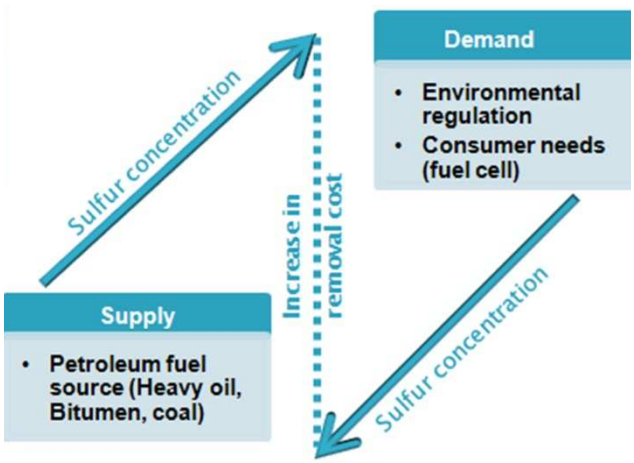

Figure I.1. Comparison of supply and demand of sulfur concentration in petroleum fuels

I.2. Literature review

I.2.1. Existing desulfurization technologies

Petroleum fuels contain varieties of sulfur compounds that differ with respect to the source, the nature of the hydrocarbon content and the distillation fraction of the crude oil. In general, the common groups of organosulfur species are mercaptans (thiols), sulfides, disulfides, and thiophenes. The first three groups are aliphatic sulfur compounds that usually reside in the lighter fractions of crude oil. Aromatic thiophenes constitute most of the sulfur species in heavier fractions. In a refinery process, three primary streams emerge from distillation of crude oil and are used for producing three major transportation fuels. Among these, the lighter naphtha fraction is used for producing gasoline, the medium kerosene fraction for jet fuel, and the heavier gas oil fraction for diesel fuel. The naphtha range consists of mostly low molecular weight sulfur compounds such as thiols, sulfides, disulfides, and light thiophene compounds (e.g. thiophene-T and benzothiophene-BT). With the descend along the distillation column, the molecular weight of thiophene derivatives increases. The gas oil fraction has a significant portion of

sulfur compounds as heavier dibenzothiophene (DBT) derivatives, such as 4-methyldibenzothiophene (4-MDBT) and 4,6-dimethyldibenzothiophene (4,6-DMDBT).

Currently, almost all of the petroleum products including transportation fuels are desulfurized in the refineries. The most widely employed desulfurization technology for petroleum derived hydrocarbons is the hydrodesulfurization (HDS) process. The HDS process can vary in terms of various factors. Primarily the process is carried out at elevated temperatures and pressures in presence of hydrogen where the sulfur species are converted to hydrogen sulfide and thus separated from the liquid stream. A common range of operating conditions is 300–400°C temperature and 3–6 MPa (1.01325 MPa = 1 atm) hydrogen pressure [6]. It is a catalytic process that employs supported and promoted molybdenum catalysts such as $CoMo/Al_2O_3$ and $NiMo/Al_2O_3$. Other than HDS, the refineries also utilize extraction processes such as Merox to remove thiols and sulfides [16].

HDS process follows the reaction mechanisms where sulfur atom is stripped off from the organosulfur compounds and the remaining hydrocarbon parts are recovered. The process is very efficient in removing most of the organosulfur species from crude oils, ranging from aliphatic mercaptans, sulfides, and disulfides to some of the aromatic thiophene derivatives. The reaction mechanism is simple and fast for mercaptans and sulfides as hydrogen reacts directly with these. However, HDS of thiophene derivatives are slower and can proceed via multiple pathways: hydrogenolysis (scission of sulfur atom) and hydrogenation (hydrogen addition of aromatic ring) [9]. The reaction pathways are shown in Figure I.2.

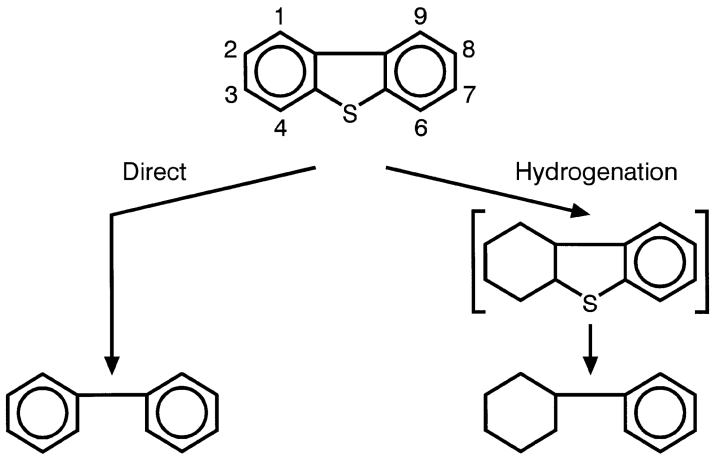

Figure I.2. Direct (hydrogenolysis) and hydrogenation pathways of HDS reaction (reproduced from K. G. Knudsen et al., Applied Catalysis A-General, 1999 [1])

HDS has been shown to perform less satisfactorily in removing DBT and its derivatives [17]. Therefore, for heavier fractions of crude oil that contain DBT compounds, desulfurization via HDS is more complicated, slow, and inefficient. Usually FCC feeds/gas oil fractions that produces diesel products contain heavier and more refractory organosulfur compounds. For this feed, the HDS process conditions are 6.9–20.7 MPa and 370–425°C, as compared to 1.38–5.17 MPa and 290–370°C for naphtha (gasoline) feed which contains more reactive sulfur species [6]. Among the sulfur compounds in diesel feed, the most refractory ones are 4,6-DMDBT and 4-MDBT. A generalized comparison of the HDS reactivities toward different thiophenic derivatives can be seen in Figure I.3. Activation energies of DBT, 4-MDBT and 4,6-DMDBT are 24, 31, and 40 kcal/mol, respectively [2]. The values of rate constant "k" for HDS reaction of BT and 4,6-DMDBT are 0.25 and 0.007 min^{-1}, respectively [6]. Thus, the HDS reactivities toward thiophene derivatives decrease in orders of magnitude with the increase in the number of aromatic rings. In addition, the attached methyl groups in 4-MDBT and 4,6-DMDBT create steric hindrances thereby decreasing the reactivity further.

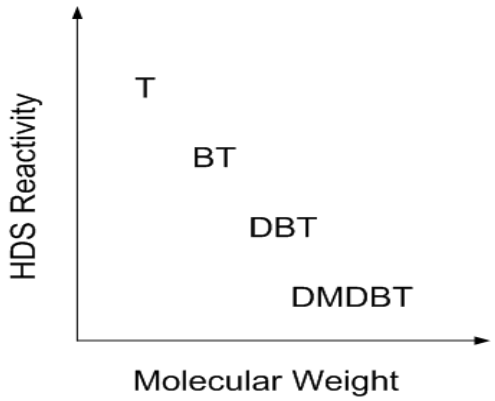

Figure I.3. Effect of different thiophenic derivatives on HDS reactivities (reproduced from K. G. Knudsen et al., Applied Catalysis A-General, 1999 [1])

Conventional HDS technology is expensive for producing ultra low sulfur fuels. The process becomes more severe in terms of catalyst volume, operating temperatures and pressures for lower target concentration of sulfur. For reducing the sulfur concentration in diesel fuel from 500 ppmw to 50 ppmw, the catalyst activity and temperature would have to increase by 420% and 38°C, respectively [1]. As the hydrotreating (HDS) process progresses, the concentration of DBT derivatives increases due to their low reactivities. Therefore, achieving low sulfur concentration by conventional HDS processes requires catalyst volumes significantly larger than the current configurations [18]. For example, the catalyst volume required for desulfurizing gas oil (diesel) fraction from 100 ppmw to 15 ppmw is more than that required for processing from 3000 ppmw to 100 ppmw [19]. Therefore, for achieving sulfur concentration tolerable to fuel cells, the HDS process would require larger reactor volume and consequent higher H_2 consumption [9, 20]. Simultaneously, some undesired reactions such as hydrogenation of olefins also take place, which complicates the process. Severe hydrotreating can also lead to the reduction of octane/cetane number, density, and aromatic content of commercial fuels [9]. Increase

in temperature and hydrogen partial pressure also initiate coke formation and deactivate the catalyst. Larger catalyst volume also makes the catalyst more prone to deactivation.

Extensive research works have been undertaken for improving HDS performance. The effects of various factors such as the nature of active sites, the nature of support materials, catalyst preparation methods, the use of more advanced and structured catalysts, operating temperatures and pressures, crude oil pretreatment and post-treatment, the change in reactor configuration etc. have been implied for this objective. Advanced catalysts such as NEBULA has been shown to improve HDS catalysis [6]. Efforts have also been given toward developing better designs for reactor systems. One example of a multifunctional, structured reactor system is the application of monolithic reactors [21]. Catalysts incorporated with monoliths have been observed to show excellent reactivity and selectivity in HDS process. Microfibrous materials can also be employed in reactor systems to ensure better contacting efficiency [22, 23]. Optimized integration of catalyst and reactor configuration culminated in processes such as catalytic distillation that has very good HDS performance [24]. However, assessing the HDS reaction kinetics of heavier thiophene derivatives, it is necessary to develop an alternative or supplementary process to HDS. Reaching the goal of “zero-sulfur” fuels due to fuel cell requirements only underlines the challenge of the task. Complimentary processes that can effectively remove the last few ppmw of sulfur from fuel and can also be applied in on board fuel stacks of diverse dimensions should be suitable.

I.2.2. Alternative processes

A common observance concerning the production of ultra clean fuel is the need for an efficient process that can remove the heavier thiophenic compounds. Several alternative

processes to HDS have been reported in the literature [6, 9, 25-31]. Among the group of alternative processes tested so far, the notable ones are extraction, catalytic and selective oxidation, alkylation, pervaporation, and adsorption. All of these except adsorption will be discussed in this section.

Desulfurization of fuel oil fraction has been carried out via extraction using a solvent. A suitable solvent is mixed with the fuel where the sulfur species is transferred to the solvent phase due to higher solubility. After proper mixing, the phases are separated and the sulfur is separated from solvent via distillation. Various solvents such as ethanol, polyethylene glycols, acetone, and advanced ones such as ionic liquids have shown satisfactory performances as solvents [32]. The process has the advantage of operating at ambient conditions. However, the selectivity of the solvents toward sulfur species is a major challenge. To enhance solubility, the modification of the sulfur species is a plausible option. The most popular and thermodynamically stable modification is the oxidation of organosulfur compounds.

Oxidative desulfurization (ODS) is a two-step process that involves oxidizing organosulfur compounds and then separating the resulting sulfones via distillation/extraction/adsorption [33]. Sulfur has a strong affinity for oxygen. The high electron density of the sulfur atom in thiophene derivatives makes these more favorable for oxidation to the respective sulfones. A separation process (e.g. adsorption, extraction, or distillation) follows the reaction process to remove the sulfone compounds. The higher polarity of sulfone compounds facilitates the separation of the sulfones from hydrocarbon streams [34]. The oxidation reaction can be expressed by the following scheme:

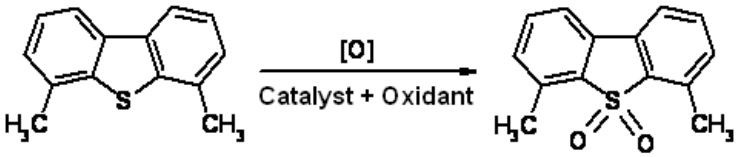

4,6-DMDBT 4,6-DMDBT Sulfone

A catalyst based on transition metals is employed in the oxidation process to catalyze the reaction. Usually molybdenum oxide (MoO_3) is used as the primary catalytic active sites. MoO_3 has been reported to be the active substances for capturing sulfur species from fuels [35, 36]. The ODS process also employs an oxidant that supplies [O] for the formation of sulfones. Different oxidants have been used for partially oxidizing the thiophenic derivatives such as hydrogen peroxide, oxygen, ozone, air, etc. Among these, H_2O_2 has been applied the most [28, 37]. Molecular oxygen has also been used for desulfurizing diesel [29]. ODS has been applied in practical applications such as UniPure and SulphCo desulfurization technologies [28, 31, 38-40].

In the recent years, bio-desulfurization has drawn much attention due to its "Green Chemistry" advantages [30, 41]. Researchers have observed that various microorganisms selectively removed sulfur species from hydrocarbon fuels at mild conditions (<100°C). The process can be operated in both aerobic and anaerobic conditions. This form of desulfurization has many advantages but the biocatalysts employed usually have low activity and low stability. Pervaporation techniques have also been tested in the recent years [42]. Notably, the S-Brane process developed by Grace Davison in 2002 follows this technique and has demonstrated good selectivities toward DBT derivatives. However, both bio-desulfurization and pervaporation techniques require auxiliary units and are more complicated and sensitive.

Alkylation of organosulfur compounds can also be applied in a desulfurization process to separate the alkylated product from the primary stream via boiling point shift. The reaction combines existing thiophenes and olefins in the fuels and produces heavier methylated thiophenes. The products, due to their high boiling points as compared to the reactants, can easily be removed via distillation. This reaction has been employed in OATS technology by British Petroleum [43]. The limiting factor of the process is the selectivity, as various side reactions take place alongside thiophene alkylation.

The processes mentioned so far bear promising solutions to the challenges faced by HDS processes. However, all of these processes are complicated and requires auxiliary units. Scalability is also a problem faced by these alternatives that make them difficult for application in small scale versions of desulfurization units for on board fuel cell systems.

I.2.3. Adsorptive desulfurization

Adsorptive desulfurization at ambient conditions can supplement hydrodesulfurization process and offers an alternative solution to the high cost of producing ultra clean fuels. The process employs a solid adsorbent material to selectively adsorb sulfur compounds from targeted streams. The process can be divided into two types: reactive and non reactive. In reactive adsorption process, sulfur atom from the compound is stripped off and the remaining hydrocarbon is recovered. This type of adsorption usually occurs at high temperature. For non reactive adsorption, the organosulfur compounds are mostly physisorbed on the surface. In this case, the operating conditions are mild (<100°C) and the material adsorbs the organosulfur compounds as whole. The adsorption process can also be employed with or without the use of auxiliary gases such as hydrogen. Regeneration of the adsorbent is necessary when a continuous process is called for.

Several media such as air, hydrogen, and steam can be used for regenerating the adsorbent. The probable applications of adsorptive desulfurization in current fuel processing systems are depicted in Figure I.4.

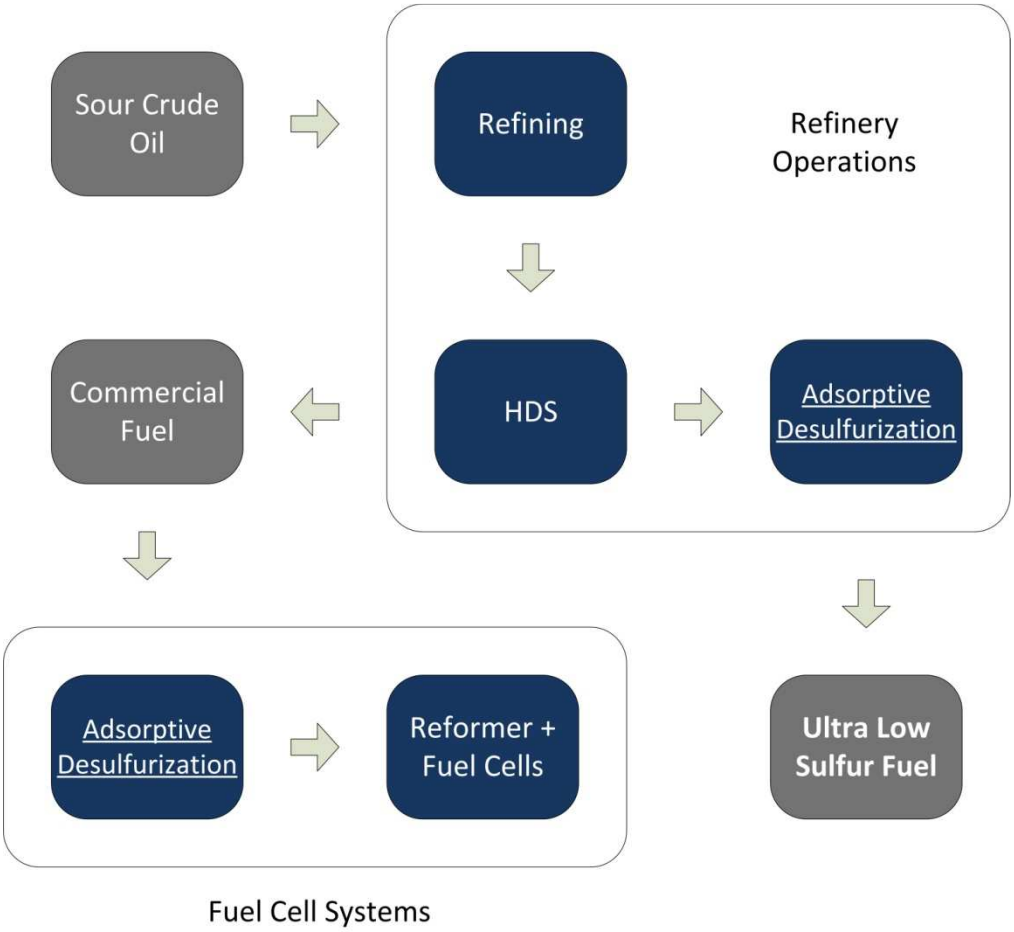

Figure I.4. Probable applications of adsorption in current fuel processing systems

High temperature/reactive adsorption of organosulfur species from petroleum fuels has been investigated extensively as discussed earlier. The "IRVAD" process developed by Black and Veatch Pritchard engineering company has shown to remove sulfur species from FCC gasoline via reactive adsorption [9]. It is a hydrogen free process that operates at elevated temperatures and pressures. The process employs moving bed technology to

adsorb and regenerate the adsorbent beds continuously. Research Triangle Institute (RTI) has developed a reactive adsorption process called TReND that has been reported to efficiently desulfurize crude oil [6]. Another successful example of adsorption process tested in a refinery is the Phillips S-zorb process [44]. Partial hydrogen pressure is employed in this process along with elevated temperatures. The reaction proceeds via following reaction [44]:

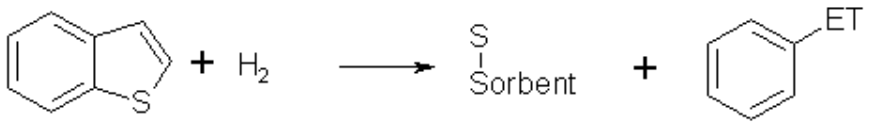

In the recent years, desulfurization by direct adsorption of organosulfur species (non reactive adsorption) at ambient conditions has gained much attention [20, 45-50]. A highly selective adsorbent or a combination of adsorption process with distillation process to pre-concentrate the feed has been shown to facilitate sub-ppmw desulfurization of hydrocarbon fuels. One of the practical applications regarding integration of adsorption in refineries is SK HDS pretreatment process. The process highlights on removal of nitrogen containing compounds from crude oil before the HDS process [51]. This has shown to enhance the HDS process significantly.

The discussion above mentions some of the successful applications of adsorption in the refinery processes. However, very few studies have been conducted for developing smaller scale versions of desulfurization processes. In the current perspective, the scalability of the adsorption process should also be included.

I.2.3.1. Adsorbent materials

Extensive research work has been carried out for developing the materials for sulfur adsorption. Several compositions have been specifically formulated and tested for liquid

phase desulfurization of hydrocarbon fuels. A complete comparative analysis of all these adsorbents is complicated due to the differences in adsorbent formulation, experimental conditions, and fuel compositions. Majority of the effective sulfur adsorbents tested so far are composed of transition metals. Among the transition metals, nickel based adsorbents have been tested more extensively for high temperature reactive adsorption [20, 52-54]. Ni supported on Al–SiO_2 [54] and MCM-41/SBA-15 [20] have been observed to work very well in desulfurizing gasoline and Ultra Low Sulfur Diesel (ULSD), respectively, at temperatures ranging from 200–250°C. IRVAD process mentioned earlier employs alumina based adsorbent with an inorganic promoter [9]; while zinc oxide based adsorbents are employed in the Philips S-zorb process [9]. High temperature adsorbents such as zinc titanate and Mn/Al_2O_3 have also been successfully employed in desulfurizing hydrocarbon fuels [9].

For low temperature applications, several adsorbents with transition metals as active sites have been shown to work very well. Low temperature operation is preferred for various applications such as use in on board Proton Exchange Membrane (PEM) fuel cells. The π-complexation adsorbents developed by ion exchange of Cu, Ag, Ce, and Ni ions into the cage structures of zeolites had very good sulfur adsorption capacities from transportation fuels [3, 27, 55]. Other than these, supported copper and palladium halide adsorbents also desulfurize high sulfur jet fuels at room temperatures via the same mechanism [45]. Solid superacid type adsorbent such as sulfated alumina has also been tested for desulfurization of commercial fuels [56].

Metal Organic Framework (MOF) materials have also been tested for adsorptive desulfurization. MOF materials such as MOF-5 and HKUST-1 have good adsorption

affinities toward organosulfur compounds e.g. BT, DBT, and 4,6-DMDBT in liquid form [57]. These MOF materials have also been tested for commercial gasoline and diesel [58]. Carbon materials are also observed to be good sulfur adsorbents even in liquid states [59]. These are one of the least expensive adsorbent materials among all the commercial ones. Carbon materials, depending on their sources, can be modified to increase its functionality as a sulfur adsorbent [25, 60]. But its selectivity is still a major challenge as seen from its poor performance for commercial fuels. Carbon also lacks the ability to regenerate at high temperature as such treatments reduce its surface area and pore structures significantly.

The adsorbent materials mentioned so far have been reported to have significant sulfur adsorption capacities from petroleum fuels. However, most adsorbent materials are in reduced form. Therefore, these adsorbents would have to undergo activation in a reducing environment (e.g. H_2, He, etc.) prior to desulfurization. Pressure drop is a major challenge for some of the supports such as MCM-41 and SBA-15, in addition to the increase in material cost. Usually an adsorber bed is larger than a typical catalyst bed; therefore the material cost would be high. Few studies have been carried out and reported in the literature regarding the regeneration procedure for these adsorbent materials. This also generates a problem in case of continuous operation because of the adsorbent's need for regeneration. Therefore, the development of a scalable adsorbent composed of inexpensive materials and possessing the ability to regenerate for indefinite cycles would be ideal for continuous operation in a desulfurization unit.

I.2.3.2. Advantages and limitations of adsorptive desulfurization

Selective adsorption of sulfur species is one of the most promising solutions for producing ultra clean hydrocarbon fuels. The process primarily requires an adsorber with or without the need of supplementary streams (e.g. hydrogen) or other external auxiliary units (e.g. separators, compressors for hydrogen). Energy efficient and environmentally benign, the process does not require operations at extreme temperatures or pressures. Some adsorption processes can even be operated at room temperature and atmospheric pressure.

Based on the adsorbent materials, adsorptive desulfurization addresses a major problem generally faced by the HDS process; the selectivity toward Poly Aromatic Sulfur Heterocycles (PASH). Heavy thiophenic derivatives such as methylated BT's and DBT's have very low reactivities with hydrogen in the presence of HDS catalysts as compared to their aliphatic counterparts, thus resist the HDS process and remain in the product streams. Selective adsorption provides novel mechanisms of capturing sulfur from hydrocarbon streams, such as π-complexation and the use of surface acidity. As a result, some of the adsorbent materials demonstrate great selectivities toward PASH molecules. This is also complemented by the absence of any extraneous reactions such as olefin hydrogenation or octane/cetane number reduction.

Adsorptive desulfurization possesses great applicability toward fuel cell applications due to its ability to deep desulfurize hydrocarbon fuels. With the variation of the adsorbent bed volume, the targeted sulfur concentration can be varied from a few ppmw to ppbw ranges. Adsorption has a significant edge over other processes in the case of application in portable desulfurization systems. As seen from the discussion above, there are marked

differences between the sulfur removal operation in the refineries and portable desulfurization paradigm. The onboard units should be compact, simple in design and should require less or no supplementary streams. Conventional HDS process requires high temperature and pressure along with auxiliary units hence it is not suitable for on board systems. The absence of major auxiliary units is a major advantage for adsorptive desulfurization. For this, the adsorption process can be scalable to any sizes and can be applied in various applications. Low temperature adsorbent within the fuel processing units allows for the “cold-starts” of hydrogen vehicles. Operating at atmospheric or mild pressures reduce the process safely challenges to a great extent. The absence of hydrogen requirements would greatly alleviate the complexity of the process. For all the features mentioned above, adsorptive desulfurization would be better suited for mobile fuel cell stacks than other commercial or prospective sulfur abatement processes. It would be an ideal process that could supplement HDS process as a polishing step.

In spite of many advantages, adsorptive desulfurization is not free from limitations. The process is primarily limited by the adsorbent capacity. Most of the adsorbent materials have very low capacities for sulfur adsorption as compared to catalytic HDS process. The lower capacity may be attributed to the facts that adsorption takes place instead of catalytic reaction and also there are mass transfer and diffusion limitations. Liquid phase adsorption proceeds much slower than gas phase; as a result the production rate would be low. It also depends upon the adsorption equilibrium thereby performs poorly for low sulfur feed. Due to its low capacity, the adsorber volume has to be significantly large considering the target production. Therefore, the economics involved regarding the cost of the adsorbent materials should be considered. Regeneration of the adsorbent bed

should also be necessary if the objective is continuous operation. In the case of regeneration by flowing gaseous streams, pressure drop becomes an issue. The choice of medium for regeneration would also be important, and easily available gases (air, steam, exhaust gases) should be appropriate for application in the regeneration process.

I.3. Silver based adsorbents

Silver has a great affinity toward sulfur as seen from the tarnishing of silver utensils. Metallic silver reacts with sulfur compounds at low temperatures that correspond to its low activation energy. Supported Ag adsorbents and catalysts have been widely used in processes such as epoxidation of propylene [61], disinfection photocatalysis [62], catalytic reduction of nitrogen oxides [63], dehydrogenation of methanol [64], decomposition of acrylonitrile [65], and many others. It is an inexpensive noble metal possessing characteristic such as reducibility at ambient conditions. Silver based adsorbent has also been tested for sulfur removal. Ag-exchanged Y-zeolite was observed to perform very well as a room temperature sulfur adsorbent [66]. Ag-zeolites have also been observed to remove dimethyl sulfides and mercaptans from natural gas [67]. $AgNO_3$ was seen to be effective in desulfurizing high sulfur jet fuels at ambient conditions [68].

The adsorption lab at Auburn University's Center for Microfibrous Materials Manufacturing (CM3) has developed a silver based adsorbent for the ultra-deep desulfurization of refined transportation and logistic fuels at room temperatures [69]. The adsorbents have demonstrated considerable sulfur adsorption capacities from fuels in liquid phase and remove sulfur down to a few ppmw ranges. It is one of the few adsorbents reported in the literature that can reduce sulfur level in oxidized form without requiring any sulfidation or activation. Saturated silver on titania adsorbent is also

thermally regenerable in air; hence it is applicable in multi-cycle desulfurization applications. The preparation technique for Ag/TiO_2 is simple, cost effective, and scalable. The adsorbent material cost can also be low since the Ag metal cost is much cheaper than other noble metals (e.g. Au, Pt, Pd) and the amount of Ag in adsorbent formulation is small (~4 wt%) [70].

The excellent performance of silver based adsorbent in desulfurization called for an extensive characterization of silver active phase. After characterizing the adsorbent via Electron Spin Resonance (ESR) and X-ray Photoelectron Spectroscopy (XPS), silver (I) oxide (silver oxidation state: +1) was observed to be the active phase for sulfur adsorption [71]. Silver being active in oxide form is accounted for its regenerability at oxidizing conditions. It was also observed that higher fraction of silver (I) oxide was present at lower loadings of silver on titania-anatase support and the optimized silver loading was around 4% by weight. Silver loading higher than 4% causes particle agglomeration and reduction in silver oxide fraction thereby lowering sulfur adsorption capacity [70].

Silver based adsorbent posses a great potential for a sulfur adsorbent operating at ambient conditions. It can be reduced at mild conditions, unlike most sulfur active transition metal. Activation of silver to its zero or low oxidation state is easy and relatively stable. Yet it is far from optimization and successful integration into a fuel cell system due to the lack of proper insight into the sulfur adsorption mechanism. Therefore a mechanistic investigation is necessary for the proper characterization of silver active sites for organosulfur adsorption.

I.4. Mixed oxide supports

I.4.1. Role of titanium oxide

In the previous work performed at CM3-adsorption lab, it was observed that metal oxide supports, especially TiO_2, had significant contribution to the overall sulfur adsorption capacity of the adsorbent [72]. The "active sites" on the supports were believed to be surface acid functional groups that were generated during calcination in air at higher temperatures [73-75]. TiO_2 acted as an electronic promoter in different catalytic processes [73]. Titania has been shown to be a better support for silver than other common metal oxide supports not only for the presence but also for the concentration of active functional groups on the surface. The active sites on titania also causes better metal dispersion than other surfaces [70]. In spite of these features, titanium oxide has lower surface area than most other commercial metal oxide supports for which the overall sulfur adsorption capacity is low. In addition, the silver loading on titania is confined to only 4% by weight. Assessing these problems, it is necessary to increase titanium oxide surface area.

One possible way of increasing titanium oxide surface area is to disperse it on high surface area supports such as silica, alumina, activated carbon, zeolites etc. Researchers have widely reported studies' regarding mixed metal oxide supports containing titanium oxide [74-80]. Some of the examples are TiO_2–SiO_2, TiO_2–Al_2O_3, Ti-MCM-41, etc. The addition of titania on alumina resulted in greater number and strength of surface acid sites [74, 81]. Titania modified supports had higher concentrations of coordinative unsaturated sites [79]. Titania dispersed mixed oxide supports such as TiO_2–SiO_2 and TiO_2–Al_2O_3 also increase the thermal stability of titania (anatase) phase [82]. Mixed oxide supports

have higher effect on catalytic reaction than their individual counterparts such as hydrodesulfurization and Claus process [83, 84]. TiO_2–Al_2O_3 mixed oxide also has very high catalytic activity toward NO reduction reaction [85] and HDS reaction [78]. Silver has been successfully applied on these mixed oxide supports for other applications such as dehydrogenation of methanol [86]. If high surface area supports are decorated with titanium oxide functional groups, it may increase the active area and enhance the sulfur loading during adsorption. Increase in total surface area may also facilitate in loading of higher amounts of oxidized silver. Therefore, more Ag could be loaded onto mixed oxide supports that in turn should increase sulfur adsorption capacity. The overall mechanism is shown in Figure I.5.

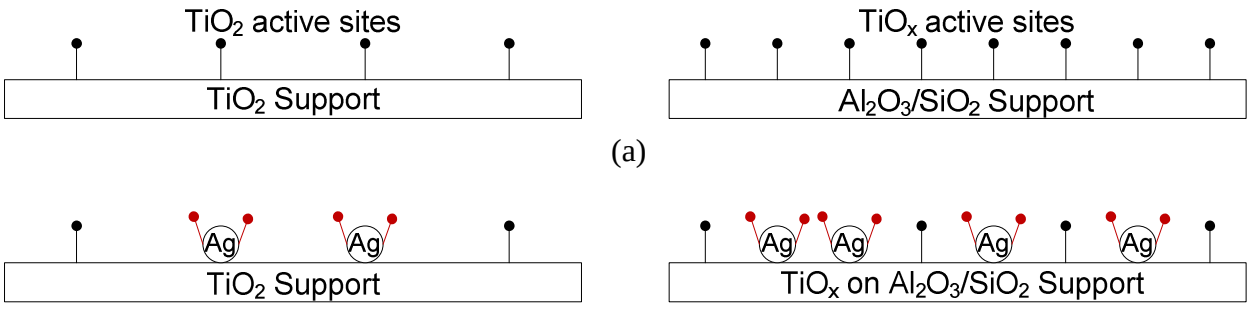

Figure I.5. Dispersion of titanium oxide sites on high surface area supports and their corresponding effects; (a) increase in titanium oxide active sites, (b) increase in silver loading

I.4.2. Formulation of titanium oxide dispersed mixed oxide supports

Mixed oxide materials containing Ti have been studied extensively in the literature [73]. There are various methods of dispersing titanium on high surface area supports, such as

incipient wetness [79, 87], co-precipitation (sol-gel) method [76, 78], atomic layer deposition [77, 84], etc. Most of the preparation methods have been developed with a view to the targeted product. Among these, incipient wetness and co-precipitation methods have been practiced most widely. The features of these two methods are illustrated in Table I.2.

Table I.2 Comparative features of incipient wetness and co-precipitation method for preparing titanium oxide containing mixed oxide supports

<table>
<tr><th></th><th>Incipient Wetness</th><th>Co-Precipitation</th></tr>
<tr><td>Features</td><td>Dispersion of Ti precursors over support surface by dry impregnation followed by drying and calcination.</td><td>Incorporation of Ti and Si/Al precursors followed by washing, filtration, drying, and calcination.</td></tr>
<tr><td rowspan="3">Advantages</td><td>Simple process</td><td>No pore blockage</td></tr>
<tr><td rowspan="2">Provide more concentration of Titanium oxide on the surface</td><td>No reduction in surface area</td></tr>
<tr><td>No limitation on Ti loading; supports with any amount of Ti can be produced</td></tr>
<tr><td rowspan="4">Limitations</td><td>The method can lead to extreme pore blockage</td><td rowspan="2">Complicated process; involving more steps and chemicals</td></tr>
<tr><td>Difficult to form monolayer</td></tr>
<tr><td>Can reduce overall surface area</td><td rowspan="2">Less amount of Titanium oxide on the surface on the basis of similar Ti loading as compared to incipient wetness.</td></tr>
<tr><td>Loading of Ti is limited</td></tr>
</table>

Besides the preparation method, different Ti precursors have also been used. Among these, three types of precursors are most common: titanium isopropoxide, titanium (IV) chloride, and titanyl oxide sulfate [73, 80, 88-90]. For adsorptive desulfurization, the objective is to increase the concentration of titanium oxide active sites on the surface. The optimization of the preparation method would help developing an ideal silver based adsorbent.

I.5. Mechanism of sulfur removal at ambient condition

Although many adsorbent materials have been tested and reported in the literature, very few of these have been investigated in detail for better understandings of the adsorption mechanisms. The reaction mechanisms regarding sulfur adsorption vary with respect to temperature, hydrogen pressure, and most of all surface characteristics of the adsorbents. For high temperature reactive adsorption in presence of hydrogen, the adsorption mechanism proceeds via hydrogenation and hydrogenolysis pathways. The adsorption mechanism of sulfur onto supported Ni–ZnO has been attributed to the sulfur scission mechanism [9].

In order to systematically develop a better understanding regarding the sulfur adsorption mechanism, the traditional HDS reaction should be properly studied. Researchers have reported previously that the removal of heavier DBT and methylated DBT is difficult via traditional pathways followed by HDS. For example, HDS of 4,6-DMDBT proceeds via hydrogenation pathways as these can be interacted mostly through π-bonding. Hydrogen is essential for this pathway so that it can react with the stripped sulfur to form H_2S. Hydrogenolysis pathway is difficult due to the steric hindrance created by the methyl group and is possible only through the active sites on the edges [2]. The phenomenon is

depicted in Figure I.6. The direct bond between the sulfur atom in methylated PASH and surface metal cation is difficult. Alternative mechanism should be employed that can bypass the attached methyl groups.

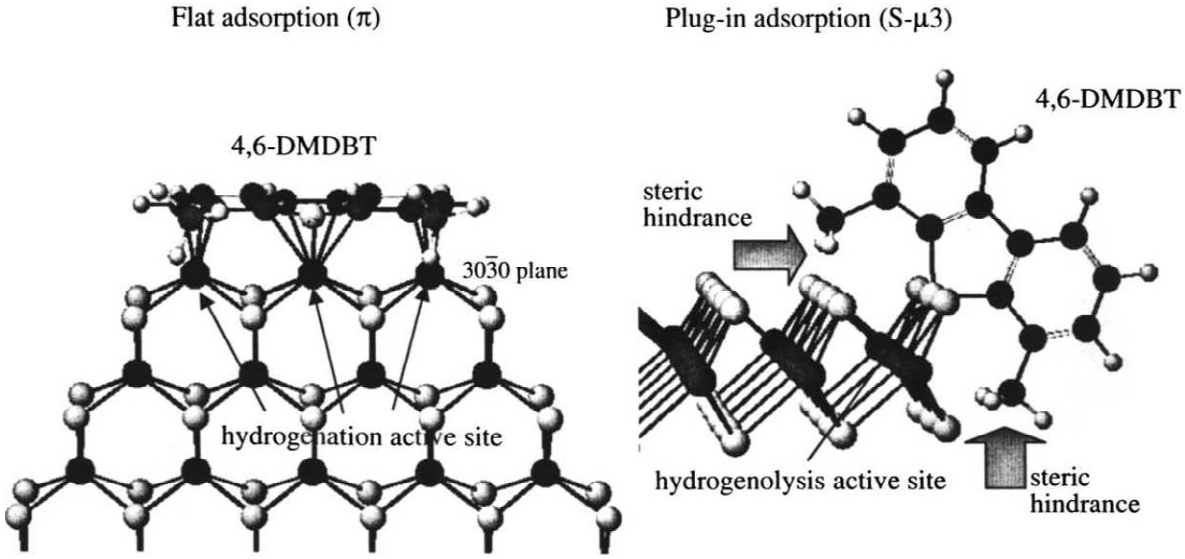

Figure I.6. Mechanisms of 4,6-DMDBT interacting with catalyst structure via hydrogenation (left) and hydrogenolysis (right) pathways (reproduced from C. Song et al., Applied Catalysis B- Environmental, 2003 [2])

Multi-cycle adsorption of sulfur species from liquid fuels at ambient conditions offers an alternative solution to the production of inexpensive ultra clean fuels. However, the area lacks clear views on the adsorption mechanism of sulfur compounds onto adsorbent surface and the surface functional groups responsible for this. Considering the activation energies, most of the desulfurization at room temperature would be physical adsorption through Van Der Waal's interactions between sulfur species and active sites. One of the notable adsorption mechanisms at room temperature ever reported is that of the π-complexation adsorbents. At low temperature, Yang and coworkers have shown π-complexation bonds between aromatic rings of sulfur species with cations of transition

metals in zeolites [27, 45]. The conjugation of π-electrons by sulfur atoms along with the back donation of electrons by the transition metal ions (e.g. Cu) results in the abovementioned bonding between these (Figure I.7).

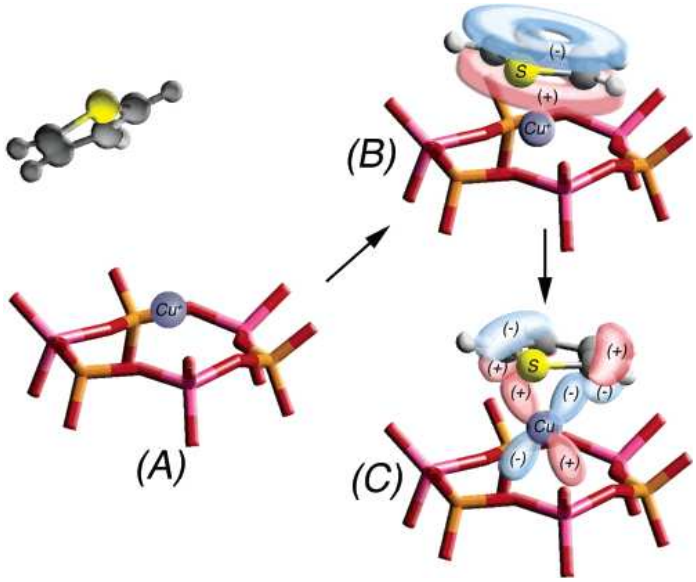

Figure I.7. Mechanisms of transition metal incorporation and sulfur adsorption; (A) Copper ion occupying the site in the zeolite; (B) S-donation of p-electrons of thiophene to the 4s orbital of copper(I); (C) d-p-backdonation of electrons from 3d orbitals of copper(I) to p-orbitals of thiophene (reproduced from A. J. Hernandez-Maldonado et al., Applied Catalysis B-Environmental, 2005 [3])

Recently, the CM3-adsorption lab has postulated a novel adsorption mechanism whereby the surface hydroxyl groups (Bronsted acid sites) form bonds with the π-electrons of the aromatic rings [4]. Characterization of the adsorbent materials with different probe molecules supported the hypothesis. The postulated scheme can be seen in Figure I.8 [4]. The sulfur adsorption mechanism involved in the case of silver adsorbents is clearly distinct from the other set of adsorbents as it performs in an oxidized form. The effect of surface acidity toward sulfur adsorption is significant in this realm. Sulfur removal from a

heterogeneous mixture such as fuel in liquid form at room temperature is a complicated process that requires much mechanistic details. Further investigation is essential for understanding the fundamental mechanisms involved. Rigorous analytical studies of the adsorbent including *in situ* techniques would help in optimizing the adsorbent formulation and the adsorption process. Computational methods should also be applied in addition to experimental techniques of performance evaluation and characterization.

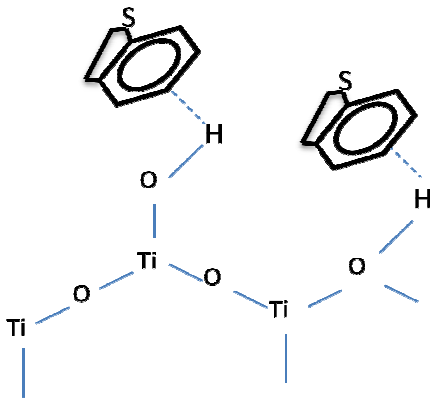

Figure I.8. Adsorption mechanism of Ag/TiO_2 adsorbents showing the bonding between aromatic rings of sulfur species with surface hydroxyl groups (reproduced from S. Nair et al., Fuel, 2013 [4])

I.6. Objectives

So far we have discussed the significance of adsorptive desulfurization in the current energy perspectives and the potentials of silver based adsorbent as a successful polishing agent following the HDS process. The studies reported in this dissertation are intended to help develop a successful application of adsorption in desulfurization units that could facilitate in meeting the demand for ultra low sulfur fuels. The objectives of this project are as follows and are also shown in Figure I.9:

- Development of adsorbent formulation for desulfurizing wide varieties of hydrocarbon fuel blends (e.g. Jet fuels and diesels).
- To develop an adsorption process that is scalable, feasible, regenerable, and effective.
- Expand the extent of desulfurization to meet fuel cell requirement (<0.1 ppmw S)
- Investigate the sulfur adsorption mechanism at ambient conditions and explore the surface acidity characteristics of silver-titanium oxide materials.
- Apply engineering fundamentals and computational studies to understand and overcome competitive adsorption and selectivity issues.

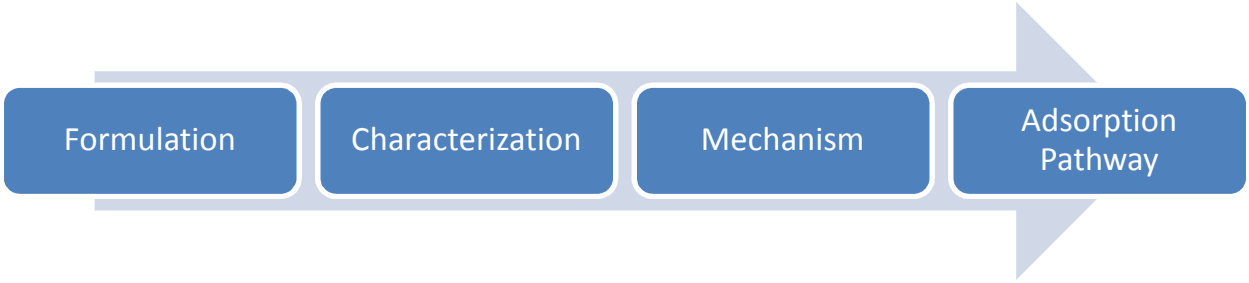

Figure I.9. The research outline

I.7. Outline:

In chapter II of this dissertation, I have presented the experimental procedures along with the characterization techniques and the comprehensive treaties on mechanism evaluation. Chapter III discusses the development, optimization and performance evaluation of mixed oxide supported silver adsorbents. It also discusses the parts per billion (ppbw) level desulfurization and regeneration of the adsorbent formulations. The adsorbent characterization is reported in chapter IV using nitrogen adsorption isotherms, oxygen

and ammonia chemisorption, x-ray diffraction (XRD), Raman and UV-vis spectroscopy, and infrared (IR) spectroscopy. This also includes the studies regarding adsorbent activation mechanism and the effect of surface acidity. Chapter V focuses on the sulfur adsorption pathways on mixed oxide supported silver adsorbents along with the effect of fuel chemistry using complimentary desulfurization and IR techniques. Chapter VI reports the investigation of adsorbent selectivity toward different sulfur and non-sulfur heterocycles using computational (density functional theory) studies.

II. Experimental Details

II.1. Adsorbent preparation

Gamma-Al_2O_3, Anatase-TiO_2 (Grade ST61120) and SiO_2 (Grade 21) were purchased from Alfa Aesar, Saint Gobain Norpro, and Grace Davison, respectively. All the supports were crushed and sieved to 850–1400 μm size (unless specified otherwise) followed by drying in a convection oven at 110°C for at least 6 h before use. The precursors for titanium and silver were purchased from Alfa Aesar and were used as received.

The blank supports used in desulfurization and characterization experiments were calcined in flowing air at 450°C for 2 h before use. For the preparation of titanium oxide dispersed mixed oxide supports, titanium precursors were dispersed onto dried (at 110°C for 6 h) Al_2O_3 and SiO_2 supports by means of incipient wetness method (dry impregnation). The concentrations of the solutions were such that the titanium metal loading was 10 wt% at the time of impregnation. In other words, the Ti:Al and Ti:Si weight ratios were 1:4.4 and 1:3.9, respectively (unless specified otherwise). Three types of titanium precursors were used; titanium (IV) chloride (99% min), titanium isopropoxide (97% +), and titanyl (IV) oxide sulfate sulfuric acid hydrate ($TiOSO_4$). The precursors were acquired from Alfa Aesar. For solution preparation, titanium isopropoxide was dissolved in iso-propanol; titanyl oxide sulfate in water; and titanium (IV) chloride was used without any solvent. The supports were then dried in the convection oven at 110°C for 6 h followed by calcination in flowing air in a tube furnace

at 550°C for 2 h. Based on previous works, the calcination temperature was optimized in terms of achieving complete conversion to titanium oxide and minimizing rutile formation [79, 84, 88-90].

The mixed oxide supports were also prepared by co-precipitation method (denoted by "CP"). Here, aluminum isopropoxide (98% +, Alfa Aesar), tetraethoxysilane (99.9%, Alfa Aesar) and titanium isopropoxide (97% +) were used as aluminum and titanium precursors, respectively. For preparing TiO_2–Al_2O_3 CP, aluminum precursor was dissolved in iso-propanol and was heated to 70°C after which titanium precursor (dissolved in iso-propanol) was added to the solution using a burette under vigorous stirring. The solutions were mixed in such a way as the Ti:Al weight ratio was 1:4.4. After 30 min, 1M HNO_3 (aq) solution was added to the mixture using a burette. After this, the mixture temperature was raised to 95°C with continuous stirring and kept there for 3 h. The mixture was then washed with de-ionized water (4 times the initial solution volume) and filtered. The residue was dried overnight at 110°C in a convection oven followed by calcination in flowing air at 450°C for 2 h. The TiO_2–SiO_2 CP mixed oxides were prepared in same way; however in this case silicon precursor was used and the Ti:Si weight ratio was 1:3.9.

Aqueous $AgNO_3$ was used as the silver precursor and was dispersed onto the supports by incipient wetness method (dry impregnation). The impregnated volume of the precursor solution was 100% of the pore volumes of the individual and mixed oxide supports, and its concentration was adjusted according to the desired metal loading on the supports. The samples were then dried in the convection oven at 110°C for 6 h followed by calcination in flowing air (unless specified otherwise) in a tube furnace at 450°C for 2 h. The

desulfurization capacities of different batches of the same formulation were within the error range of 10%. This deviation was observed in all desulfurization experiments reported in this dissertation. All the gases used in the adsorbent treatments were purchased from Airgas South Inc.

II.2. Challenge fuels

Both commercial fuels and model fuels were employed as challenges in the desulfurization experiments in liquid form. JP5 and JP8 jet fuels were collected from NAVSEA Philadelphia and TARDEK, respectively. ORD and ULSD were acquired from local sources near Auburn, Alabama, USA. The initial sulfur contents of JP5, JP8, ORD, and ULSD were 1172, 630, 452, and 7.5 ppmw, respectively. Benzene (99%), benzothiophene or BT (98% +), 1-butanethiol or 1-C4T (98%), and diethyl sulfide or DES (96%) were purchased from Alfa Aesar while thiophene or T (98%), 4,6-dimethyldibenzothiophene or 4,6-DMDBT (97%) and n-octane (97% +) were acquired from Acros Organics. These compounds were used in model fuel preparation. The model fuels used in the desulfurization experiments were prepared by mixing the sulfur (1-C4T, DES, T, BT, 4,6-DMDBT) and non-sulfur species (benzene) with n-octane. The major sulfur species in the fuels were identified using analytical standards collected from Chiron AS.

II.3. Desulfurization experiments

II.3.1. Static saturation tests

For the desulfurization experiments, both static saturation tests and dynamic breakthrough tests were carried out in order to assess the sulfur adsorption capacities of

the adsorbents. In each saturation test, the fuel was mixed with the adsorbent and the mixture was agitated mechanically for 48 h at ambient conditions. The equilibrated fuel was analyzed to measure the outlet total sulfur content, which was used to calculate equilibrium sulfur adsorption capacity. The equilibrium saturation capacity was calculated from the following formula:

$$Q_{Sat} = \frac{(1 - \frac{C}{C_0})\rho_f V_f C_0}{1000}$$

Where, Q_{Sat} = Equilibrium saturation capacity (mg S/g adsorbent)

C = Sulfur concentration of fuel after saturation (ppmw)

C_0 = Initial sulfur concentration of fuel (ppmw)

ρ_f = Density of fuel (g/ml)

V_f = Volume of fuel/adsorbent weight (ml/g)

All the saturation experiments were carried out at room temperature and ambient pressure. The density of the commercial fuels varied from 0.8–0.85 (g/ml), and that of model fuel was between 0.7–0.75 (g/ml). The values were calculated experimentally.

II.3.2. Dynamic breakthrough tests

The breakthrough experiments were conducted using logistic, commercial, and model fuels as challenges. Each time, the adsorbent was loaded onto a quartz adsorber in a vertical packed column configuration and was supported on both sides by quartz wool. The adsorbents were not activated prior to the experiment. Fuel flowed upward vertically with a flow rate of 0.5 ml/min and WHSV of 2.5 h^{-1} (LHSV~2 h^{-1}) using a Cole-Parmer Masterplex Digistaltic peristaltic pump. Upward flow minimized bed channeling and ensured complete wetting of all adsorbent particles. All the breakthrough experiments

were performed at room temperature and atmospheric pressures. Outlet fuel was sampled at regular intervals and analyzed. The outlet sulfur concentration (C) was normalized by inlet sulfur concentration (C_o). The breakthrough curves were obtained by plotting C/C_0 against either time (min) or cumulative volume of fuel per unit weight of adsorbent (ml/g). The breakthrough capacity was calculated at the 10 ppmw sulfur threshold limit. For calculating the capacity at saturation, linear integration method was applied. The breakthrough capacity was calculated using the following formula:

$$q_b = \frac{\rho_f V_f (C_0 - C_T)}{1000}$$

Where, q_b = Breakthrough capacity (mg S/g adsorbent)

C_0 = Initial sulfur concentration of fuel (ppmw)

C_T = Threshold sulfur concentration (ppmw)

ρ_f = Density of fuel (g/ml)

V_f = Volume of fuel/adsorbent weight (ml/g)

The value of C_T was 10 ppmw, unless specified otherwise. For calculating the capacity at saturation, linear integration method was applied. The following formulas were applied for calculating the capacity at saturation.

$$V_n = \frac{t_n v}{W}$$

$$q_{sat} = \frac{\rho_f \sum_n \left[(V_n - V_{n-1}) \left\{ (C_0 - \frac{(C_n + C_{n-1})}{2} \right\} \right]}{1000}$$

Where, V_n = Cumulative volume of fuel per unit weight of adsorbent (ml/g)

t_n = Cumulative time (min)

v = Volumetric flow rate (ml/min)

W = Adsorbent weight (g)

q_{sat} = Capacity at saturation (mg S/g adsorbent)

ρ_f = Density of fuel (g/ml)

C_0 = Initial sulfur concentration of fuel (ppmw)

C_n = Sulfur concentration of outlet fuel at n point (ppmw)

For regeneration, the saturated bed was heated at 110°C for 1 h in flowing air, followed by 230°C for 2 h, and finally 450°C for 1 h. After regeneration, the rejuvenated adsorbent bed was cooled down to room temperature and used again for breakthrough experiments in desulfurizing challenge fuels. The setups for adsorption and regeneration process are schematically shown in Figure II.1.

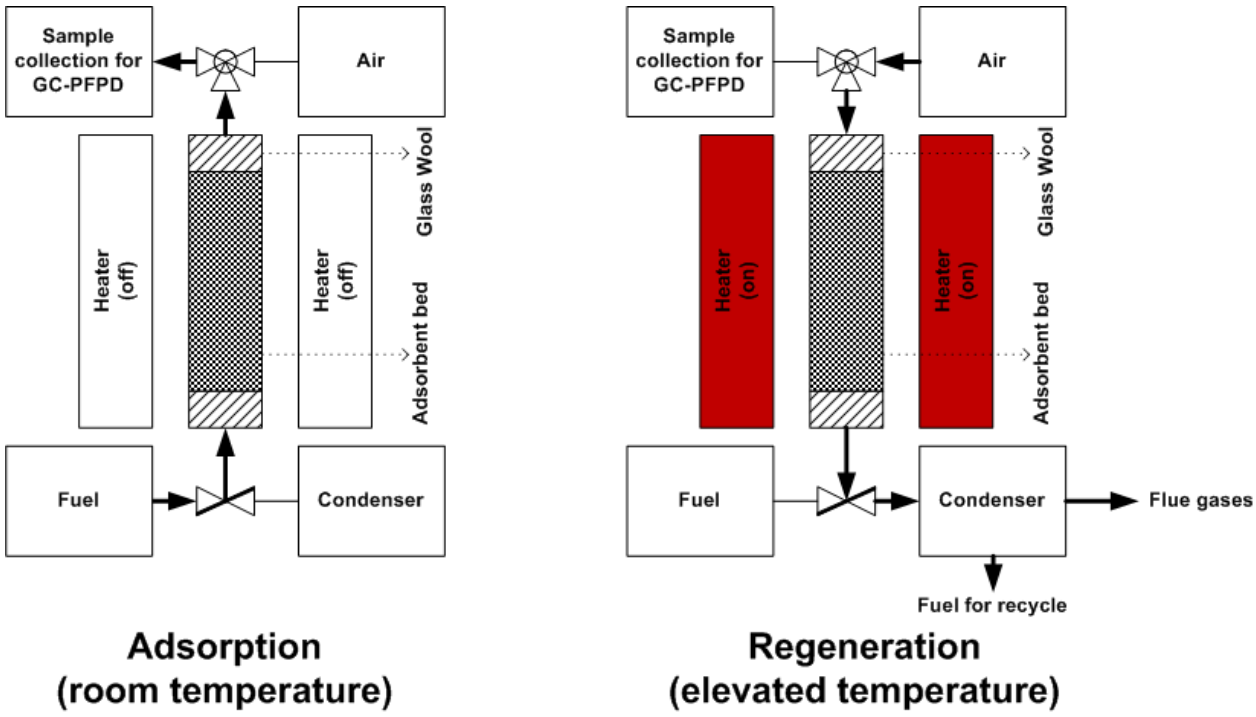

Figure II.1. Experimental setup for breakthrough test; adsorption at room temperature (left), regeneration at elevated temperature (right)

II.4. Analysis of fuel

The total sulfur content of the fuel was measured using an Antek 9000S Total Sulfur Analyzer (TSA) equipped with a photomultiplier tube. The column temperature for every sample analysis was 1050°C. UHP oxygen and helium (source: Airgas South) were used as pyro and carrier gases, respectively. The lower detection limit of TSA was measured to be 200 ppbw.

To determine the sulfur content as well as sulfur speciation, fuel samples were analyzed in a Varian CP3800 Gas Chromatograph (GC) equipped with a Pulsed Flame Photometric Detector (PFPD). The GC used a Restek XTI-5 crossboard column of 30 m length and 0.25 mm ID. The sample injection volume was 1μL with split ratios between 0 and 100. For analysis, the column temperature was initially at 100°C for 3 min and was then raised to 300°C at 10°C/min and was kept there for 2 min. Both GC-PFPD and TSA were calibrated using standard samples prepared by successive dilution of JP5, ORD, and also using model fuels containing octane-sulfur mixtures with known sulfur concentrations. For dilution of commercial fuels, n-octane was used to dilute the fuels to make standard solutions of different sulfur concentration ranging from $C/C_0 = 0$ to 1. Successive dilution of ULSD was also carried out to prepare standard solutions. The solutions were used to calibrate the GC-PFPD so that it can measure ultra low concentration of sulfur (e.g. 75 ppbw). The calibration curve of GC-PFPD prepared by successive dilution of ULSD is shown in Figure II.2.

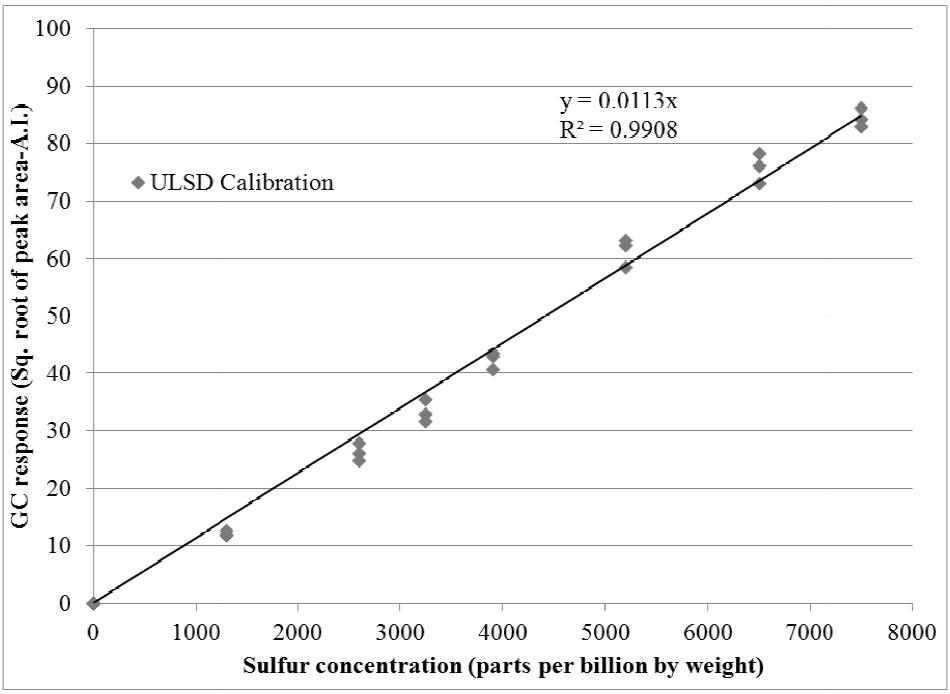

Figure II.2. Calibration curve of GC-PFPD prepared by successive dilution of ULSD (Split: 0)

II.5. Characterization of adsorbents

II.5.1. Nitrogen physisorption

Nitrogen physisorption was conducted to calculate BET (Brunauer-Emmett-Teller) surface areas, pore volumes, and average pore sizes of the adsorbents in a Quantachrome Autosorb AS1 analyzer. The analysis was carried out at -196^{0}C. Prior to the analysis, all the samples were outgassed at 150^{0}C for 2 h for moisture removal. Sample weight was between 0.1–0.15 g during each analysis.

II.5.2. Oxygen chemisorption

Selective oxygen chemisorption was also carried out in the Quantachrome Autosorb AS1 equipment to measure the silver dispersion on the supports. Different gases such as H_2, O_2, CO etc. have been used as adsorbate gases to measure active metal dispersion on

supports surfaces. Among them, oxygen was observed to work the best in terms of calculating the total oxygen uptake [91]. O_2 has been proved more effective for measuring silver surface area than other gases such as H_2, CO [70, 92, 93]. The samples tested via O_2 chemisorption had to undergo pretreatment before analysis. In each pretreatment process, the sample surface was cleaned by heating it at 150^0C for 30 min in vacuum (3.99×10^{-11} kPa) followed by reduction at 400^0C for 1 h in hydrogen (atmosphere pressure). After that, the sample cell was evacuated again to remove the physically adsorbed H_2. It was assumed that all the silver on the surface was in reduced metallic phase. For successful monolayer chemisorption of oxygen on silver surface, the optimized temperature ranges were observed to be between 170–220°C [91, 94]. In the present work, O_2 chemisorption was carried out at 170^0C at different relative pressures (P/P_0) and oxygen uptake at $P/P_0 = 0$ was calculated by extrapolating the linear portion of the graph to the y-axis. It was assumed that the physisorbed oxygen was negligible at that temperature; therefore combined oxygen uptake was used for calculation. Oxygen chemisorption on the supports surfaces such as TiO_2, SiO_2, and Al_2O_3 is negligible compared to that on silver. Detailed procedures of oxygen chemisorption analysis along with calculation methods of dispersion, active metal surface area, and average crystalline size have been stated elsewhere [70]. The adsorption stoichiometry was defined to be one oxygen atom to one silver atom [95, 96]. From total oxygen uptake, dispersion (D), active metal surface area (s), and average crystallite size was calculated from the following expressions:

$$D = \frac{N_m SM}{100L}$$

$$s = \frac{N_m S A_m}{166}$$

$$d = \frac{100Lf}{sZ}$$

Where, N_m = Oxygen uptake (μmol/g)

S = Adsorption Stoichiometry

M = Molecular weight of metal

L = Percentage metal loading

A_m = X-sectional area occupied by each surface atom ($Å^2$/Ag atom)

Z = Density of silver

f = Shape factor

The values of A_m and Z for Ag was 8.696 $Å^2$/Ag atom and 10.5 g/ml, respectively. The value of f was 6 as the particle was assumed to be spherical.

II.5.3. X-ray diffraction

Extent of titanium oxide on support surfaces was estimated using X-Ray Diffraction (XRD). A Bruker D-8 x-ray diffractometer equipped with CuKα source was used at 40KV/40mA. For each sample, the XRD scan range was 30–90° and scan speed was 0.1 second/step (~5.85°/min).

II.5.4. Scanning electron microscopy

The surface topography of fresh and regenerated adsorbents was acquired using a JOEL 7000-F Scanning Electron Microscope (SEM). The voltage of the equipment was 40 KV during imaging. The samples were analyzed without using any metal sputtering.

II.5.5. Raman spectroscopy

Raman spectroscopy was carried out *ex situ* in a RENishaw inVia Raman spectrometer at room temperature. A 514.5 nm Ar ion laser was employed using a resolution of 4 cm^{-1}. The adsorbent samples prepared for Raman studies were in 251–354 μm particle size ranges.

II.5.6. UV-DRS spectroscopy

UV-DRS measurements were performed using a commercial AvaSpec-2048 UV-vis spectrometer at a range of 200–800 nm (reflectance mode). The spectrometer was equipped with a pulsed Xe light source and a UV-vis DRS immersion probe. The probe was directly inserted into the adsorbent sample and analysis was carried out in a closed and dark vessel at room temperature. More information related to the experimentation can be found elsewhere [97]. The UV-DRS spectra were analyzed using Kubelka-Munk equation [98]. The absorbance data were used to calculate the band gap of TiO_2 at room temperature [99].

II.6. Ammonia adsorption

To determine overall surface acidity, NH_3 adsorption was carried out in the Quantachrome Autosorb AS1 instrument. Prior to each adsorption analysis, the sample was calcined (*in situ*) at 400 °C in air followed by evacuation for 30 min. Adsorption was conducted at 175 °C. During every analysis, combined (representing reversibly + irreversibly adsorbed NH_3) and additional weak points (representing reversibly adsorbed NH_3) were collected. The weak point was then subtracted from the combined point to calculate the strong (irreversibly adsorbed NH_3) point. Experimental details regarding NH_3 adsorption have been reported previously [100, 101].

II.7. IR Spectroscopy

Adsorbent samples treated with sulfur and non-sulfur probe molecules were analyzed via IR Spectroscopy. A Thermo Scientific Nicolet IR 100 spectroscope was used for this purpose. The analysis range was between 1000–4000 cm^{-1} and the spectral resolution was 4 cm^{-1}. The adsorbent samples prepared for IR studies were in 251–354 μm particle size ranges. A customized IR cell with ZnSe windows was employed for this study. Figure II.3 shows the experimental setup along with the IR cell and auxiliary units for treatment steps. The pretreatment procedures are described in Table II.1. Each adsorbent sample was pressed to a self supporting thin pellet by a Carver hydraulic press (model no. 3925) at 16000 psi followed by calcination in air at 450 °C for 2 h. Then the sample was loaded onto the cell and underwent through pretreatment (Table II.1). Here, the sample was heated to 200°C for 60 min in air, followed by evacuation (100 mTorr or 13.33 Pa) during the cooling down to room temperature (22°C). After every pretreatment, the sample was treated with different probe molecules. Both the pretreatment and exposure to adsorbate steps were performed *in situ*.

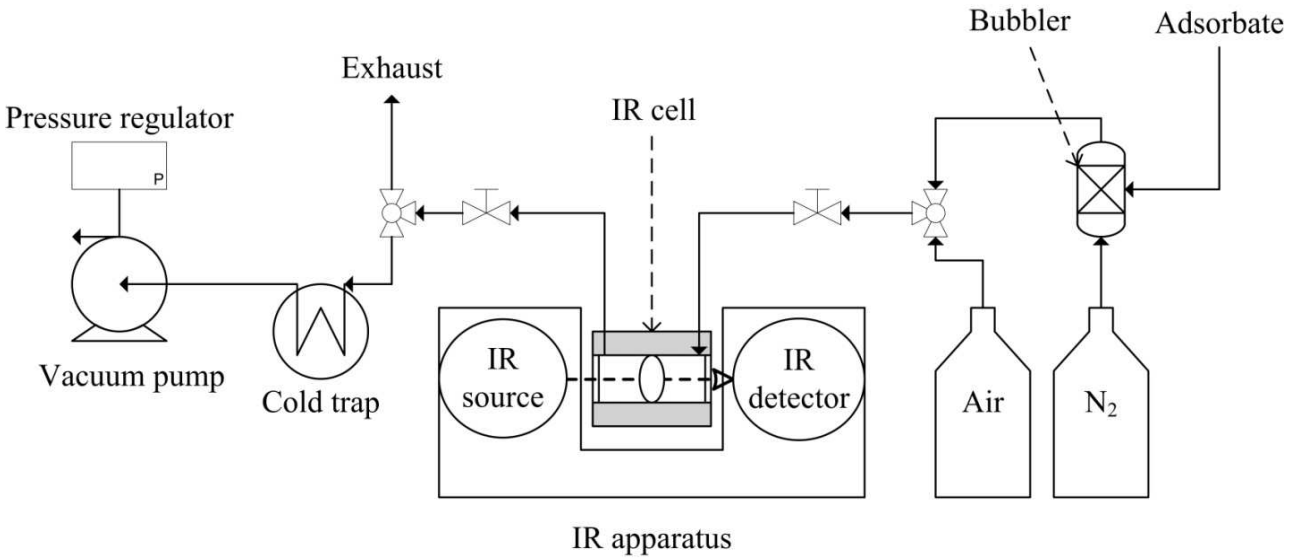

(a)

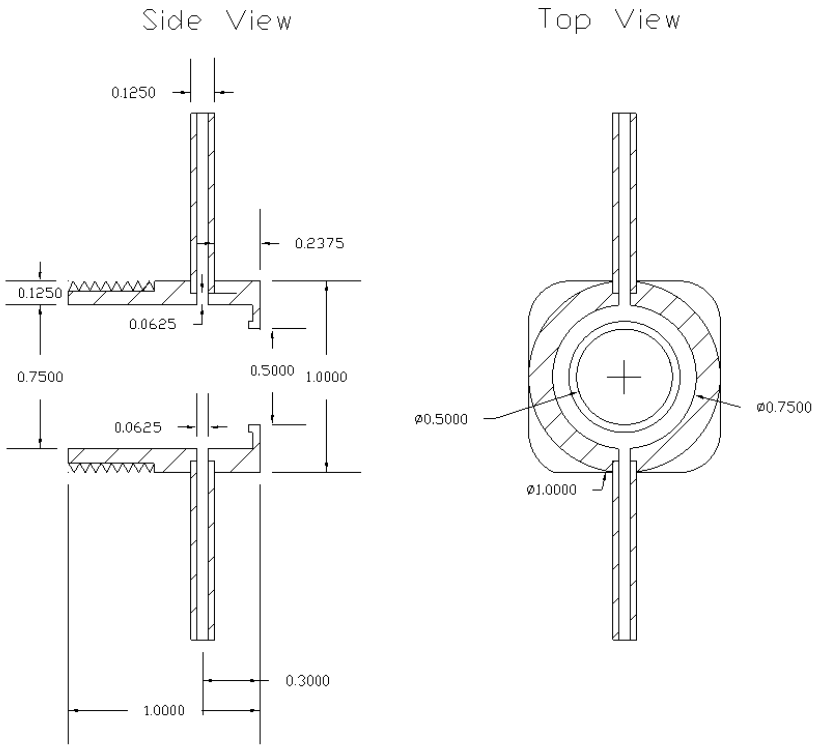

(b)

Figure II.3. (a) Experimental setup for *in situ* Infrared (IR) analysis; (b) Mechanical drawing of the IR cell.

Table II.1 Pretreatment steps before IR analysis

Steps	Temperature (°C)	Time (min)	Pressure
Drying	200	60	Atmospheric (Air flow)
Evacuation + Cooling	22	-	100 mTorr (13.33 Pa)

III. Adsorptive desulfurization of jet and diesel fuels using Ag/ TiO_2–Al_2O_3 and Ag/TiO_2–SiO_2 adsorbents

Abstract:

The objective of this work is to examine the performance of Ag/TiO_2–Al_2O_3 and Ag/TiO_2–SiO_2 for adsorptive desulfurization of JP5, JP8, Off-Road Diesel (ORD), and Ultra Low Sulfur Diesel (ULSD) at ambient conditions. These adsorbents were observed to be effective for desulfurizing liquid hydrocarbon feeds that ranged from 7.5 to 1172 ppmw S and comprised of diverse sulfur compositions. In fixed bed continuous adsorption tests, 4 wt% Ag/TiO_2–Al_2O_3 demonstrated saturation capacities of 10.11, 6.11, and 7.4 mg S/g adsorbent for JP5 (1172 ppmw S), JP8 (630 ppmw S), and ORD (452 ppmw S), respectively. In equilibrium saturation experiments, the adsorbent was able to desulfurize ULSD down to less than 75 ppbw S and this was achievable even when the initial concentration of non-sulfur aromatics was greater than 25,000 times higher. Dispersing TiO_2 onto high surface area alumina and silica substrates increased the sulfur adsorption capacities of both. This enhancement in adsorption capacity increased still further with silver addition. Higher Ag loading (up to ~12 wt% Ag) on TiO_2–Al_2O_3 proved beneficial to sulfur adsorption capacity when compared to TiO_2 (up to ~4 wt% Ag), indicating that the mixed oxide supports were able to host more active silver oxides. The adsorption selectivity toward different sulfur compounds present in the fuels varied during the fixed bed adsorption tests. The adsorbent had the greatest affinity for BT's and

the least for TMBT's and DMDBT's (the selectivity order from the strongest to weakest adsorption was: BT>MBT>DMBT>DBT≈MDBT>TMBT≈DMDBT). $Ag/TiO_2–Al_2O_3$ was thermally regenerable in air for multiple cycles at temperatures ranging from 110 to 450°C. The effects of titanium loading, silver loading, preparation methods, and titanium precursor on sulfur adsorption capacity are also presented.

III.1. Introduction

Sulfur and its derivatives are major contaminants in hydrocarbon fuels. Desulfurization of fuels has gained importance due to environmental concerns, and many countries are enacting laws limiting maximum sulfur emissions. For example, the maximum sulfur concentration in highway diesel in the US has been limited to 15 ppmw since 2006, down from 500 ppmw [6-8]. Other transportation fuels are also being regulated to reduce sulfur content. Desulfurization also has a significant impact on the successful application of fuel cell technologies. Transportation fuels such as gasoline, diesel, and jet fuel are ideal for on-board fuel cell systems because of their high energy density, availability, and operational safety factors. However, the development of fuel cell systems is restricted due to the demand of ultra low sulfur feeds in their reformation systems [11]. Sulfur poisons precious metal electrodes in fuel cells and reforming catalysts, therefore only fuels with less than 100 ppbw sulfur content are allowable in fuel cell systems such as Proton Exchange Membrane (PEM) fuel cells [6, 12]. High temperature Solid Oxide Fuel Cells (SOFC) typically require less than 30 ppm S in the feed prior to reforming [13].

Most of the organosulfur compounds are generally removed from hydrocarbon fuels by conventional Hydrodesulfurization (HDS) process in refineries. It is a catalytic process requiring high temperature (300–400°C) and pressure (3–6 MPa) in the presence of

hydrogen [6]. In the recent years, refineries are facing higher amounts of sulfurous crude oil as feedstock due to the diminishing crude oil reserves and producing larger volume of products from high sulfur heavy oil fractions. This, along with the demand for ultra clean fuel, are increasing the desulfurization cost [15]. Especially for achieving the sulfur concentration tolerable to fuel cells, the HDS process has to increase its reactor volume and H_2 consumption [9, 20]. HDS also has less satisfactory performance in removing Poly Aromatic Sulfur Heterocycles (PASH) [17]. Hence, it is necessary to develop an alternative or supplementary process to HDS for deep desulfurizing fuel. Among several alternative processes reported earlier [6, 9, 25-31], desulfurization by direct adsorption of organosulfur species at ambient conditions has gained much attention [20, 45-50, 102]. Adsorptive desulfurization provides great applicability and has several advantages such as its selectivity toward PASH, scalability, and the ability to desulfurize hydrocarbon fuels to near zero sulfur content. It also does not require hydrogen or any other auxiliary units. Adsorptive desulfurization can supplement HDS process as a polishing step and offers an alternative solution to the high cost of producing ultra clean fuels.

The adsorption lab at the Auburn University Center for Microfibrous Materials Manufacturing (CM3) has developed a silver based adsorbent for the desulfurization of high sulfur refined fuels at room temperatures [69, 70]. It is one of the few adsorbents reported in the literature that can reduce sulfur down to ppmw level in “oxidized” form without requiring any sulfidation or activation. After characterizing the adsorbent via X-ray Photoelectron Spectroscopy (XPS) and Electron Spin Resonance (ESR), silver (I) oxide was observed to be the active phase for sulfur adsorption [71]. Metal oxide supports, especially TiO_2, had significant contribution to the overall sulfur adsorption

capacity in addition to the silver active sites [72]. The “active sites” on the supports were believed to be the surface acid sites that were generated during calcination in air at higher temperatures [73-75]. Titanium oxide has shown to be a better support for silver than other common metal oxide supports not only for the presence but also for the concentration of surface acid sites. The active sites on titania also causes better metal dispersion than other surfaces [70]. In spite of these features, TiO_2 is not available in high surface area as compared to most other commercial metal oxide supports for which the overall sulfur adsorption capacity is low. In addition, the silver loading on titania is confined to only 4 wt% above which causes particle agglomeration and reduction in silver oxide fraction thereby lowering sulfur adsorption capacity [70]. Assessing these problems, we tried to increase active titanium oxide surface area.

One possible way of increasing titanium oxide surface area is to disperse it onto high surface area supports such as SiO_2, Al_2O_3, activated carbon, zeolites etc. Mixed metal oxide supports containing titanium oxide have been widely reported in the literature [74-80]. Titanium oxide modified supports have higher concentration of coordinative unsaturated sites [79]. The addition of titanium oxide on alumina resulted in greater number and strength of surface acid sites [74, 81]. Silver has been successfully applied on these mixed oxide supports for other applications such as dehydrogenation of methanol [86]. If high surface area supports are decorated with titanium oxide functional groups, it may increase the active area for sulfur adsorption. Increase in overall surface area may also facilitate in loading of higher amount of oxidized silver. All these changes may result in higher sulfur adsorption capacity.

The previous works conducted at CM3-adsorption lab were focused primarily on desulfurizing high sulfur jet fuels (JP5 and JP8). It is known that the sulfur compositions in hydrocarbon fuels vary widely with respect to their volatility cuts. The sulfur concentration and the type of sulfur compounds present would obviously affect the adsorbent capacity and selectivity. Therefore it is necessary to study the effect of various types of organosulfur compounds on sulfur adsorption.

The objective of this work was to study the performance of silver adsorbents supported on titanium oxide dispersed mixed oxides for desulfurizing challenge fuels comprised of various sulfur compounds. TiO_2–Al_2O_3 and TiO_2–SiO_2 mixed oxide supports were prepared and silver was supported on these materials. The adsorbents were tested in desulfurizing JP5, JP8, Off-Road Diesel (ORD) and Ultra Low Sulfur Diesel (ULSD). The effects of titanium and silver loading were also investigated by means of desulfurization experiments. The mixed oxides were prepared via two different methods (incipient wetness and co-precipitation) and were compared. The effect of titanium precursor was studied by testing TiO_2–Al_2O_3 supports prepared by three different titanium precursors. Nitrogen physisorption was carried out to measure the BET surface area and pore volume. Breakthrough characteristics of the adsorbent for JP5, JP8, ORD, and ULSD challenge fuels were examined to assess the selectivity of the adsorbent toward different sulfur compounds present in refined fuels. The reasons behind varying selectivity were also discussed. Multi-cycle capability of Ag/TiO_2–Al_2O_3 was tested by regenerating saturated adsorbent in air at elevated temperatures. The surface topography of the adsorbent after regeneration was studied using Scanning Electron Microscopy (SEM).

III.2. Experimental

The preparation of $Ag/TiO_2–Al_2O_3$ and $Ag/TiO_2–SiO_2$ adsorbents has been mentioned in section II.1. The Ti:Al and Ti:Si weight ratio were constant all throughout this chapter (1:4.4 and 1:3.9, respectively), however Ag loading was varied from 4–12 wt%. The challenge fuels used have been discussed in section II.2. However, the model fuel used in the fixed bed continuous adsorption experiments (breakthrough experiments) was prepared by mixing 3500 (±25) ppmw benzothiophene (BT) with n-octane. The fuel was employed in the experiments to compare the adsorbents with different metal loadings.

For the desulfurization experiments, both static saturation tests and dynamic breakthrough tests were carried out in order to assess the sulfur adsorption capacities of the adsorbents. In the saturation experiments, JP5 and ULSD were used as the primary fuels. The fuel to adsorbent ratio was 20 ml of fuel per g of adsorbent for JP5 and 10 ml of fuel per g of adsorbent for ULSD. The experimental procedures and the capacity calculation methods are described in section II.3.1. The breakthrough experiments were conducted using JP5, JP8, ORD, ULSD, and model fuel. The experimental details of breakthrough tests, regeneration, and analysis can be found in section II.3.2 and section II.3. The bed weight, diameter, and volume were 10 g, 1.6 cm, and 15–16 cm^3, respectively. The analytical techniques used in adsorbent characterization have been described in section II.5.

III.3. Results and discussion

III.3.1. Adsorbent formulation

III.3.1.1. Support comparison and characterization

The equilibrium saturation capacities of the commercial and the mixed oxide supports were evaluated through saturation experiments at room temperature and atmospheric pressure. Figure III.1 and Table III.1 illustrate the comparison between the capacities of the supports that indicate considerable increase in sulfur adsorption capacities in the case of mixed oxide supports. TiO_2–Al_2O_3 support had higher capacity than individual anatase-TiO_2 or γ-Al_2O_3 supports. For TiO_2–SiO_2 support, the contribution of titanium oxide on sulfur adsorption capacity was higher. Table III.1 shows the saturation capacities of the supports per unit area basis. Among the individual supports materials, titania had the highest saturation capacity per unit surface area but had the lowest overall surface area. The TiO_2–Al_2O_3 support had moderate capacity per unit area, but the overall saturation capacity was higher. It is important to note that instead of Y-zeolites; silica and alumina supports were used to reduce diffusion limitations during operations at ambient conditions.

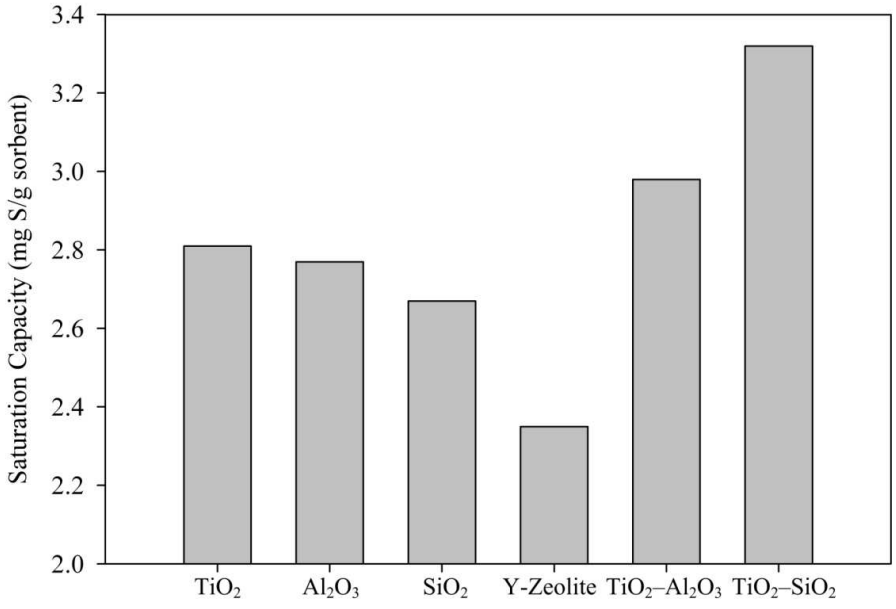

Figure III.1. Equilibrium saturation capacities of different metal oxide supports acquired from saturation tests with JP5 (1172 ppmw S) for 48 h (Fuel to adsorbent ratio: 20 ml/g)

Table III.1 Surface properties and equilibrium saturation capacities (per unit area basis) of different metal oxide supports acquired from N_2 physisorption tests and 48 h saturation experiments with JP5 (1172 ppmw S)

Supports	BET Surface Area (m^2/g)	Pore volume (cc/g)	Capacity (mg S/g adsorbent)	Capacity (μg S/ m^2 surface area)
TiO_2	154	0.41	2.81	18.25
Al_2O_3	267	1.12	2.77	10.37
SiO_2	319	1.06	2.67	8.37
Y-Zeolite	660	0.83	2.35	3.56
TiO_2–Al_2O_3 (Ti:Al = 1:4.4)	237	0.75	3.32	14.01
TiO_2–SiO_2 (Ti:Si = 1:3.9)	304	0.80	2.98	9.80

Nitrogen physisorption tests reveal that there were significant changes in BET surface areas of the mixed oxide supports (Table III.1). TiO_2–Al_2O_3 and TiO_2–SiO_2 supports had 54% and 97% more surface areas than TiO_2. The TiO_2–Al_2O_3 support had better desulfurization performance than TiO_2–SiO_2. Apparently there was better interaction between TiO_2 and Al_2O_3 than that between TiO_2 and SiO_2. Comparing the saturation capacities and BET surface areas of TiO_2–Al_2O_3 and Al_2O_3 supports, there was an increase of 3.64 μg S/m^2 surface area in sulfur adsorption capacity for TiO_2–Al_2O_3 support. To ascertain the extent of titanium oxide dispersion, the supports were examined

via x-ray diffraction (XRD) where the graph of TiO_2–Al_2O_3 sample showed no titanium/anatase-TiO_2/rutile-TiO_2/brookite-TiO_2 peaks apart from the γ-alumina peaks (not shown here). This is common for mixed oxide supports, as observed by other researchers [74]. A similar scenario was also observed in the case of TiO_2–SiO_2 support. The probable explanations for this absence are either the titanium oxide particle size (anatase/rutile/brookite) is too small to be detected by XRD or titanium oxide is in some amorphous and disordered phase. Either way, it was evident that titanium phase was nanodispersed onto the supports. The measurement of titanium oxide active surface area in the mixed oxide supports and the study concerning interactions between titanium oxide and support materials are currently being pursued.

Mixed oxide supported silver adsorbents were tested in equilibrium saturation and breakthrough tests and were analyzed via N_2 physisorption. Silver loadings were 4% by weight for each sample. The promotional effect of Ag addition was higher on mixed oxide supports than on individual supports. Table III.2 shows the BET surface areas, pore volumes, and equilibrium saturation capacities of silver supported adsorbents from N_2 physisorption tests. The capacities were calculated from 48 h saturation experiments using a JP5 challenge (fuel to adsorbent ratio: 20 ml/g). The capacities of these two adsorbents were increased by 217% and 147%, respectively after Ag addition. Compared to the saturation capacity of 4% Ag/TiO_2, capacities of both the adsorbents were higher [70]. Figure III.2 exhibits the breakthrough performances of Ag/TiO_2–Al_2O_3 and Ag/TiO_2–SiO_2 and their comparison with Ag/TiO_2 and Ag/Al_2O_3 in fixed bed adsorption tests with JP5 as challenge fuels. The capacities at breakthrough (10 ppmw threshold limit) and at saturation of 4% Ag/TiO_2–Al_2O_3 were 0.90 and 10.11 mg S/g adsorbent,

respectively. The capacities were high when compared to 4% Ag/TiO_2 (0.79 and 5.65 mg S/g adsorbent). The 4% Ag/TiO_2–SiO_2 adsorbent had poor breakthrough capacity (0.67 mg S/g adsorbent), but had a decent saturation capacity (7.73 mg S/g adsorbent). So, Ag/TiO_2–Al_2O_3 and Ag/TiO_2–SiO_2 adsorbents had better desulfurization performances than Ag/TiO_2 and Ag/Al_2O_3 for JP5 challenge. The extent of silver (I) oxide present on these supports and the effect of surface acidity are currently under investigation.

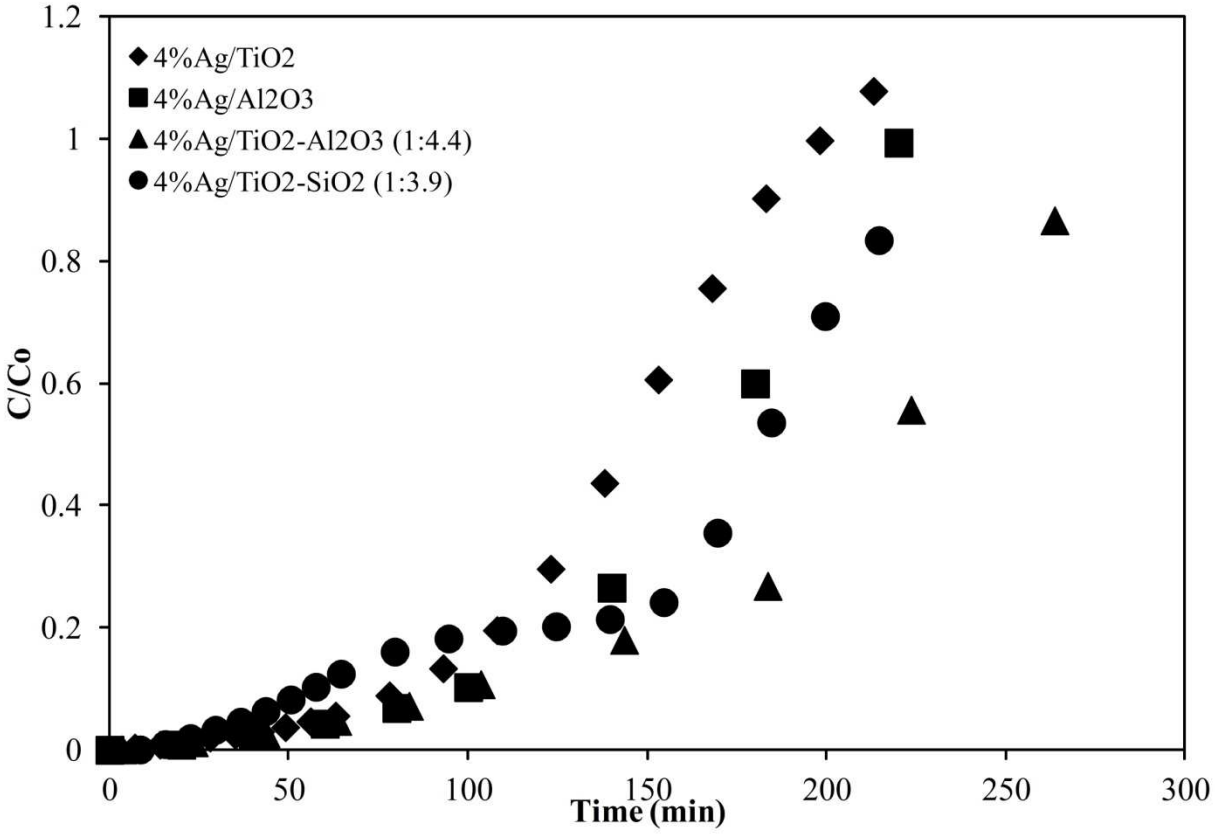

Figure III.2. Breakthrough performances of Ag loaded on titanium oxide dispersed supports and their comparisons with Ag loaded on individual supports (Bed wt.: 10g, WHSV: ~2.5h^{-1}, fuel: JP5-1172 ppmw S)

Table III.2 Surface properties and equilibrium saturation capacities (per unit area basis) of different metal oxide supports acquired from N_2 physisorption tests and 48 h saturation experiments with JP5 (1172 ppmw S)

Adsorbents	BET surface area (m^2/g)	Pore volume (ml/g)	Capacity (mg S/g adsorbent)	Capacity (μg S/ m^2 surface area)
4% $Ag/TiO_2–Al_2O_3$ (Ti:Al=1:4.4)	222	0.61	10.55	47.52
4% $Ag/TiO_2–SiO_2$ (Ti:Si = 1:3.9)	263	0.66	7.36	27.98

III.3.1.2. Effect of support precursor

Precursors play a significant role in achieving desired phases of active centers for catalytic reactions and adsorption. Titanium oxide phases vary extensively for the types of precursor used and the preparation techniques. For sulfur adsorption from liquid fuels, the anatase form of titania experimentally appeared to perform better than rutile form. Hence, for preparation of titania dispersed supports, efforts were made to optimize the type of titanium precursors to achieve highest amount of anatase phase on the surface. For titanium, three types of precursors are commonly used: titanium isopropoxide, titanium (IV) chloride, and titanyl oxide sulfate [73, 80, 88-90]. There are also various methods of preparing mixed oxide supports, such as incipient wetness [79, 87], sol-gel method [76, 78], atomic layer deposition [77, 84] etc. However, in our case, incipient wetness method was purposefully employed because this method is simple and causes more presence of TiO_2 on the support surface than the bulk phase [89]. Silver (4% by weight) impregnated on these supports were tested in breakthrough tests for desulfurizing

JP5 (Figure III.3). Ag/TiO_2–Al_2O_3 adsorbent prepared by titanium isopropoxide had higher capacities at breakthrough (0.90 mg S/g adsorbent at 10 ppmw threshold limit) and at saturation (10.11 mg S/g adsorbent) than the other two (0, 5.89 mg S/g adsorbent for titanyl oxide sulfate and 0.38, 7.92 mg S/g adsorbent for titanium chloride, respectively). This corresponds to the higher concentration of dispersed titanium oxide phase on the surface [74]. Besides precursor effect, the effect of impregnation sequence of Ag and Ti precursors was also tested, i.e. Ag was impregnated onto alumina support prior to Ti impregnation. The adsorbent had poor performance in sulfur adsorption.

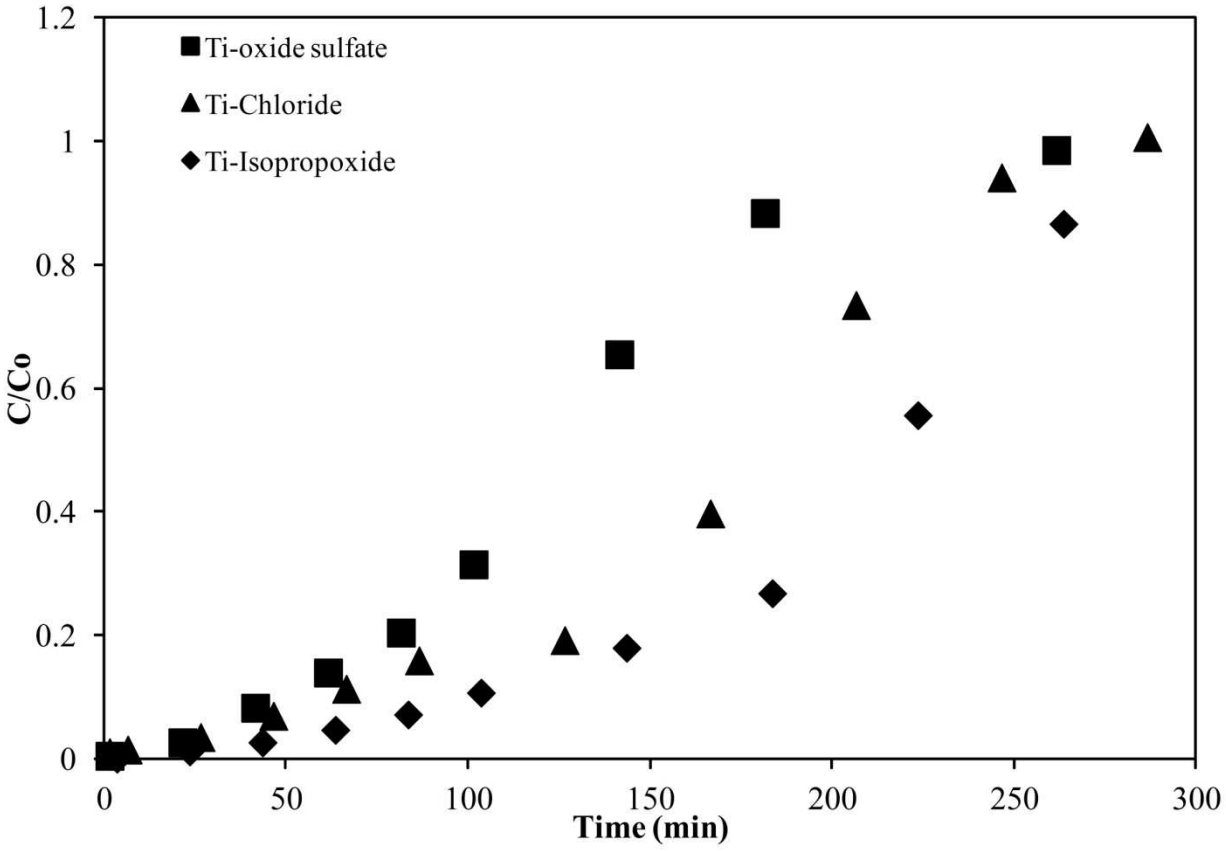

Figure III.3. Breakthrough performance comparison of 4% Ag supported on TiO_2–Al_2O_3 prepared from different titanium precursors (Bed wt.: 10g, WHSV: ~2.5h^{-1}, fuel: JP5-1172 ppmw S)

III.3.1.3. Effect of titanium loading

The effect of titanium loading was also tested for sulfur adsorption. Figure III.4 illustrates the breakthrough characteristics of model fuel (3500 ppmw BT in n-octane) by adsorbent with different titanium loadings. The Ti:Al ratio by weight for the three samples during support preparation were 1:9.7, 1:4.4, and 1:2.6, that corresponds to 5%, 10%, and 15% Ti loading by weight on alumina support at the time of impregnation, respectively. The silver loading for these adsorbents was 12% by weight. The $Ag/TiO_2–Al_2O_3$ (Ti:Al = 1:4.4) adsorbent had the optimized loading of titanium oxide for sulfur adsorption, for which the capacities at breakthrough and at saturation were 10.67 and 12.23 mg S/g adsorbent, respectively. Higher Ti loading caused pore blockage and reduced surface area that offset the increase in titanium oxide concentration.

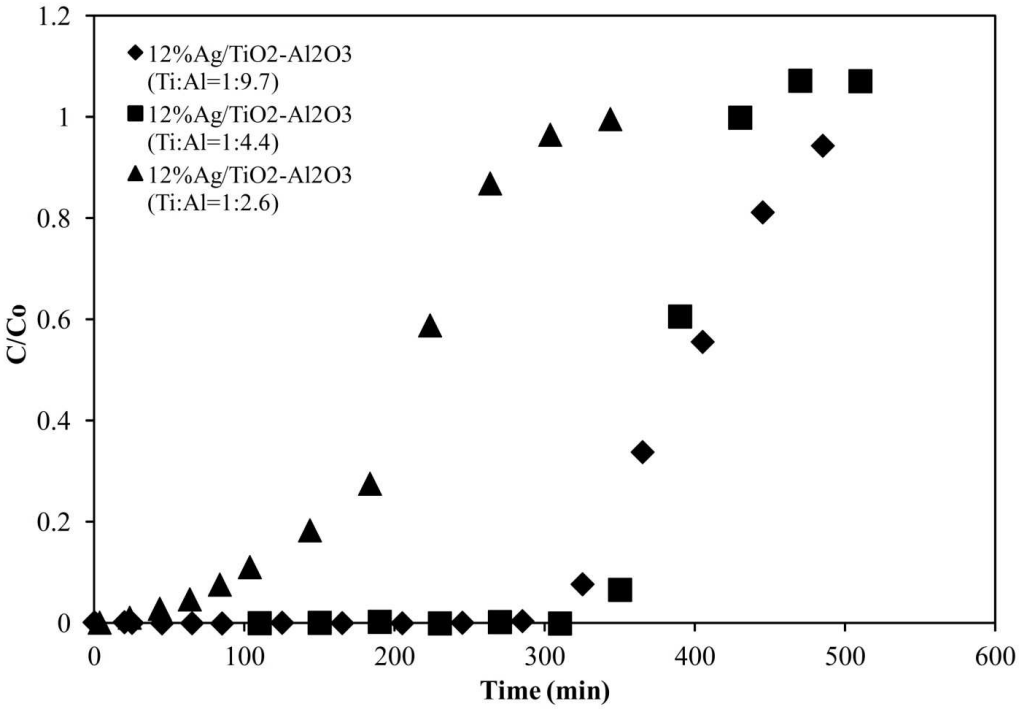

Figure III.4. Breakthrough performance comparison of 12% Ag on $TiO_2–Al_2O_3$ supports with varied Ti loadings (Bed wt.: 10g, WHSV: ~$2.5h^{-1}$, fuel: model fuel - 3500 ppmw S)

III.3.1.4. Effect of support preparation

The mixed oxide supports prepared via different methods can function differently, as described in section I.4.2. The effect was studied here. The TiO_2–Al_2O_3 and TiO_2–SiO_2 mixed oxides were prepared via incipient wetness impregnation and co-precipitation (CP) methods and were compared by means of saturation and breakthrough experiments. For this, JP5 was used as the challenge fuels. Figure III.5 shows the saturation capacity comparison between the resulting mixed oxides adsorbents. For most of the adsorbents, the mixed oxides prepared by incipient wetness method had higher saturation capacities than the ones prepared by co-precipitation methods. For silver supported mixed oxides, the increase in saturation capacities was more significant. This was true for both Ag/TiO_2–Al_2O_3 and Ag/TiO_2–SiO_2. Figure III.6 demonstrates the breakthrough curves of Ag supported on TiO_2–Al_2O_3 supports prepared via incipient wetness (IW) and co-precipitation (CP) methods. The Ag loading was 4 and 12 wt%. In both Ag loadings, incipient wetness was observed to be the preferred method for mixed oxide preparation. This illustrated the beneficial effect of titanium oxides on sulfur adsorption. In the mixed oxides prepared by incipient wetness method, more titanium oxide was on the support surface. This provided more concentrated sulfur adsorption sites. As a result, the sulfur adsorption capacity was increased. Titanium oxide also increases Ag dispersion, therefore the silver impregnation on TiO_2–Al_2O_3 (prepared via IW method) resulted in significant increase in capacity.

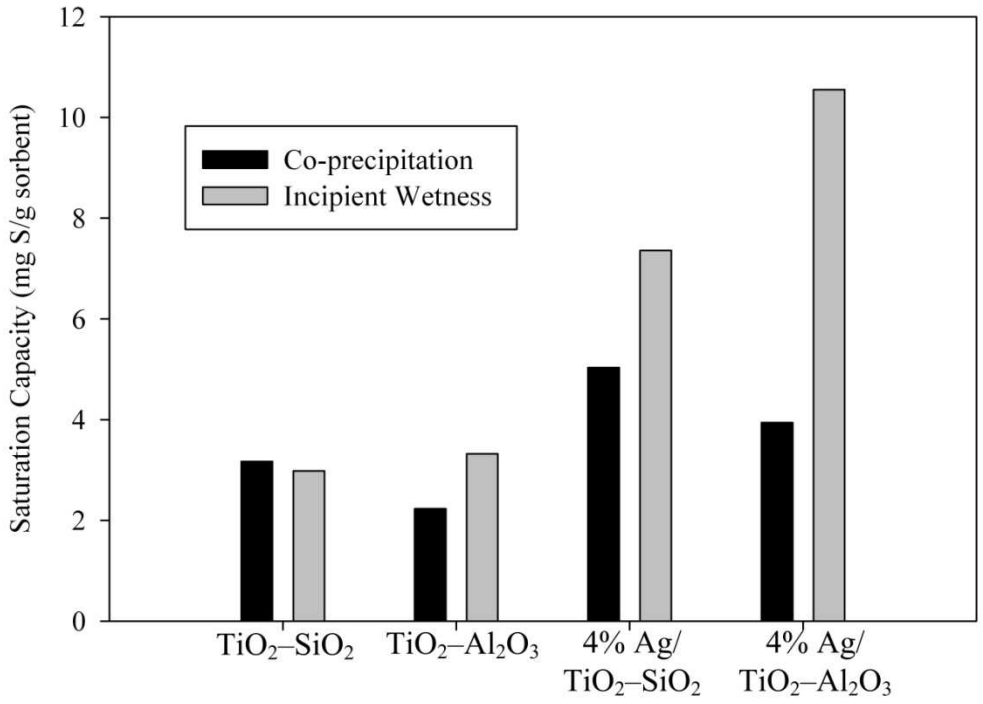

Figure III.5. Equilibrium saturation capacities of neat and silver supported mixed oxides prepared by incipient wetness and co-precipitation methods. The capacities were acquired from saturation tests with JP5 (1172 ppmw S) for 48 h (Fuel to adsorbent ratio: 20 ml/g)

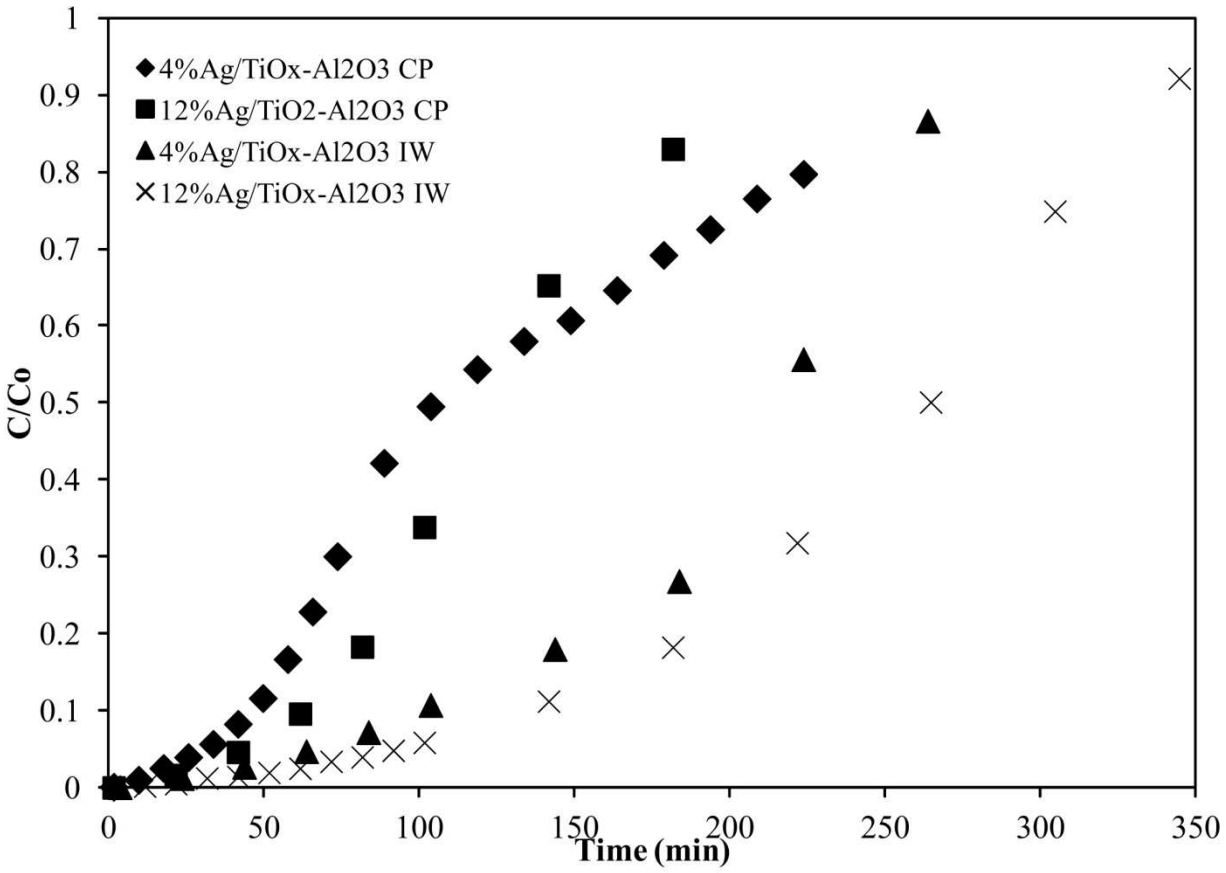

Figure III.6. Breakthrough performances of Ag supported on TiO_2–Al_2O_3 supports prepared via incipient wetness (IW) and co-precipitation (CP) methods (Bed wt.: 10g, WHSV: ~2.5h^{-1}, fuel: JP5-1172 ppmw S)

III.3.1.5. Effect of silver loading

One of the objectives of this work was to facilitate higher silver loading in active form by increasing titanium oxide surface area. The effect of silver loading was studied on TiO_2–Al_2O_3 support to test this. Figure III.7 illustrates the breakthrough of sulfur in JP5 (1172 ppmw sulfur) using TiO_2–Al_2O_3 (Ti:Al = 1:4.4 by weight) impregnated with 4, 8, 12, and 16% Ag by weight. Up to 12 wt% Ag loading on TiO_2–Al_2O_3 was beneficial to sulfur adsorption, with breakthrough (at 10 ppmw threshold) and saturation capacities of 1.51 and 12.73 mg S/g adsorbent, respectively. This was up from 4 wt% for Ag on TiO_2

support implying the effect of higher surface area. Previous studies conducted at CM3 reported development of pore clogging with increased Ag loading (more than 4 wt% Ag) on TiO_2 support [70]. In this work, similar phenomenon was observed where the atomic utilization of silver was lower at higher loadings. The obstruction of sulfur active sites by large Ag particles was greater in 16% Ag loaded adsorbent to affect the sulfur adsorption capacity. In this case, agglomeration of Ag led to the formation of large particles and lower Ag dispersion. The large Ag particles blocked the pores, thereby decreasing sulfur adsorption capacity, similar to Ag/TiO_2 adsorbents [70]. From these observations, the optimized Ag loading on TiO_2–Al_2O_3 mixed oxide supports were estimated to be ca. 10% by weight.

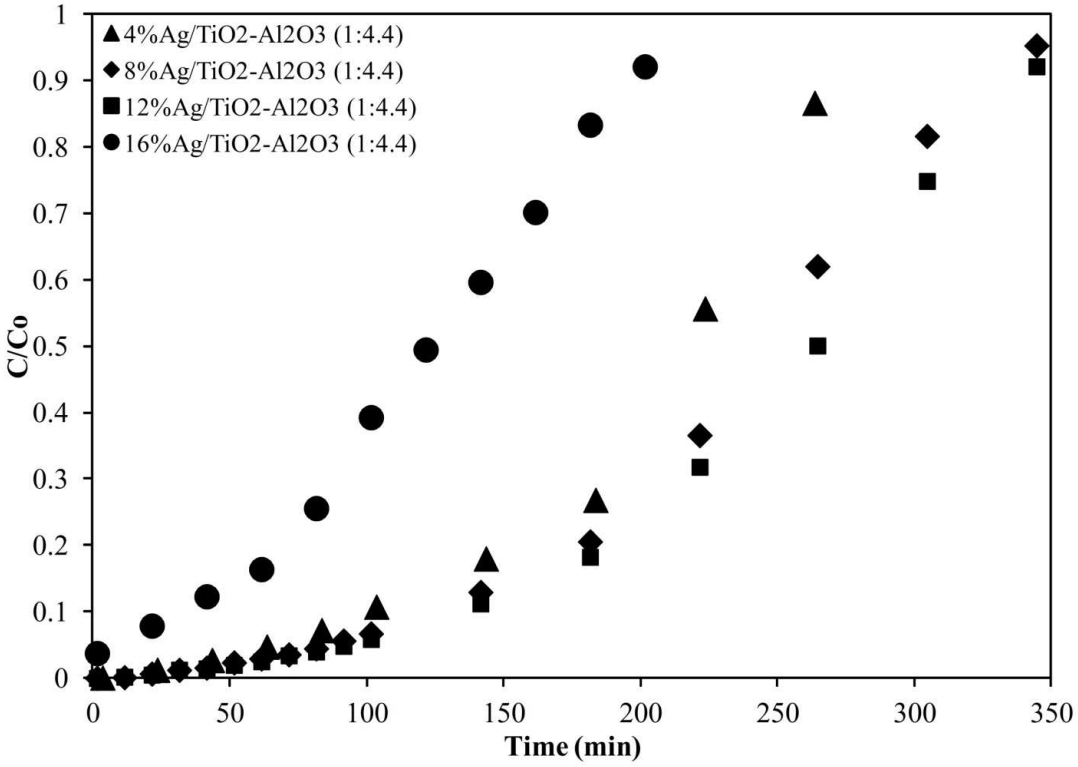

Figure III.7. Breakthrough performance comparison of TiO_2–Al_2O_3 adsorbents with 4, 8, 12, and 16 wt% Ag loading (Bed wt.: 10 g, WHSV: ~2.5h^{-1}, fuel: JP5-1172 ppmw S)

III.3.2. Effect of various sulfur compounds in commercial fuels

Commercial petroleum fuels have diverse mixtures of hydrocarbons considering their origin from different distillation fractions of crude oil in the refinery. Diversity in sulfur compounds is no exemption. The sulfur species can vary with respect to the number of aromatic rings and alkyl side chains attached to thiophene (T). These factors can affect the sulfur adsorption capacity. The PFPD chromatograms of Figure III.8 illustrate the sulfur peaks of JP5, JP8, ORD, and ULSD showing different sulfur species. As illustrated from the figure, JP5 and JP8 contain almost similar sulfur compound, although JP8 contains more trimethyl benzothiophenes (TMBT). JP5 and JP8 have approximately 9% and 29% of the total sulfur compounds as TMBT's, respectively. Generally diesel is generated from the heavier fractions of crude oil. As a result, it contains greater quantities of aromatic compounds and also heavier sulfur heterocycles. The chromatogram depicts that dibenzothiophene (DBT) derivatives constitute significant portion of the sulfur species in ORD, majority of which were DBT and 4-methyl dibenzothiophene (4-MDBT). Other than ORD, ULSD also contains substituted DBT as sulfur heterocycles, among which 4,6-DMDBT is the major sulfur compound. The organosulfur compounds in ULSD are the most refractory sulfur species present in petroleum fuels. Silver based adsorbents have different capacities for these thiophenic compounds as observed earlier using model fuels [72]. In addition, there are high concentrations of aromatic hydrocarbons and additives in these refined fuels that also compete for the active sites on the acid adsorbents. In case of ULSD, the concentration of non-sulfur aromatics is >25000 times higher than that of sulfur heterocycles. This overwhelming concentration of non-sulfur heterocycles may have a significant effect on sulfur adsorption. The effect can

also be observed from the difference in breakthrough capacities of the adsorbent for model fuel and JP5 (10.67 and 1.51 mg S/g adsorbent). In this case, the structure of different organosulfur compounds and the presence of different non-sulfur heterocycles adversely affected the breakthrough capacity. It is therefore necessary to gauge the influence of these factors through performance comparison between different commercial and logistic fuels.

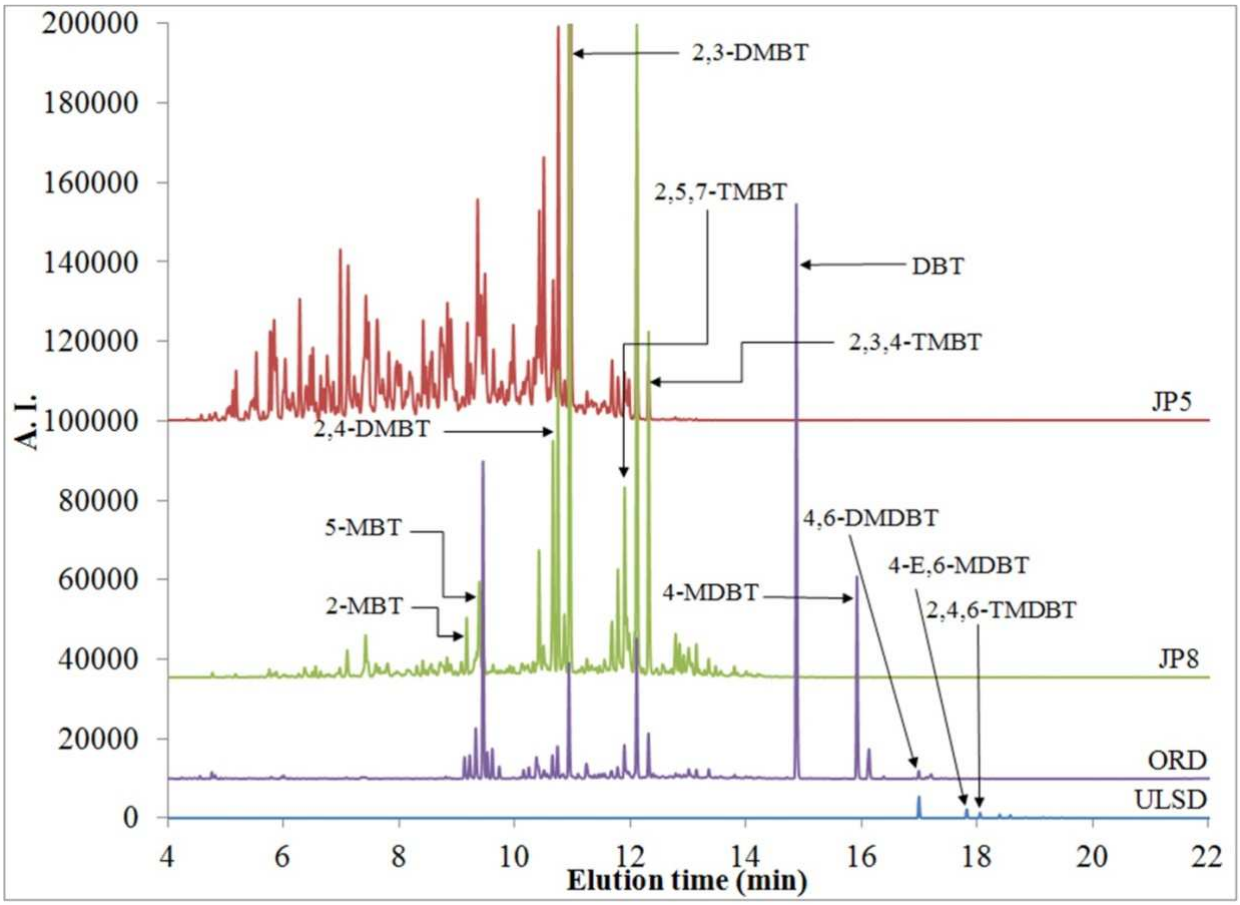

Figure III.8. GC-PFPD chromatograms of JP5 (1172 ppmw S), JP8 (630 ppmw S), ORD (452 ppmw S), and ULSD (7.5 ppmw S) exhibiting sulfur species present.

The fuels were used as challenges in breakthrough experiments using 4% $Ag/TiO_2–Al_2O_3$ (Ti:Al = 1:4.4) adsorbent. Their breakthrough characteristics and sulfur adsorption capacities are shown in Figure III.9 and Table III.3, respectively. The breakthrough

capacity (calculated at 10 ppmw threshold limit) for JP5 (1172 ppmw sulfur) was the best among the fuels. However, JP5 was the quickest to saturate the adsorbent due to its higher initial sulfur content. For JP8, the curve broke initially but had a secondary breakthrough at around 350 min and C/Co ≈ 0.55 (outlet sulfur concentration~350 ppmw S). Incoming methyl benzothiophene (MBT) was preferentially adsorbed while more sterically hindered BT (e.g. TMBT's) remained in outlet fuel. Secondary breakthrough marks the saturation of adsorbent by MBT's. In the case of ORD, the curve broke early and had a secondary breakthrough similar to JP8; though in this case at around 500 min and C/Co ≈ 0.45 (outlet sulfur concentration ~200 ppmw). Figure III.10 demonstrates the GC-PFPD chromatograms of outlet ORD samples at different times of breakthrough. Initially, sterically hindered TMBT's were the first group of sulfur species breaking through (at 60 min). DBT and 4-MDBT were the following ones as seen from the chromatogram at 300 min. However, the chromatogram of outlet ORD at 500 min (Figure III.10) shows that the adsorbent was slowly saturated with these compounds. The reason for this might be the replacement of the adsorbed aromatic compounds by DBT and its derivatives. The adsorbent continued to adsorb the entire inlet MBT's till saturation.

The sulfur adsorption capacity of 4% $Ag/TiO_2–Al_2O_3$ (Ti:Al = 1:4.4) for ULSD was significantly lower than those of the jet fuels and ORD. The possible reasons for this are the low initial sulfur concentration of ULSD and the effect of aromatic hydrocarbons and heteroatoms competing for the adsorption sites. The methyl groups in DBT derivatives e.g. 4,6-DMDBT caused steric hindrances to adsorption on the metal cations. However, the surface acid sites (hydroxyl groups) were able to adsorb the sulfur compounds. The

breakthrough curve leveled off at C/Co ≈ 0.5–0.6 and stayed in this range till 2000 min or 100 ml fuel/g adsorbent (shown in-set of Figure III.9). The adsorbent continued to adsorb till 6000 min or 300 ml fuel/g adsorbent. Plausible explanation for this might be the replacement of adsorbed aromatic hydrocarbons by incoming sulfur compounds. In the breakthrough tests, the adsorbent had the greatest affinity for BT's and the least for TMBT's and DMDBT's. The adsorbent selectivity order from the strongest to weakest adsorption was observed to be: BT>MBT>DMBT>DBT≈MDBT>TMBT≈DMDBT. Identification of the sites active for sterically hindered sulfur species and the estimation of adsorption energies are currently being pursued.

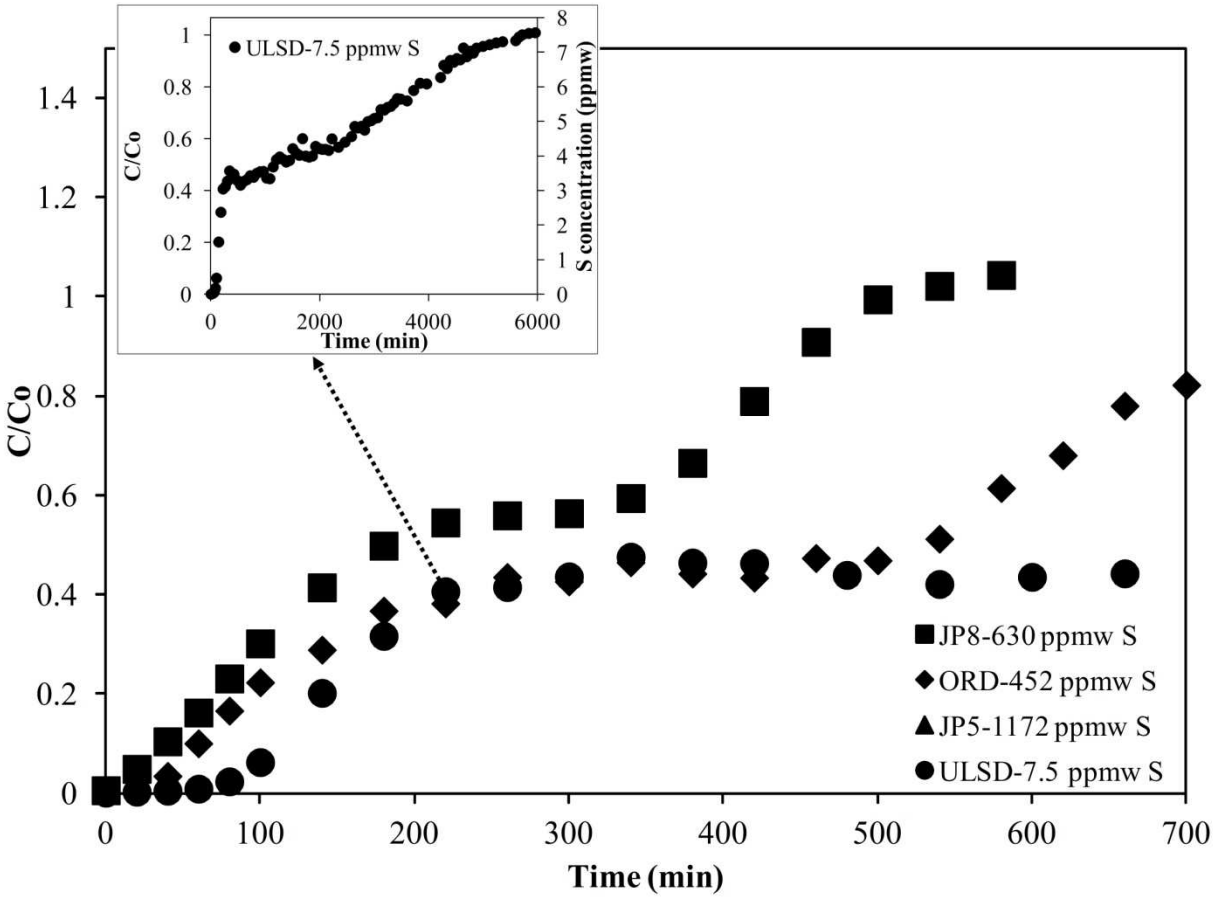

Figure III.9. Breakthrough performance comparison of 4% $Ag/TiO_2–Al_2O_3$ (Ti:Al =1:4.4) for desulfurizing JP5, JP8, ORD, and ULSD (Bed wt.: 10g, WHSV: ~2.5h^{-1}).

Inset figure: Extended breakthrough characteristics of ULSD challenge using 4% $Ag/TiO_2–Al_2O_3$ (Ti:Al =1:4.4)

Table III.3 Sulfur adsorption capacities for 4% $Ag/TiO_2–Al2O_3$ (Ti:Al = 1:4.4) adsorbent for JP5 (1172 ppmw S), JP8 (630 ppmw S), ORD (452 ppmw S), and ULSD (7.5 ppmw S)

Fuel	Breakthrough capacity at 10 ppmw threshold limit (mg S/g adsorbent)	Capacity at saturation (mg S/g adsorbent
JP5	0.9	10.11
JP8	0.12	6.11
ORD	0.64	7.40
ULSD	-*	0.59

* The initial sulfur content of ULSD was lower than 10 ppmw

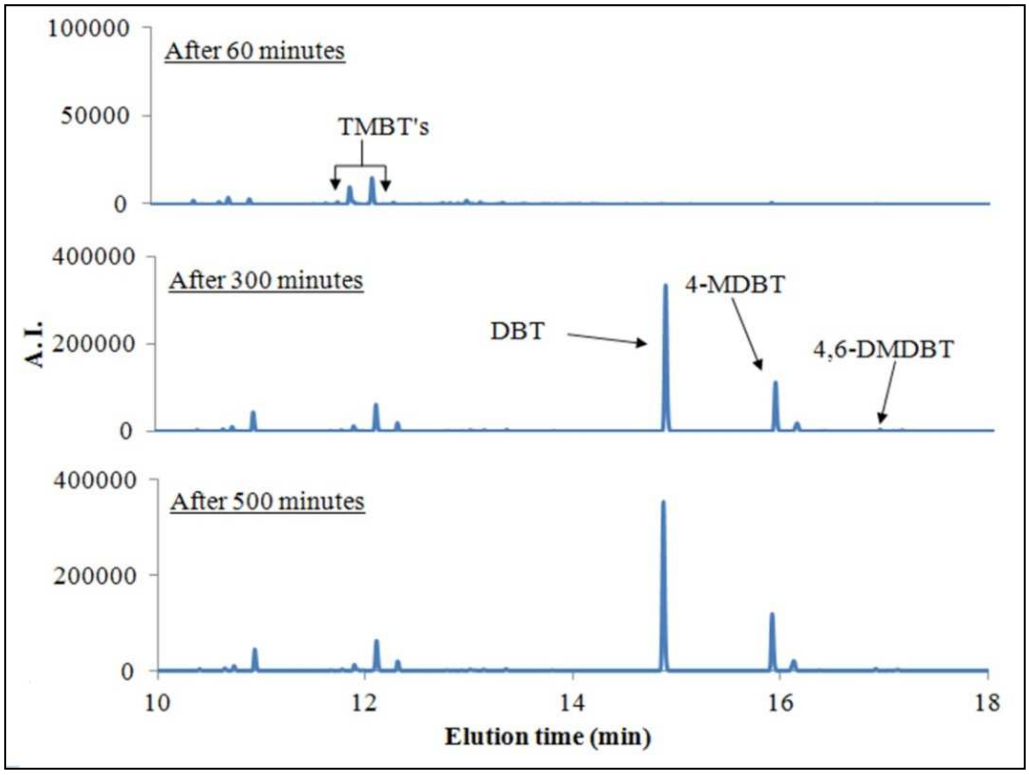

Figure III.10. GC-PFPD chromatograms of outlet ORD (452 ppmw S) sampled at 60, 300, and 500 min of breakthrough experiment with 4% $Ag/TiO_2–Al_2O_3$ (Ti:Al = 1:4.4) adsorbent; (Bed wt.: 10 g, WHSV: ~2.5 h^{-1})

Equilibrium saturation experiment using 4% $Ag/TiO_2–Al_2O_3$ (Ti:Al = 1:4.4) with a ULSD challenge was carried out where the fuel to adsorbent ratio was 10 ml/g. The GC-PFPD chromatograms in Figure III.11 show the sulfur species present in ULSD before and after saturation experiment. The sulfur species were undetectable in the fuel after saturation as shown from the chromatogram. The lower detection limit calibrated for the GC-PFPD method in splitless mode was 75 ppbw. So, the adsorbent was able to remove >99% of the sulfur species and desulfurize ULSD to almost zero sulfur content. This demonstrates the excellent selectivity of the adsorbent toward thiophenic sulfur compounds.

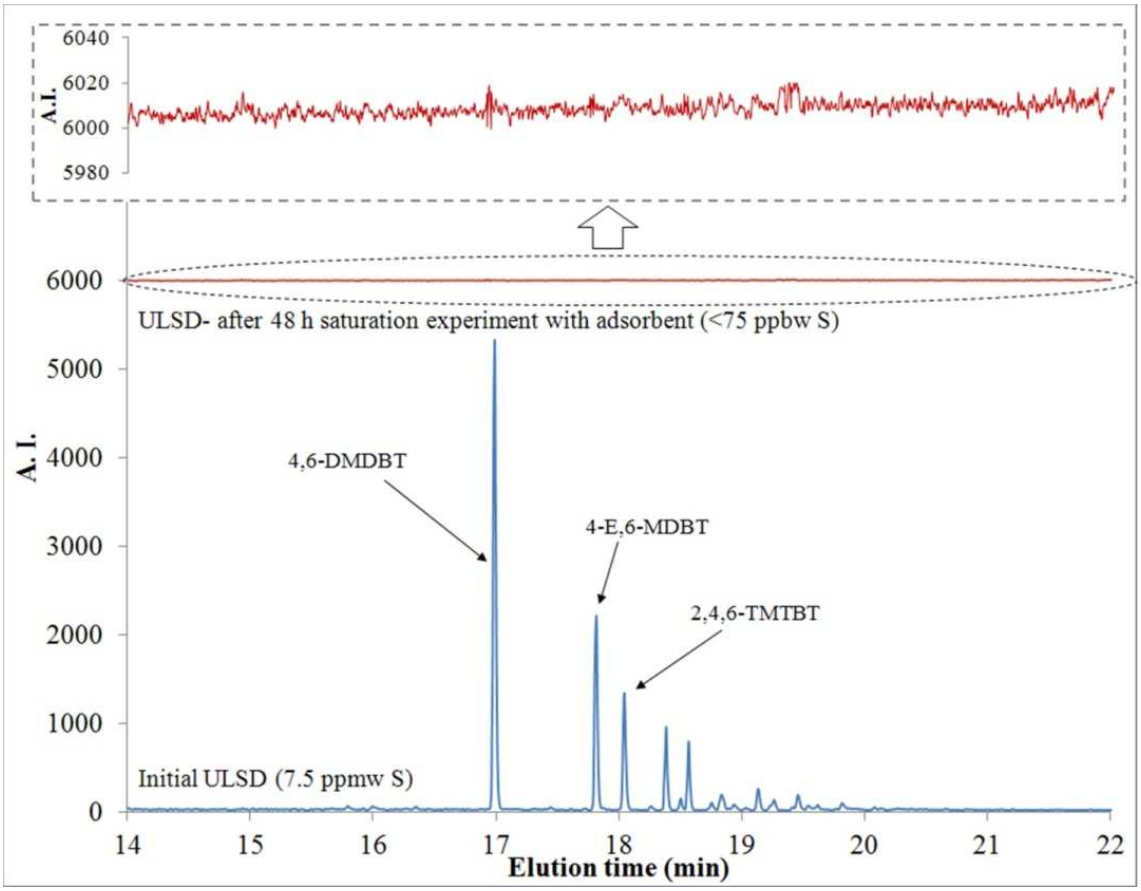

Figure III.11. GC-PFPD chromatograms of ULSD before (below) and after (above) equilibrium saturation experiment using 4% $Ag/TiO_2–Al_2O_3$ (Ti:Al = 1:4.4) adsorbent (Saturation time: 48 h, fuel to adsorbent ratio: 10 ml/g)

III.3.3. Regeneration

The regenerability of silver adsorbent supported on $TiO_2–Al_2O_3$ was tested by heating the saturated adsorbent bed in flowing air. The temperature was slowly ramped to ensure appropriate evacuation of hydrocarbons and PASH residues from the adsorbent bed. After this, the bed was cooled down and tested again in breakthrough tests. The adsorbent was taken through 5 cycles of adsorption-regeneration using JP5. Figure III.12 illustrates the breakthrough curves for fresh and regenerated 12% $Ag/TiO_2–Al_2O_3$ (Ti:Al = 1:4.4) adsorbents. The breakthrough performance was consistent for multiple cycles. To check

the surface topography of the adsorbent after regeneration, the samples were studies via SEM. Figure III.13 shows the SEM images of fresh and regenerated adsorbent after five cycles. No significant difference could be seen between the two samples, indicating stability in multi cycle heat treatment. Usually for supported metal catalysts, especially supported on γ-alumina, multiple heat treatment can cause metal sintering, thereby reducing activity. The phenomenon was not observed here, implying that titanium oxide stabilizes silver oxide phase interacting with alumina [103].

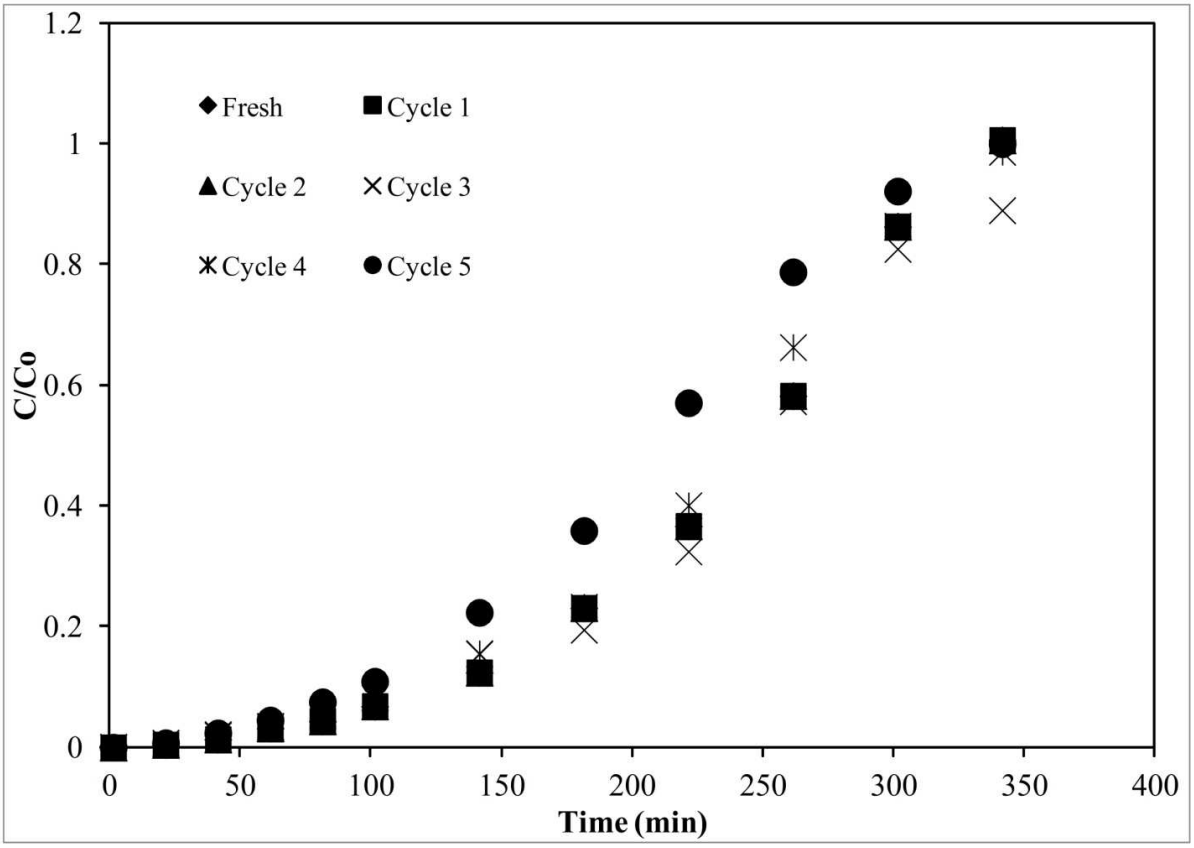

Figure III.12. Breakthrough performance comparison of fresh and regenerated 12% $Ag/TiO_2–Al_2O_3$ (Ti:Al = 1:4.4) adsorbents (Bed wt.: 10g, WHSV: ~$2.5h^{-1}$, fuel: JP5-1172 ppmw S)

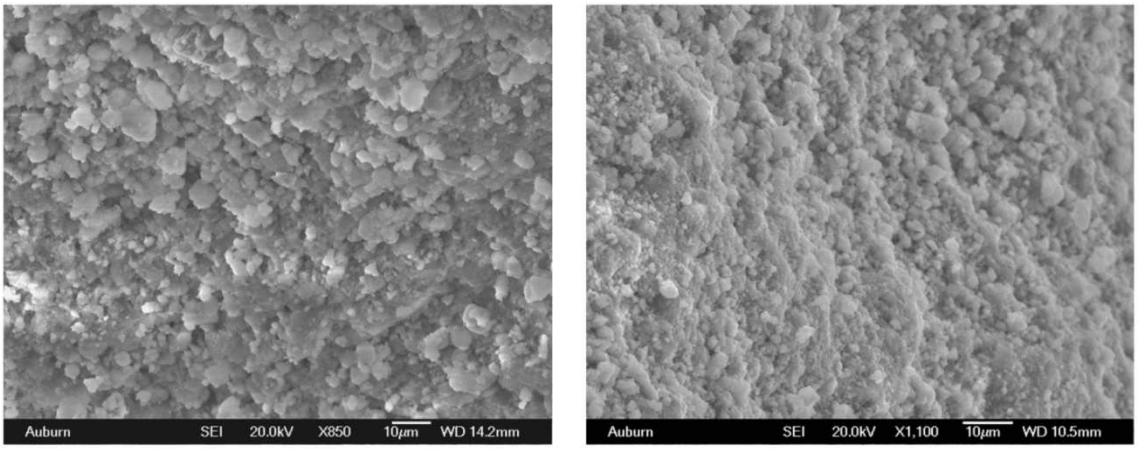

Figure III.13. SEM images of fresh and regenerated (After 5 cycles) 12% $Ag/TiO_2–Al_2O_3$ (Ti:Al = 1:4.4) adsorbent

III.4. Conclusions

Silver on $TiO_2–Al_2O_3$ and $TiO_2–SiO_2$ mixed oxide supports were observed to be effective sulfur adsorbents for both high and low sulfur containing fuels. The adsorbents enhanced the sulfur adsorption capacity (mg S/g adsorbent) and lowered the exit sulfur threshold (ppmw S). In continuous breakthrough experiments, 4% $Ag/TiO_2–Al_2O_3$ (Ti:Al = 1:4.4) demonstrated saturation capacities of 10.11, 6.11, and 7.40 mg S/g adsorbent for JP5 (1172 ppmw S), JP8 (630 ppmw S), and ORD (452 ppmw S), respectively. The adsorbent was able to desulfurize ULSD (7.5 ppmw S) down to less than 75 ppbw S in the saturation experiments. Incorporation of TiO_2 onto high surface area Al_2O_3 and SiO_2 increased the number of sulfur adsorption sites. The mixed oxide supports were also able to host more silver oxides (up to ~12 wt% Ag) as demonstrated by the increase in capacity. The 12% $Ag/TiO_2–Al_2O_3$ (Ti:Al = 1:4.4) adsorbent had a saturation capacity of 12.73 mg S/g adsorbent for a JP5 challenge in breakthrough experiments. The mixed oxides prepared by incipient wetness method were more effective in sulfur adsorption

because of greater presence of titanium oxides on the surface. Differences in desulfurization performance were observed for different fuels and attributed to variations in organosulfur species. Methyl and ethyl groups attached to thiophenic derivatives created steric hindrances to adsorption on the silver cations. After examining the breakthrough performance of 4% $Ag/TiO_2–Al_2O_3$, the order of adsorption affinity toward the sulfur species (from the strongest to weakest adsorption) was observed to be: BT>MBT>DMBT>DBT≈MDBT>TMBT≈DMDBT (based on their order of appearance at the bed outlet). The adsorbent maintained its capacity and stability after multiple cycles of adsorption-regeneration operations with JP5 challenge. Thus, silver on mixed oxide supports would provide better efficacy by enhancing the capacity and the extent of desulfurization while maintaining regenerability, scalability, and operability at ambient conditions. Future work will focus on the characterization of the adsorbents and on the mechanism for the adsorption of sulfur heterocycles at ambient conditions.

IV. Mechanism of hydrocarbon fuel desulfurization using $Ag/TiO_2–Al_2O_3$ adsorbent

Abstract

Silver supported on mixed oxides have shown promises as an advanced sulfur adsorbent with deep desulfurizing ability and scalability to be fitted into on-board fuel cell systems. However, its application into a workable technology requires thorough understanding of the sulfur adsorption mechanism. This chapter presents the characterization of $Ag/TiO_2–Al_2O_3$ (10 wt% Ag, Ti/Al = 1:4.4) adsorbent for applications in pre-reformate cleaning of Proton Exchange Membrane (PEM) fuel cells. The adsorbent demonstrated effective sulfur adsorption capacities at ambient conditions (13.06 mg S/g adsorbent for model hydrocarbon fuel containing benzothiophene). This was achieved through greater TiO_2 (<4 nm, from x-ray diffraction) and Ag dispersions (~23% for 10 wt% Ag, from O_2 chemisorption). Anatase-TiO_2 dispersion on Al_2O_3 provided increased adsorbent activity (3.27 eV band gap, from UV-vis spectroscopy), higher surface acidity (~14 cc/g NH_3 uptake at P = 800 mm Hg, from NH_3 chemisorption), and exerted in more defect sites (α-Lewis acid sites) for Ag incorporation. $TiO_2–Al_2O_3$ provided both strong and weak Brønsted sites (from infrared studies using Ammonia, 2,6-lutidine, trimethyl chlorosilane, and thiophene as probe molecules). Organosulfur adsorption on $Ag/TiO_2–Al_2O_3$ adsorbent was primarily attributed to surface hydroxyls (via hydrogen/σ bonding) and surface bound silver oxides (via π bonding).

IV.1. Introduction

Logistic and transportation fuels are ideal for producing hydrogen in portable fuel cell systems for their higher energy density, availability, and operational safety. However, the sulfur compounds in these fuels can poison fuel cell electrodes and reforming catalysts. As a result, fuels with ultra low sulfur content (<0.1 ppmw) are tolerable at the anode side of systems such as Proton Exchange Membrane (PEM) fuel cells [11, 104]. Desulfurization of transportation and logistic fuels for these applications is tricky because of their differences in sulfur concentration (15 ppmw S in ultra low sulfur diesel and 500–3000 ppmw S in jet fuels). Among several desulfurization processes [9, 37, 105-107], adsorptive desulfurization is promising in producing inexpensive ultraclean fuels for on-board fuel cell systems because of its low energy requirements and scalability. However, the challenging step for its feasible application is the development of a high capacity adsorbent formulation that can desulfurize fuel down to parts per billion (ppb) levels and can work for a variety of fuel blends. Among several adsorbent formulations studied so far [20, 102, 105, 108, 109], silver based adsorbents have shown effective desulfurization capability at ambient conditions and regenerability [70, 72]. Recently, TiO_2 has been dispersed onto high surface area Al_2O_3 and SiO_2 supports (via Ti-isopropoxide impregnation followed by calcination) in order to increase the active surface area and Ag loading. The novel $Ag/TiO_2–Al_2O_3$ and $Ag/TiO_2–SiO_2$ adsorbents have enhanced sulfur adsorption capacities for both logistic and commercial fuels [110]. In addition, the formulation can desulfurize fuels down to parts per billion by weight (ppbw) levels and render them applicable to fuel cell systems [110].

The optimized application of this formulation calls for an effort to understand the sulfur adsorption mechanisms involved. In previous works, Ag adsorbent supported on TiO_2 was characterized through electron spin resonance (ESR) and x-ray photoelectron spectroscopy (XPS), where silver (I) oxide (Ag_2O) was observed to be the active Ag phase [70, 71]. Our earlier observations also led us to the premise that both silver and titania have individual sulfur adsorption capacities [110]. Further characterization of the adsorbent is necessary to investigate the dispersed Ag and TiO_2 phases, the amount of dispersion, and the possibility of a synergistic effect among the sites.

Previously we observed a relationship between sulfur adsorption capacity and surface acidity regarding Ag/TiO_2 adsorbent [100]. The enhancement in surface acidity was similar to that in sulfur adsorption capacity in terms of calcination and metal impregnation. The adsorbent was observed to be more selective toward the aromatics with more basic or electron rich functional groups (e.g. N>S>O) [100]. In our recent work, the use of acidic TiO_2–Al_2O_3 and TiO_2–SiO_2 mixed oxides has resulted in higher sulfur adsorption capacities [110]. Mixed metal oxides can exert in higher concentration of surface acid sites than either of its components alone [74] and also facilitate active metal dispersion by creating more defect sites [111, 112]. As a result, more active silver phase might be incorporated onto these mixed oxide supports. This would in turn increase the sulfur adsorption capacity. Hence further studies on these adsorbents would determine the influence of surface acidity on adsorbent activation. The acquired knowledge regarding sulfur adsorption mechanism would further facilitate more advanced adsorbent formulation and the adsorption process optimization for implementation in fuel cell systems. This study would also help to tailor the adsorbent formulation and the

adsorption process according to different fuel blends (e.g. high sulfur jet fuels or low sulfur diesels).

In this study, we studied the desulfurization mechanism of $Ag/TiO_2–Al_2O_3$ adsorbent for applications in PEM fuel cell power systems. Desulfurization experiments were carried out to gauge the contributions of Ag and TiO_2 phases. X-ray Diffraction (XRD), Raman spectroscopy, UV-vis. Diffuse Reflectance Spectroscopy (UV-DRS), and O_2 chemisorption were employed to identify the active phases and to study the effects of Ag and TiO_2 dispersions. The adsorbent acidity was measured via NH_3 adsorption, while Infrared (IR) spectroscopy was employed to identify the surface acid sites on the neat and Ag supported $TiO_2–Al_2O_3$. The postulated sulfur adsorption mechanisms are discussed.

IV.2. Experimental

The adsorbent preparation steps have been mentioned in section II.1. The Ti:Al and Ti:Si weight ratio were constant all throughout this chapter (1:4.4 and 1:3.9, respectively), however Ag loading was 10 wt%. During final calcination, air was used as the calcination gas unless specified otherwise. The model fuel used in the equilibrium saturation experiments was prepared by mixing 3500 (±25) ppmw S as benzothiophene (BT) with n-octane.

For the desulfurization experiments, static saturation tests and fixed bed continuous adsorption (breakthrough) experiments were carried out with model fuel. Comprehensive treatises on the saturation tests and the capacity calculation methods are described in section II.3.1.The fuel to adsorbent ratio was 20 ml of fuel per g of adsorbent. The experimental details of breakthrough tests and analysis can be found in section II.3.2 and section II.3. The bed weight, diameter, volume, and overall aspect ratio (bed length:bed

diameter) were 10 g, 1 cm, 15–16 cm^3, and 22, respectively. The analytical techniques used in adsorbent characterization have been described in section II.5. Experimental details on the ammonia chemisorption and IR spectroscopy can be found in section II.6 and II.7. For the IR analysis in this work, anhydrous ammonia (source: Airgas), 2,6-lutidine, trimethyl chlorosilane (TMCS), and thiophene (T) (source: Alfa Aesar) were used as probe molecules. The pretreatment, probe molecule treatment, and IR analysis steps were performed *in situ.*

IV.3. Results

IV.3.1. Effect of TiO_2 and Ag dispersion on sulfur adsorption capacity

Saturation experiments were conducted using model fuel to compare the sulfur adsorption capacities. Figure IV.1 shows the saturation capacities of anatase TiO_2, TiO_2–Al_2O_3, and Ag/TiO_2–Al_2O_3. TiO_2–Al_2O_3 showed 89% higher capacity than TiO_2 and silver incorporation further increased the sulfur capacity by 91% as compared to TiO_2–Al_2O_3. Titania dispersion resulted in smaller crystals and more edges and corners, consequently increasing the active sites for sulfur adsorption. The resulting TiO_2–Al_2O_3 provided sites for higher Ag loading, as observed previously [110]. Assuming the difference in capacities of TiO_2–Al_2O_3 and Ag/TiO_2–Al_2O_3 came from silver sites only, the ratio of adsorbed sulfur molecules to the amount of Ag molecules were 0.21:1. Therefore, around 21% of the Ag atoms (in the form of silver oxides) were active in sulfur adsorption. This is also practically significant since we are decreasing the amount of more expensive materials (Ag and TiO_2) by diluting them, and are increasing the sulfur adsorption capacity as well. This is to be noted here that we used model fuels to rule out competitive adsorption issues. The differences in sorption behavior for different

organosulfur compounds and the effect of non sulfur aromatics were investigated previously [110].

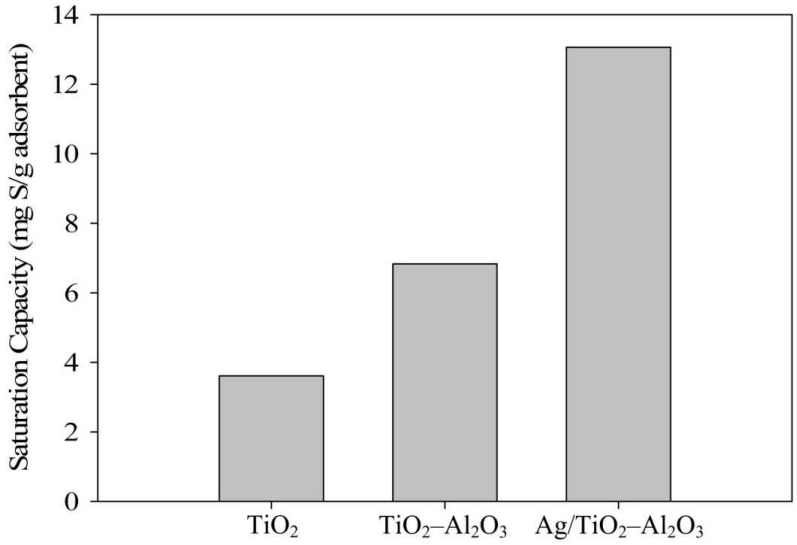

Figure IV.1. Sulfur adsorption capacities estimated from saturation experiments (fuel: model fuel-3500 ppmw S as BT + C8, fuel to adsorbent ratio: 20 ml/g, saturation time: 48 h)

IV.3.2. TiO_2 phase determination

Figure IV.2 (left) shows the XRD graphs of TiO_2–Al_2O_3, TiO_2–SiO_2, and individual oxides for reference. The TiO_2–Al_2O_3 sample diffractogram showed only γ–Al_2O_3 peaks while the TiO_2–SiO_2 sample diffractogram did not show any peak. The absence of any titanium/anatase-TiO_2/rutile-TiO_2/brookite-TiO_2 peaks implied that either the supported titanium oxide was present in an amorphous and disordered phase or the TiO_2 (rutile/anatase/brookite) particles were too small to be detected by XRD. Figure IV.2 (right) shows the XRD signatures of Ag/TiO_2–Al_2O_3 along with Ag and Ag_2O for references. The absence of any peak representing Ag phase (i.e. Ag, Ag_2O, or AgO)

indicated that Ag phase was below the detection limit of XRD. In both cases, titanium and silver phases were adequately dispersed (as nanoparticles) on the supports.

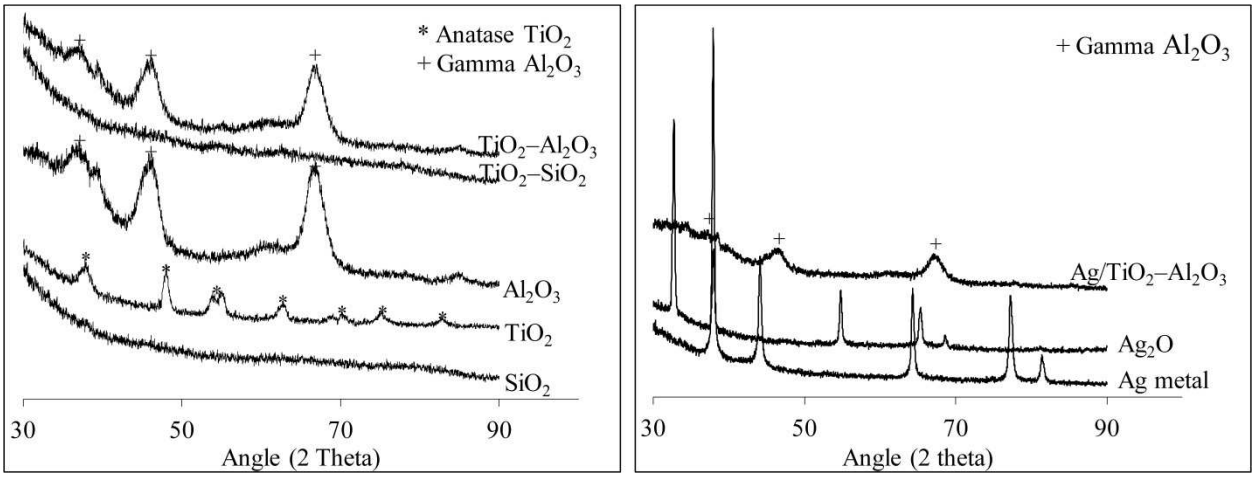

Figure IV.2. Left: XRD patterns of TiO_2–Al_2O_3 (Ti/Al = 1:4.4), TiO_2–SiO_2 (Ti/Si = 1:3.9) mixed oxides and TiO_2, Al_2O_3, SiO_2 supports for reference. Right: XRD patterns of 10 wt% Ag/TiO_2–Al_2O_3 (Ti/Al = 1:4.4) adsorbent and Ag_2O, Ag powders for reference

To determine the TiO_2 phase on TiO_2–Al_2O_3 and Ag/TiO_2–Al_2O_3, Raman spectroscopy was employed. Raman spectroscopy has shown higher sensitivity for metal oxides, as reported previously [73]. It is extremely sensitive to the formation of crystalline anatase and rutile phases of TiO_2 [113]. Figure IV.3 illustrates the Raman spectra of neat and Ag supported TiO_2–Al_2O_3 at 100–1000 cm^{-1} ranges. The anatase-TiO_2 and γ-Al_2O_3 spectra are also shown for reference. The TiO_2–Al_2O_3 spectrum showed bands at 141.5 (E_g), 196 (E_g), 395 (B_{1g}), 515 (B_{1g}/A_{1g}), and 636 cm^{-1} (E_g), which were indicative of anatase-TiO_2 [114-116]. This pointed out that the prominent phase of TiO_2 in TiO_2–Al_2O_3 was in anatase form [73, 79, 115]. No band representing rutile phase was observed in the spectrum [114]. In addition, no band representing –C–H or –C–C vibrations was observed at higher (1000–3000 cm^{-1}, not shown here for brevity) wavenumbers [117].

Therefore, there was no presence of titanium precursors, ensuring complete decomposition to titania during calcination. The $Ag/TiO_2–Al_2O_3$ sample spectrum showed similar bands, although in this case the bands were shifted. The shifting might have occurred because of the change in anatase symmetry (Ti–O–Ti) and might have resulted from silver addition [115]. In the case of gamma-alumina samples, no significant band was seen. Therefore, the titanium oxide in $TiO_2–Al_2O_3$ and $Ag/TiO_2–Al_2O_3$ were present in anatase phase.

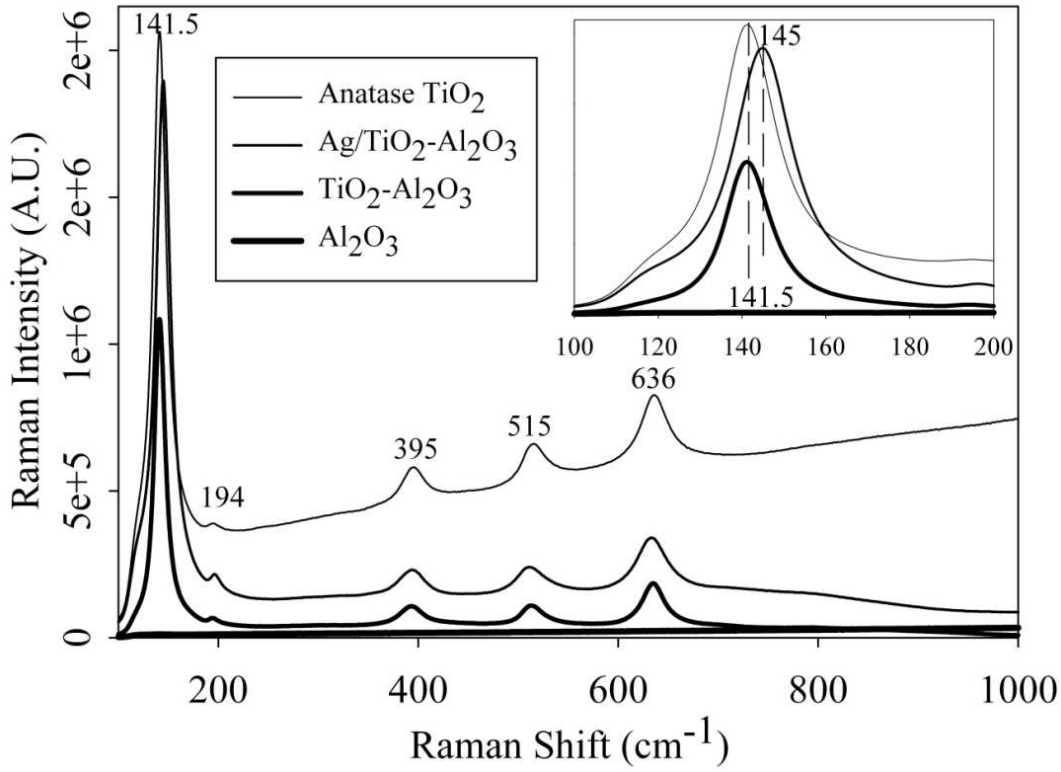

Figure IV.3. Raman spectra of $TiO_2–Al_2O_3$ (Ti/Al = 1:4.4), 10 wt% $Ag/TiO_2–Al_2O_3$ (Ti/Al = 1:4.4), anatase TiO_2, and γ-Al_2O_3

IV.3.3. Effect of $Ag–TiO_2$ dispersion

The electronic spectra of neat and silver-supported mixed oxides along with TiO_2 (as reference) are shown in Figure IV.4. Background spectra were subtracted from all sample

spectra ($BaSO_4$ for TiO_2, Al_2O_3 for TiO_2–Al_2O_3 and Ag/TiO_2–Al_2O_3). The adsorption edge of TiO_2–Al_2O_3 was higher than that of TiO_2. The adsorption edge of Ag/TiO_2–Al_2O_3 was the highest and showed adsorption edge in the visible region. The in-set table in Figure IV.4 exhibits the band gap calculated from UV-DRS absorption data. The band gap of dispersed TiO_2 was much lower than that of anatase-TiO_2, indicating higher activity resulting from dispersion. Silver incorporation further lowered the band gap. The presence of Ag^+ can shift TiO_2 absorption edge toward visible range by creating oxygen vacancies and enabling charge transfer between Ag^+ and TiO_2 [98]. The visible light activation and band gap reduction can enable the material to transfer electrons more easily, therefore it can facilitate the subsequent bonding with organosulfur species upon adsorption [98].

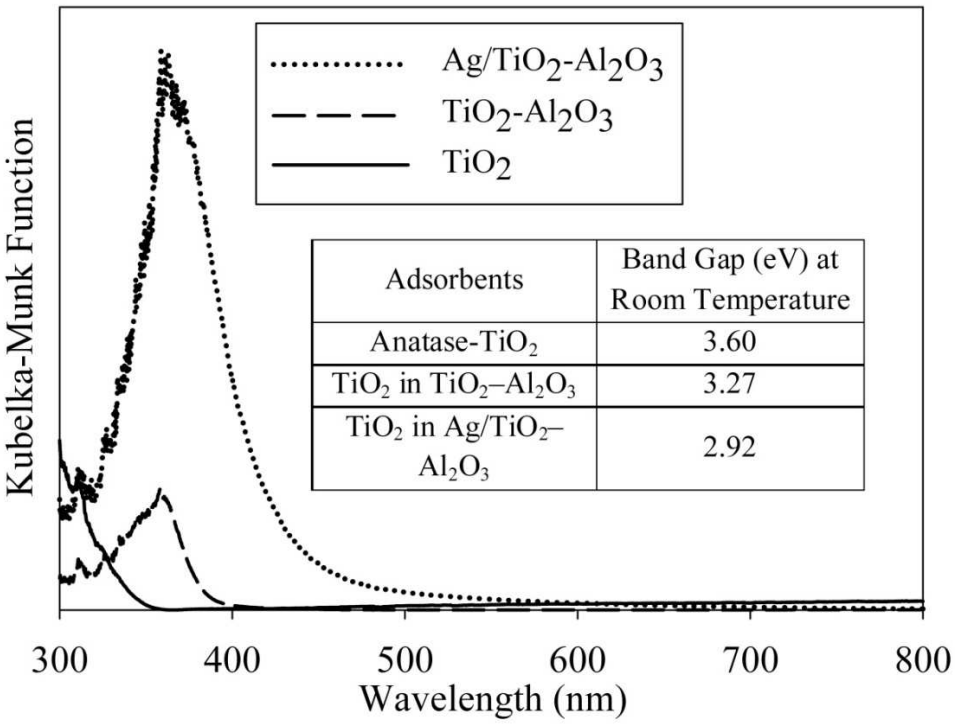

Adsorbents	Band Gap (eV) at Room Temperature
Anatase-TiO_2	3.60
TiO_2 in TiO_2–Al_2O_3	3.27
TiO_2 in Ag/TiO_2–Al_2O_3	2.92

Figure IV.4. UV-vis diffuse reflectance spectra (Kubelka-Munk function versus wavelength) of TiO_2–Al_2O_3 (Ti/Al = 1:4.4), 10 wt% Ag/TiO_2–Al_2O_3 (Ti/Al = 1:4.4), and

anatase TiO_2. In-set table: Band gap calculated from UV-vis diffuse reflectance spectroscopy [37]

IV.3.4. Silver phase determination- Influence of treatment environment

The effect of calcination gases on desulfurization performance was studied to determine the active silver phase. $Ag/TiO_2–Al_2O_3$ after $AgNO_3$ impregnation was calcined in different gases: air, nitrogen, and hydrogen. The gases represented oxidizing, neutral (partial reducing), and reducing environments, respectively. The calcination temperature was kept at 450^0C for each case. After calcination, the cooling process was carried out in the respective gas environment (*in situ*). After each cooling process, the adsorbent bed was charged with model fuel without exposing it to ambient air. Figure IV.5 shows the breakthrough performances of these adsorbent samples. Table IV.1 presents the adsorbent capacities at breakthrough and at saturation. The oxidized adsorbent demonstrated the highest capacity, reiterating that the adsorbent was active in an oxidized form. Most of the sulfur adsorbents reported in literature are active in reduced forms [20, 45, 47, 68]. This unique feature makes the desulfurization and regeneration processes much simpler and cheaper since no expensive gases are required.

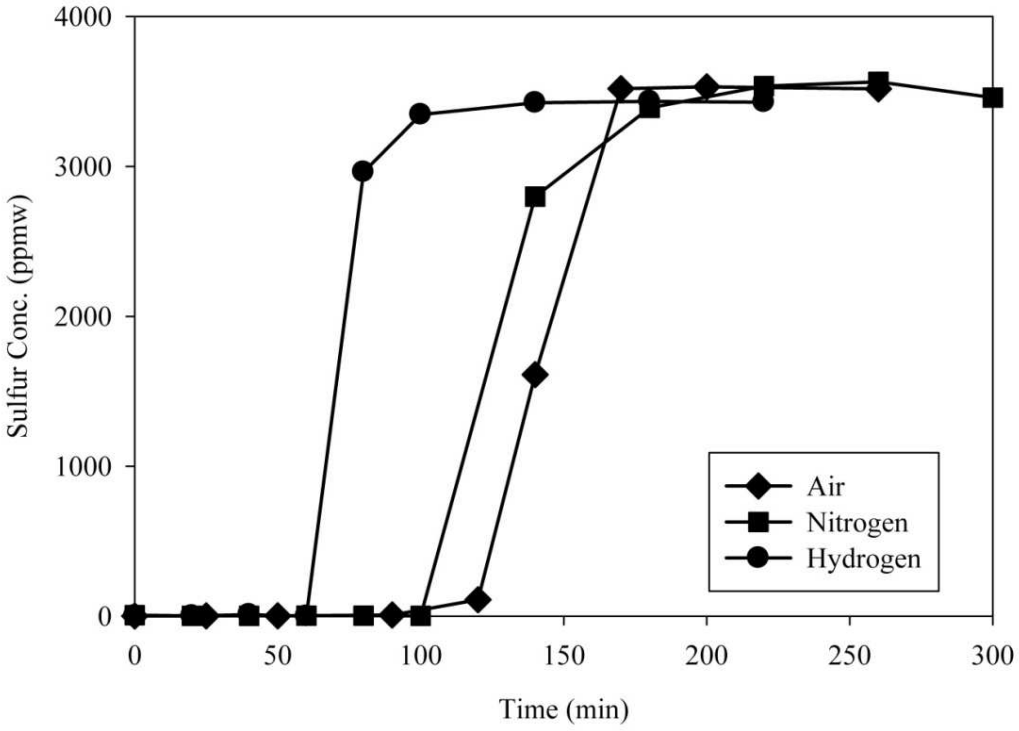

Figure IV.5. Breakthrough performance comparison 10 wt% $Ag/TiO_2–Al_2O_3$ (Ti/Al = 1:4.4) adsorbents calcined in air, nitrogen, and hydrogen for desulfurizing model fuel (3500 ppmw S as benzothiophene + n-octane)

Table IV.1 Sulfur adsorption capacities estimated from breakthrough experiments using model fuels

Adsorbents	Calcination Gas	Breakthrough Time (min)	Breakthrough Capacity at 10 ppmw (mg S/g)	Capacity at Saturation (mg S/g adsorbent)
$Ag/TiO_2–Al_2O_3$	Air	116	14.37	17.63
	Nitrogen	100	12.39	15.98
	Hydrogen	60	7.43	9.46

IV.3.5. Effect of Ag dispersion on TiO_2–Al_2O_3

The Ag dispersion on different supports was estimated via oxygen chemisorption studies [92, 93]. Table IV.2 presents the Ag surface areas and Ag dispersions of Ag/TiO_2, Ag/Al_2O_3, and Ag/TiO_2–Al_2O_3 (10 wt% Ag loading in each sample). The O_2 uptake of blank TiO_2–Al_2O_3 is also shown. The value, however minor, represents the error range of estimated values (3–5%). This O_2 uptake might have also indicated the sub-stoichiometry in TiO_2.The highest silver surface area was observed in the mixed oxide, which was 55% and 65% higher than those in TiO_2 and Al_2O_3. Therefore, TiO_2 increased the silver incorporation sites when dispersed on Al_2O_3. The TiO_2–Al_2O_3 support was able to create more defect sites; thereby increasing silver dispersion and eventually enhancing sulfur adsorption capacity. This finding was in agreement with our previous work where higher Ag loading (up to 12 wt% Ag) on TiO_2–Al_2O_3 brought about beneficial effect to sulfur adsorption, as compared to that on TiO_2 (only 4 wt% Ag) [110]. The Ag dispersion on Ag/TiO_2–Al_2O_3 was measured to be 22.89%. Compared with the sulfur adsorption capacity of Ag (0.21 mol S/mol Ag, see section 3.1), approximately 92% of the exposed Ag participated in sulfur adsorption.

Table IV.2 Silver surface areas and dispersions measured from oxygen chemisorption (temperature: 170°C)

Samples	Monolayer Uptake (μmol/g)	Silver Surface Area (m^2/g)	Dispersion (%)
TiO_2–Al_2O_3	6.2	-	-
10 wt% Ag/TiO_2	137.2	7.19	14.80
10 wt% Ag/Al_2O_3	128.7	6.74	13.89
10 wt% Ag/TiO_2–Al_2O_3	212.1	11.11	22.89

IV.3.6. Measurement of surface acidity in mixed oxide supported silver adsorbents

IV.3.6.1. NH_3 adsorption

The acid site concentrations of individual and mixed metal oxide supports have been measured via NH_3 adsorption. It is an effective method to quantitatively measure surface acid site concentrations [78]. In this work, we used NH_3 as the probe molecule since it can interact with both Lewis and Brønsted sites. NH_3 is a strong base and can be adsorbed on both strong and weak Lewis sites. Strong Brønsted sites can also protonate NH_3 molecules to form NH_4^+. Figure IV.6 illustrates the NH_3 uptakes (both strong and weak) of individual and mixed oxides at 800 mmHg. Before adsorption, all samples have been activated at 400 °C, as stated in the experimental section. The NH_3 uptakes of TiO_2–Al_2O_3 (strong) and of TiO_2–SiO_2 (weak) were the highest, followed by those of Al_2O_3, TiO_2, and SiO_2. The higher surface acidity of TiO_2–Al_2O_3 implied the synergistic effect of mixed oxides. Titania dispersion on SiO_2 also increased its surface acidity as compared to SiO_2 alone. Hence, titania dispersion resulted in surface acidity enhancement.

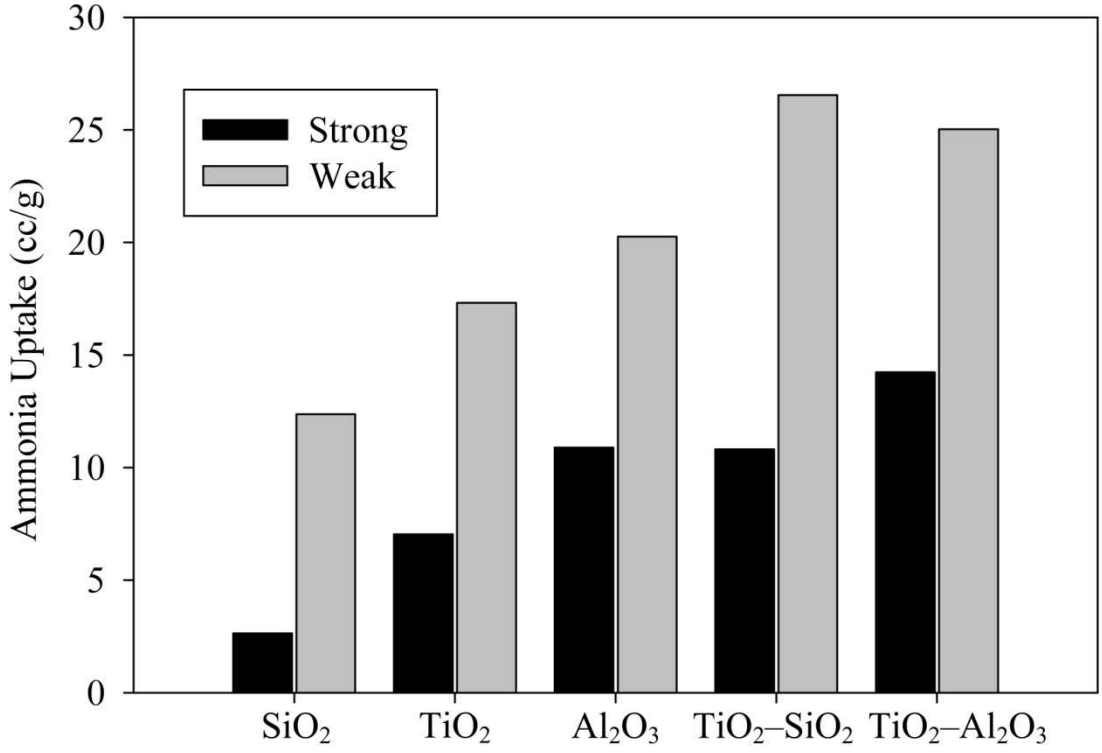

Figure IV.6. Ammonia uptake of anatase SiO_2, TiO_2, γ-Al_2O_3, TiO2–SiO_2 (Ti/Si = 1.3.9), and TiO_2–Al_2O_3 (Ti/Al = 1:4.4) at 800 mmHg measured from adsorption experiments (temperature: 175 °C)

IV.3.6.2. IR spectroscopy using probe molecules

IR spectroscopy using probe molecules is a well established method for qualitative measurement of surface acidity [81, 118]. The IR spectra of samples before and after treatment with probe molecules are shown in Figure IV.7–10. Table IV.3 represents the corresponding assignments. All the bands represented chemisorbed species since the cell was evacuated prior to analysis. Figure IV.7 shows the spectra of calcined and pretreated TiO_2–Al_2O_3 and Ag/TiO_2–Al_2O_3 samples. The –OH stretching vibrations was seen at 3500–3750 cm^{-1} in the spectra [119, 120]. After Ag incorporation, the overall intensity of

–OH decreased slightly, implying that some of the hydroxyls were replaced after Ag impregnation [121]. However, an additional –OH stretching band (3727 cm^{-1}) was observed in the $Ag/TiO_2–Al_2O_3$ sample spectrum. The formation of these –OH groups might have been closely related to Ag impregnation. The bands at these region (3720–3740 cm^{-1}) have been reported to be the –OH groups at corners and edges [122]. Therefore these –OH groups were single surface hydroxyls.

Ammonia: In the IR study, NH_3 was used as a probe molecule to detect strong Brønsted and Lewis acidity [78]. Figure IV.7 shows the IR spectra of NH_3 treated samples. In the treated sample spectra, bands representing some of the hydroxyl groups (3650–3750 cm^{-1}) were low in intensities as compared to those in the untreated spectra. The 3727 cm^{-1} band in $Ag/TiO_2–Al_2O_3$ + NH_3 sample spectrum was also absent, indicating the interaction of NH_3 with these sites. Broad bands were observed at 3200–3450 cm^{-1} in the $TiO_2–Al_2O_3$ + NH_3 spectrum and at 3100–3450 cm^{-1} in the $Ag/TiO_2–Al_2O_3$ + NH_3 spectrum. These bands have been assigned to a combination of N–H stretching vibrations of adsorbed NH_3 molecules [123] and the NH_4^+ vibrations resulting from interactions with hydroxyl groups [124]. Hence significant amount of Lewis sites and active hydroxyl groups were present on the adsorbents samples. However, only the single surface hydroxyl groups participated whereas the bridged ones (3400–3600 cm^{-1}) appeared to be inaccessible to NH_3 treatment.

At the 1200–1800 cm^{-1} wavenumbers, both treated spectra showed a strong band centered at 1620 cm^{-1}. The band has been assigned to a combination of the $\delta(NH_3)_{as}$ deformations of adsorbed ammonia molecules [123] and possibly of adsorbed NH_2 [122]. The 1620 cm^{-1} band was broader in the $TiO_2–Al_2O_3$ + NH_3 spectrum. This might have resulted from

adsorbed water [120]. Water might have been produced from the reaction between NH_3 and –OH groups ($NH_3 + OH \rightarrow NH_2 + H_2O$). This phenomenon was observed only in the TiO_2–Al_2O_3 sample. Broad shoulders at ca. 1248 and 1200 cm^{-1} in the NH_3 treated TiO_2–Al_2O_3 sample spectrum were observed. In the treated Ag/TiO_2–Al_2O_3 sample spectrum, the band was shifted to ca. 1180 cm^{-1}. These three bands denoted $\delta(NH_3)_s$ vibrations of coordinatively bound ammonia on Lewis sites [125, 126]. The presence of two different bands in TiO_2–Al_2O_3 sample spectrum indicated the presence of two different Lewis sites [125]. During silver impregnation, one of these Lewis sites (defect mediated sites) might had been blocked, exposing the Brønsted sites [125]. Therefore, only one major band representing coordinated NH_3 molecules (1180 cm^{-1}) was observed in the Ag/TiO_2–$Al_2O_3 + NH_3$ spectrum. The NH_3 treated TiO_2–Al_2O_3 sample spectrum had a broad band centered at 1460 cm^{-1}, which has been assigned to the asymmetric deformation vibrations of NH_4^+ on surface Brønsted sites [124, 125]. The band was absent in Ag/TiO_2–$Al_2O_3 + NH_3$ sample spectrum, indicating that Ag ions replaced the –OH groups (representing this band in TiO_2–Al_2O_3) during silver impregnation stage.

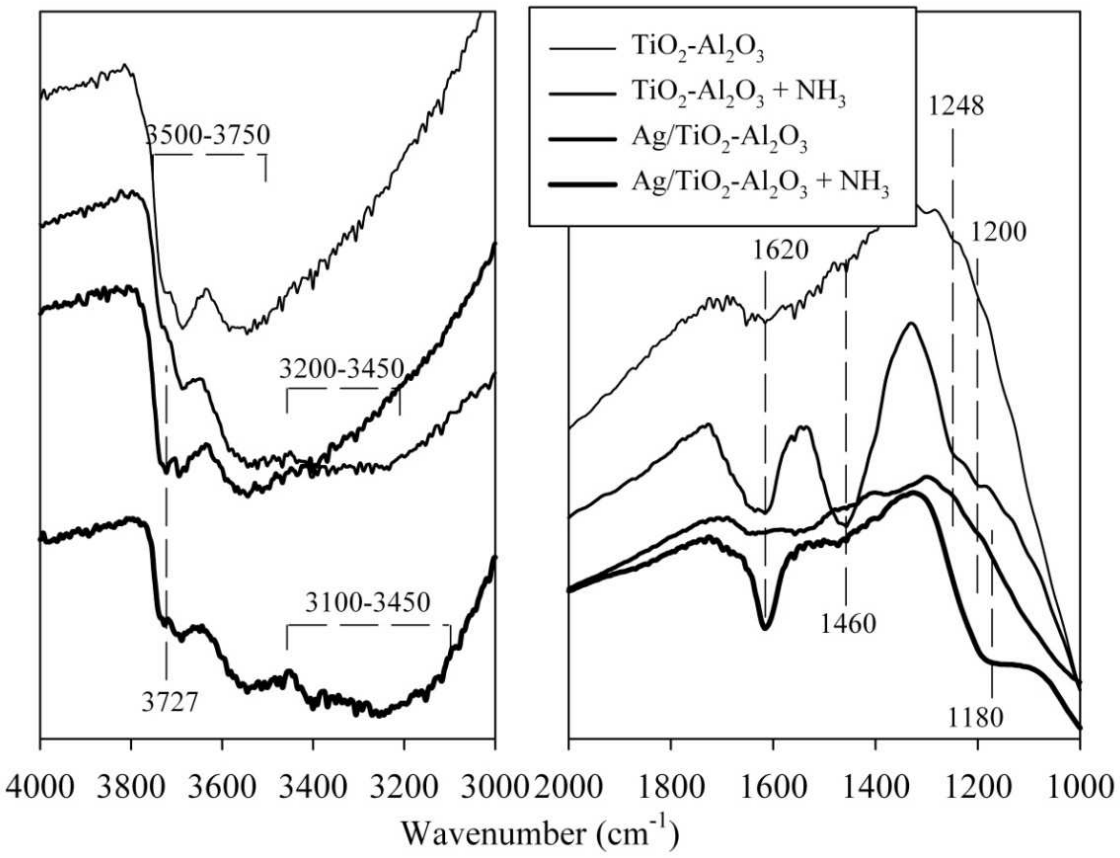

Figure IV.7. *In situ* IR spectra (in transmission mode; Y-axis in transmittance-A.U.) of calcined and pretreated TiO_2–Al_2O_3 (Ti/Al = 1:4.4) and 10 wt% Ag/TiO_2–Al_2O_3 (Ti/Al = 1:4.4) adsorbent samples before and after treatment with ammonia

2,6-lutidine: Figure IV.8 exhibits the spectra of 2,6-lutidine treated samples. 2,6-lutidine has been used to detect weak Brønsted acidity [127]. The sterically hindered amine is preferentially adsorbed on proton acid sites even in presence of strong Lewis sites and thus can act as a good titrant for the Brønsted sites [128]. Both treated sample spectra showed several bands (Figure IV.8). The common υ_{8b} and υ_{8a} vibrations of ligated lutidine molecules was seen at 1575 and 1613 cm^{-1}, respectively [129]. However, these bands were very strong and broad, that might have hidden additional bands in between. Another strong and broad band centered at 1461 cm^{-1} was observed in both treated

spectra. These bands represented Lewis sites on the adsorbent surface. A small band was observed at 1540 cm^{-1} in the $Ag/TiO_2–Al_2O_3$ + 2,6-lutidine sample spectrum. This band has been assigned to the vibrations of lutidine molecules adsorbed on Brønsted sites [129, 130]. This indicated the presence of weak Brønsted sites on $Ag/TiO_2–Al_2O_3$. The $TiO_2–Al_2O_3$ + 2,6-lutidine sample spectrum showed the bands representing protonated species at 1626 and 1640 cm^{-1} [127]. These bands represented the strong Brønsted sites (single surface hydroxyl groups at edges and corners) that might have formed bonds with the sterically hindered lutidine. These active sites may be able to remove sterically hindered 4,6-dimethyldibenzothiophenes from fuels such as ultra low sulfur diesel, as observed before [110].

At higher wavenumbers, the bands representing aliphatic (2929, 2978 cm^{-1}) and aromatic (3066 cm^{-1}) –C–H stretching vibration was seen in the $Ag/TiO_2–Al_2O_3$ + 2,6-lutidine sample spectrum [122]. This suggested that $Ag/TiO_2–Al_2O_3$ had higher adsorption capacity for lutidine than $TiO_2–Al_2O_3$. The broad bands at 3200–3500 and 3100–3500 cm^{-1} in lutidine treated $TiO_2–Al_2O_3$ and $Ag/TiO_2–Al_2O_3$ spectra have been attributed to the perturbed hydroxyl groups interacting with lutidine molecules.

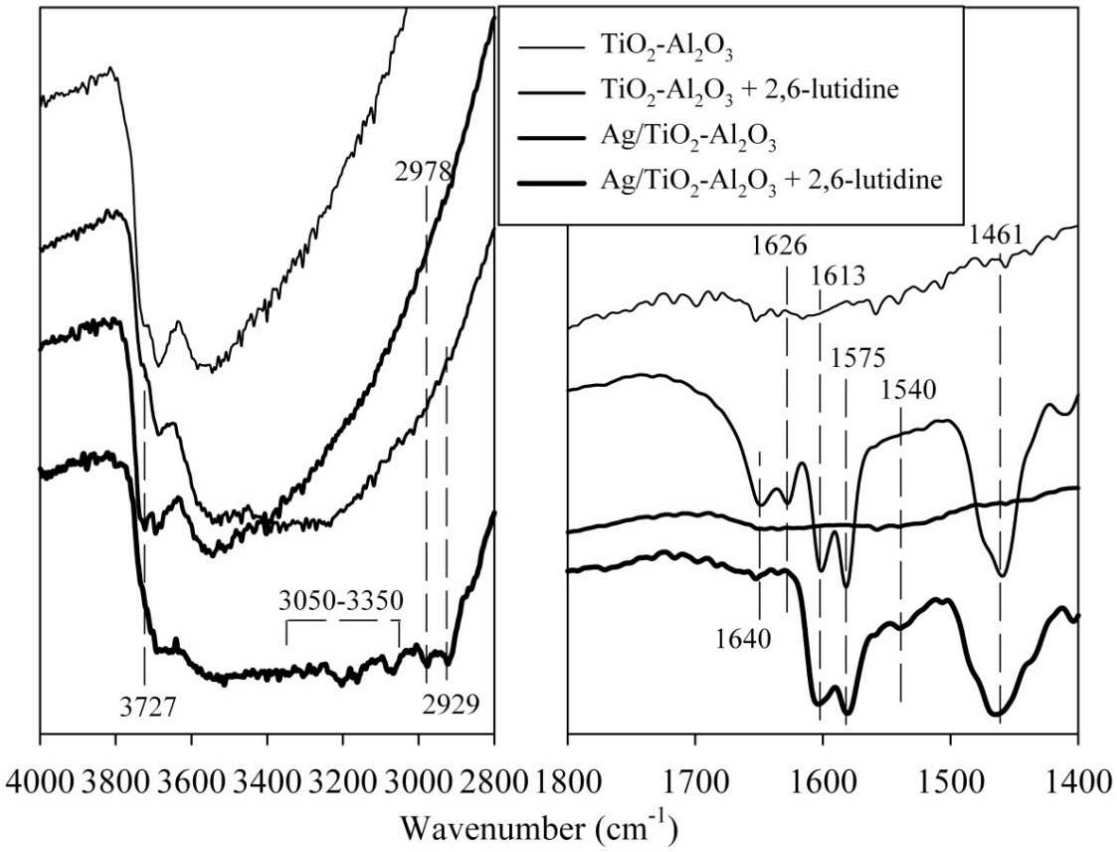

Figure IV.8. *In situ* IR spectra (in transmission mode; Y-axis in transmittance-A.U.) of calcined and pretreated TiO_2–Al_2O_3 (Ti/Al = 1:4.4) and 10 wt% Ag/TiO_2–Al_2O_3 (Ti/Al = 1:4.4) adsorbent samples before and after treatment with 2,6-lutidine

TMCS: Figure IV.9 shows the IR signatures of TMCS treated adsorbent samples. TMCS has been used to detect vicinal and geminal hydroxyls (single –OH groups) [131]. The participation of hydroxyl groups were evident from the spectra (Figure IV.9), where a significant decrease in hydroxyl band intensities and subsequent formation of broad bands at lower wavenumbers (3100–3500 cm^{-1}) were observed. The decrease in intensities of –OH stretching bands therefore confirmed the presence of single surface hydroxyl groups, which included the –OH groups formed after Ag incorporation (3727

cm^{-1}). Besides these, the bands representing TMCS molecules were also observed in the sample spectra (2954, 1449, 1412, and 1255 cm^{-1}).

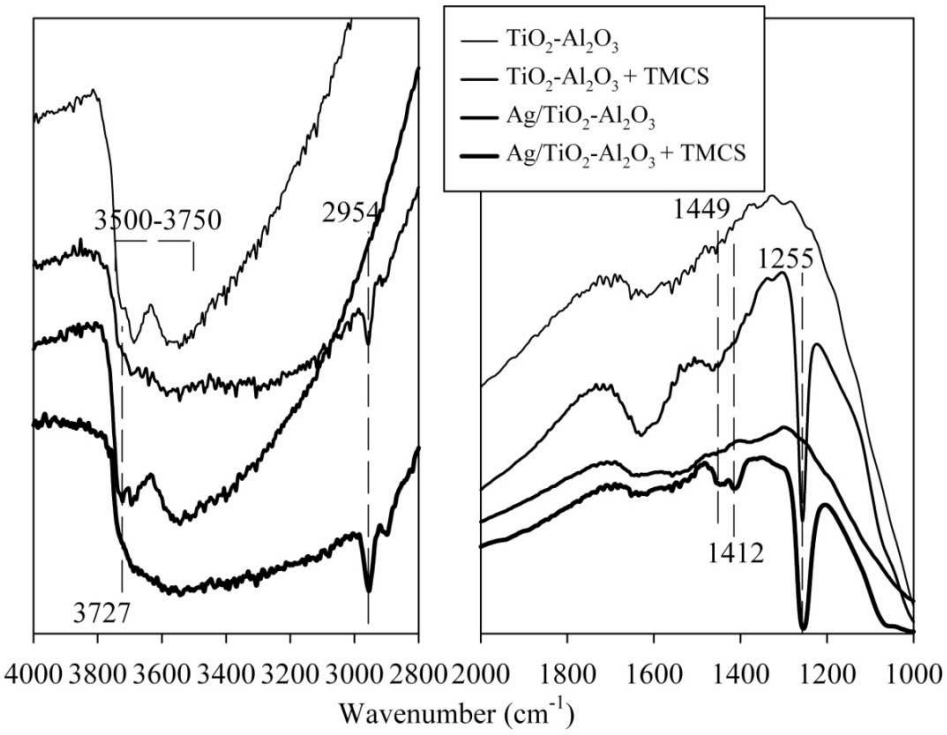

Figure IV.9. *In situ* IR spectra (in transmission mode; Y-axis in transmittance-A.U.) of calcined and pretreated TiO_2–Al_2O_3 (Ti/Al = 1:4.4) and 10 wt% Ag/TiO_2–Al_2O_3 (Ti/Al = 1:4.4) adsorbent samples before and after treatment with trimethyl chlorosilane (TMCS)

IV.3.7. Determination of sulfur adsorption sites

To determine the sulfur adsorption sites, TiO_2–Al_2O_3 and Ag/TiO_2–Al_2O_3 adsorbent samples were treated with thiophene in vacuum (100 mTorr) followed by IR analysis. In the 1200–1800 cm^{-1} wavenumber region of Ag/TiO_2–Al_2O_3 + T sample spectrum (Figure IV.10), three distinct bands at 1641 (H–O–H bending vibrations of water impurities), 1393 (perturbed C=C stretching vibrations of thiophene rings), and 1249 cm^{-1} (in plane –C–H bending vibrations of thiophene rings) were seen [122, 132-134]. The 1393 and 1249 cm^{-1} bands were red-shifted from those representing free thiophene molecules

(1409 and 1256 cm^{-1}) [123], indicating that the orientation of adsorbed thiophene molecules was parallel to the adsorbent surface. This pointed to the π-interactions of thiophene molecules with surface sites [134]. The 1393 and 1249 cm^{-1} bands were absent in TiO_2–Al_2O_3 + T sample spectrum, implying that the Ag ions were primarily responsible for π-interactions. This was in agreement with the literature that reported the adsorption of sulfur heterocycles on metal ions via π electrons [3]. The red-shift of the bands representing –OH groups from 3700–3750 cm^{-1} to 3100–3450 cm^{-1} reiterated their participation in adsorbing thiophene molecules. The –C–H stretching vibrations of adsorbed thiophenes was also evident from the band at 3080 cm^{-1} [122].

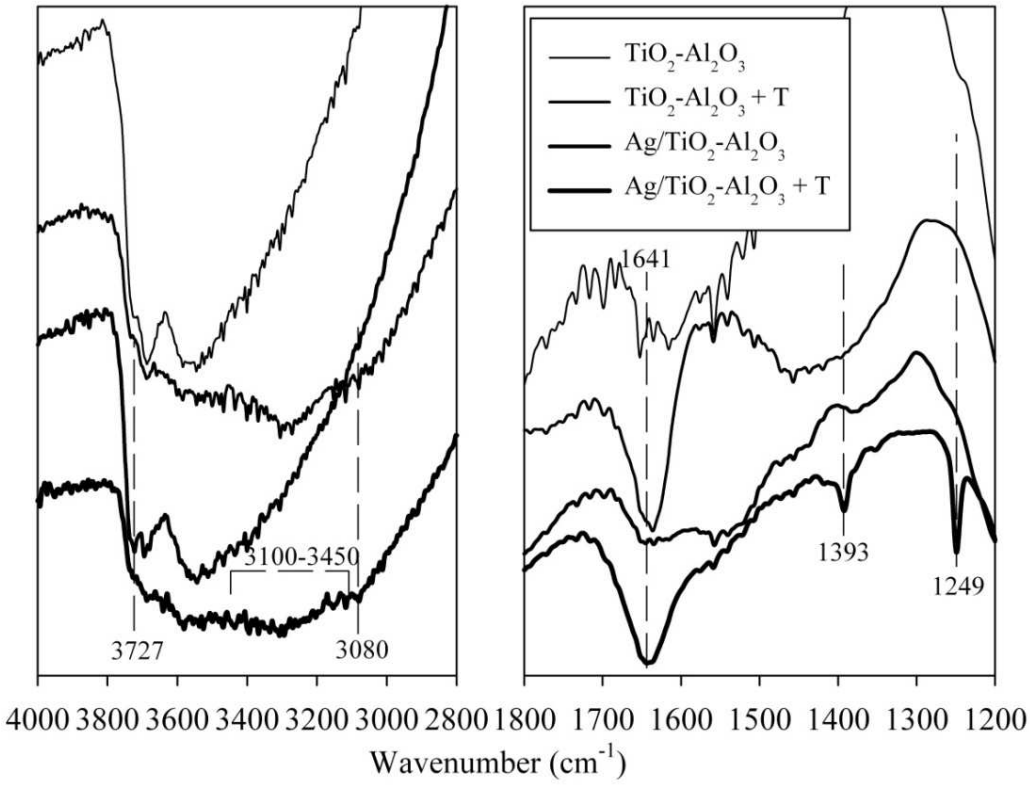

Figure IV.10. *In situ* IR spectra (in transmission mode; Y-axis in transmittance-A.U.) of calcined and pretreated TiO_2–Al_2O_3 (Ti/Al = 1:4.4) and 10 wt% Ag/TiO_2–Al_2O_3 (Ti/Al = 1:4.4) adsorbent samples before and after treatment with thiophene (T)

Table IV.3 IR bands and their respected assignments for calcined adsorbents before and after treatment with different adsorbate molecules (The "×" symbols indicate observed bands in untreated/treated TiO_2–Al_2O_3 and Ag/TiO_2–Al_2O_3 sample spectra)

Treatment	Wave-number (cm^{-1})	Assignments	TiO_2–Al_2O_3	Ag/TiO_2–Al_2O_3	Reference
No treatment	3500–3750	–OH stretching vibrations	×	×	[119, 120]
	3727			×	
Ammonia	1180	υ_2 vibrations of coordinatively bound NH_3		×	[125, 126]
	1200, 1248		×		
	1460	$\upsilon_4(\delta_{as})$ asymmetric deformation of NH_4^+	×		[124, 125]
	1600–1650	Combination of $\delta(NH_3)_{as}$ deformations of adsorbed NH_3 & of adsorbed NH_2	×	×	[122, 123]
	3200–3450	Combination of N–H stretching vibrations (NH_3) and NH_4^+ vibrations after interacting with –OH	×	×	[123, 124]
2,6-lutidine	1461	Lutidine, coordinatively bound on LAS	×	×	[78, 127]
	1540	Lutidine on BAS		×	[130]
	1575, 1613	υ_{8b} and υ_{8a} vibrations of lutidine, coordinatively bound on LAS	×	×	[127, 129]
	1626, 1640	Lutidine chemisorbed on BAS	×		[127]
	2929, 2978, 3066	–C–H stretching vibrations of aliphatics and aromatics		×	[122]
	3050–3350	Perturbed (–OH) stretching vibrations	×	×	[121, 135, 136]
Trimethyl chlorosilane (TMCS)	1255	υ_4 symmetric deformation of $–CH_3$	×	×	[131]
	1412	$–CH_3$ deformation		×	
	1449		×	×	
	2954	Adsorbed TMCS groups	×	×	
Thiophene	1249	δ(–C–H) bending vibrations in plane		×	[123]
	1393	Perturbed $\delta(C=C)_s$ vibrations of T rings		×	[133, 134]
	1641	H–O–H bending vibrations of water	×	×	[120]
	3080	–C–H stretching vibrations of T rings	×	×	[122]
	3100–3450	Perturbed (–OH) stretching vibrations	×	×	[121, 135, 136]

IV.4. Discussion

Enhanced sulfur adsorption capacity was achieved by dispersing Ag and TiO_2 onto high surface area supports such as Al_2O_3. $Ag/TiO_2–Al_2O_3$ reduced the outlet sulfur concentration to PEM fuel cell application range, as seen previously [110], therefore it possessed adsorption sites that were highly selective for sulfur heterocycles. Consequent addition of TiO_2 and Ag reduced band gap, as observed by UV-DRS measurements. NH_3 adsorption indicated higher overall surface acidity in $TiO_2–Al_2O_3$ mixed oxides. The XRD signatures of adsorbent samples did not show any titanium oxide peaks. However, Raman indicated that the supported TiO_2 was in anatase phase. Therefore, the anatase TiO_2 particles on $TiO_2–Al_2O_3$ mixed oxide were in dispersed states with particle sizes lower than the XRD detection limit (ca. <4 nm). This resulted in higher acidity of anatase as well as greater exposed areas at corners and edges. In addition, the concentration of coordinatively unsaturated sites (CUS) was increased, paving the way to higher Ag dispersion. This was supported by the O_2 chemisorption results that indicated the highest Ag dispersion for $Ag/TiO_2–Al_2O_3$. The CUS also facilitated the formation of hydroxyl groups strong enough to protonate species upon adsorption. This was supported by the IR spectra of $TiO_2–Al_2O_3$ samples treated with NH_3 (1540 cm^{-1}) and 2,6-lutidine (1626 and 1640 cm^{-1}). Silver is most likely to be incorporated with TiO_2 as single atom, as observed from the XRD results discussed before and from the EXAFS studies reported by others [137].

From the above findings, the following mechanism for Ag impregnation can be postulated (shown schematically in Figure IV.11(a), IV.11(b), and IV.11(c)). When Ag is impregnated, it occupies either the CUS Lewis sites or the Brønsted sites (produced after

the relaxation of Lewis sites by moisture in air). Among the CUS Lewis sites, Ag occupies the α-Lewis sites (4 coordinated Ti^{4+} ions) [125]. This was evident from the IR spectra of NH_3 treated samples. In addition, Ag replaces some of the strong –OH groups, especially the ones at corners and edges. This was supported by the absence of bands representing protonated species (1540 cm^{-1} in the NH_3 treated sample spectrum and 1626 and 1640 cm^{-1} in the lutidine treated sample spectra) in the treated $Ag/TiO_2–Al_2O_3$ sample spectra. However, new –OH groups (represented by the 3727 cm^{-1} band in pretreated $Ag/TiO_2–Al_2O_3$ sample spectrum) were observed after Ag addition, resulting from Ag impregnation. This phenomenon was in agreement with the literature reported by other researchers [125]. These –OH groups were believed to be the single surface hydroxyl groups (as evident from the IR spectrum of TMCS treated $Ag/TiO_2–Al_2O_3$), and were weak in strength (as evident from the 1540 cm^{-1} band in lutidine treated $Ag/TiO_2–Al_2O_3$ spectrum). The above discussion was only focused on $Ag–TiO_2$ interactions. Besides this, a fraction of Ag might have also been impregnated on the Al_2O_3 surface. However, we assumed that most of the Ag was impregnated on TiO_2 surface, based on the iso-electric points of anatase-TiO_2 and γ-Al_2O_3. There might also be a possibility of –OH presence on Ag surfaces as AgOH, as observed by others [138]. However, no evidence for such specie was observed in this work.

The IR spectra of thiophene treated adsorbent samples lead to the premise that thiophene molecules were adsorbed parallel to the $Ag/TiO_2–Al_2O_3$ surface, whereas such interaction was absent in $TiO_2–Al_2O_3$. Therefore, Ag primarily adsorbs sulfur compounds via π-interactions, while the –OH groups primarily adsorb via direct hydrogen/σ bonding

between the S atoms and H^+ cations. Figure IV.11(d) and IV.11(e) schematically show the adsorption mechanisms.

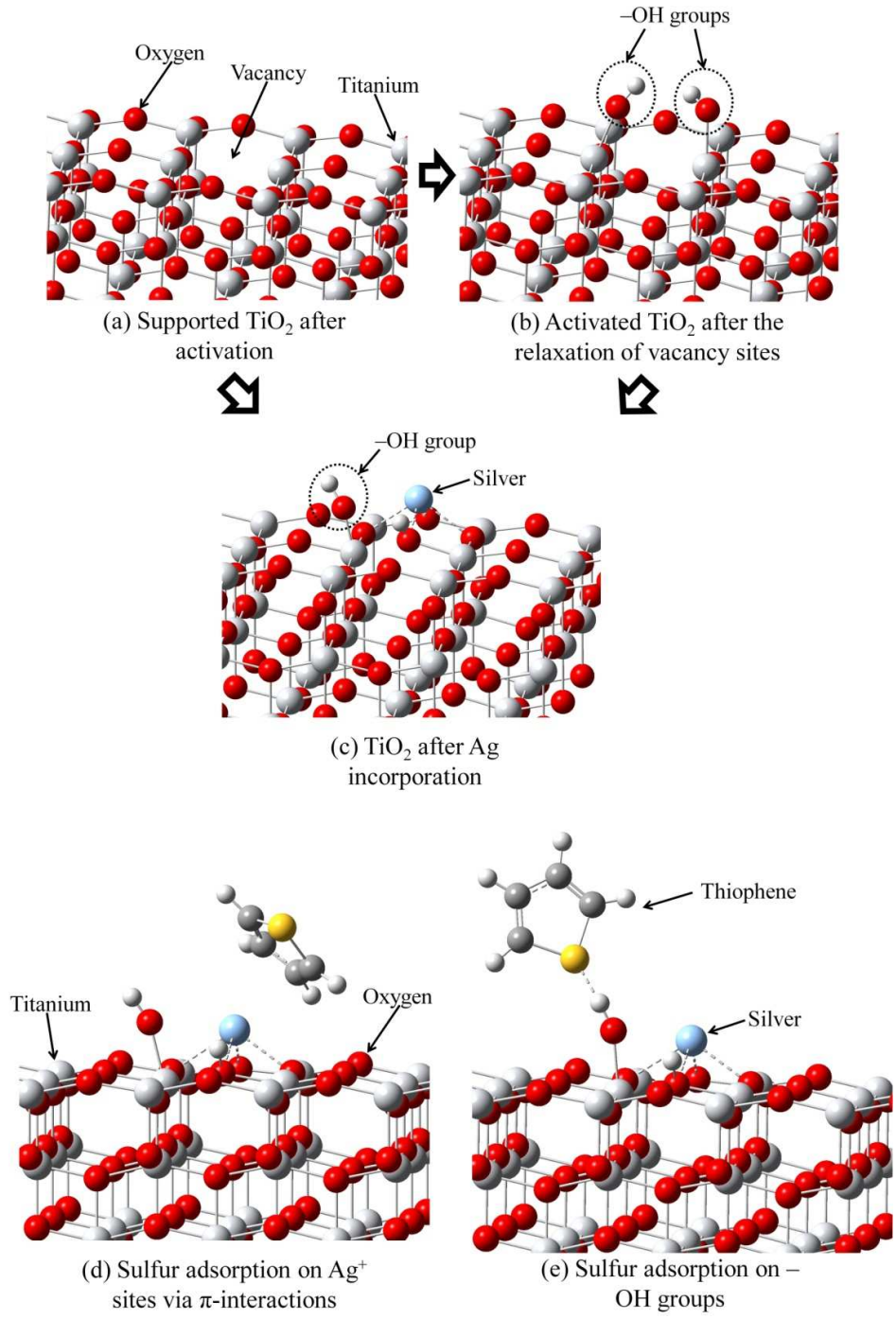

Figure IV.11. (a), (b), (c): The sequence of Ag impregnation on TiO_2–Al_2O_3; (d), (e) Sulfur adsorption mechanisms on Ag/TiO_2–Al_2O_3.

IV.5. Conclusions

$Ag/TiO_2–Al_2O_3$ demonstrated enhanced capability in desulfurizing liquid hydrocarbon feeds for PEM fuel cell systems. The adsorbent had 262% higher saturation capacity than titania alone (based on work with model fuel). TiO_2 dispersion on Al_2O_3 resulted in the formation of highly dispersed (<4 nm) anatase phase and the consequent increase in activity (lower band gap) and in surface acidity (higher NH_3 uptake). The breakthrough experiments indicated silver oxides as the active silver phase for sulfur adsorption. The higher number of defect sites on $TiO_2–Al_2O_3$ provided more sites for Ag incorporation, resulting in higher Ag dispersion (55% higher than Ag/TiO_2). Approximately 92% of the Ag sites (exposed Ag atoms in the form of silver oxides) participated in sulfur adsorption (benzothiophene) at room temperature (0.21 mol S/mol Ag). IR signatures of the adsorbent samples treated with probe molecules revealed single surface hydroxyl groups on the TiO_2 edges and corners. Silver addition brought in additional –OH groups (3727 cm^{-1}). These –OH groups contributed in the adsorption of thiophenic molecules, as observed by the respective IR signatures. The Lewis sites of $TiO_2–Al_2O_3$ mixed oxides paved a way to increased amount of surface bound silver oxides, while the Brønsted sites (hydroxyl groups) actively participated in sulfur adsorption. Ag addition not only enhanced the sulfur adsorption capacity, but also enabled the adsorbent to adsorb sulfur heterocycles via π-interactions (1393 and 1249 cm^{-1}) as well. The adsorbent formulation showed promises for application in an upstream desulfurization unit for fuel cell applications. The adsorbent mechanism consisted of multiple adsorption sites, which can be useful for treating different fuel blends.

V. Investigation of Organosulfur Adsorption Pathways from Liquid Fuels onto $Ag/TiO_2–Al_2O_3$ Adsorbents at Ambient Conditions

Abstract:

The adsorption mechanisms for aliphatic and aromatic sulfur compounds onto $Ag/TiO_2–Al_2O_3$ (10 wt% Ag, Ti:Al = 1:4.4 by weight) adsorbent were investigated in this paper. The mesoporous mixed oxide supported silver adsorbent demonstrated promising sulfur adsorption capacities (~10 mg S/g adsorbents) from liquid hydrocarbon fuels (JP5, JP8, and Off Road Diesel-ORD). However, its performance was significantly hindered by the presence of non-sulfur aromatics. *In situ* infrared (IR) spectra of $TiO_2–Al_2O_3$ and $Ag/TiO_2–Al_2O_3$ samples treated with various model fuels revealed dissociative chemisorption pathways for different sulfur species. The aliphatic (1-butanethiol and diethyl sulfide) and aromatic (thiophene, benzothiophene, dibenzothiophene, 4,6-dimethyldibenzothiophene) sulfur compounds underwent dissociative and reactive adsorption on the surface acid sites at room temperature. The surface hydroxyl groups adsorbed the sulfur aromatics primarily via hydrogen bonding (3100–3400 cm^{-1}), and possible dissociated products were saturated/partially saturated aliphatic compounds. The presence of non-sulfur aromatics (benzene) reduced the sulfur adsorption capacity (~18% for $Ag/TiO_2–Al_2O_3$) due to its competitive adsorption on the adsorbent via π-interactions.

V.1. Introduction

Airborne sulfur compounds originating from hydrocarbon fuel combustion are one of the primary health hazards present in the air. Sulfur concentration increase in the atmosphere due to the burning of fossil fuels has been a major concern and countries around the world are regulating the maximum allowable sulfur concentration in commercial fuels. To comply with these restrictive regulations, the sulfur removal technologies have become more severe and complicated [6-8]. Current desulfurization process, namely hydrodesulfurization (HDS) employs extremely high temperatures and hydrogen pressures for desulfurizing hydrocarbon fuels. Such technology is difficult to apply in the reformation stages for on-board fuel cell systems. The use of commercial and logistic fuels as feedstocks in vehicular fuel cells requires a desulfurization step prior to the reformation stage in order to prevent sulfur poisoning of the reforming catalysts and of the fuel cell electrodes [11]. Thus, a simple, compact, and cost effective desulfurization technology is highly desirable in fuel processing for hydrogen production.

Among the alternative processes to HDS tested so far [6, 9, 25-31], selective adsorption of sulfur species is one of the most promising solutions for producing ultra clean hydrocarbon fuels. Adsorptive desulfurization addresses a major problem faced by the HDS process: the selectivity toward Poly Aromatic Sulfur Heterocycles (PASH). Adsorption has a significant edge over the other processes in portable desulfurization applications because of its simplicity, compact design, and hydrogen free operation. It can be feasibly implemented as a polishing agent supplementing HDS process. There has been much research work on developing the materials for sulfur adsorption [3, 20, 25, 27, 52, 53, 55, 102]. Among them, supported silver adsorbents have demonstrated excellent sulfur adsorption capacities for logistic and commercial fuels at ambient conditions [69,

70]. Oxidized silver removes sulfur down to sub ppmw levels without requiring any activation step or any hydrogen stream. Its operability at ambient temperatures and atmospheric pressure allows for the "cold-starts" of hydrogen vehicles and greatly reduces the challenges due to process safely. Recently, silver adsorbents supported on TiO_2 dispersed supports have shown to enhance sulfur adsorption by increasing TiO_2 active sites and providing more seats for silver incorporation [110]. The novel oxide adsorbent can also be applied in continuous desulfurization units since it is completely regenerable. The preparation technique for supported silver adsorbents is simple, cost effective, and scalable.

Sulfur removal from liquid heterogeneous mixtures at room temperature is a complicated process thus detailed investigation is essential for understanding the mechanisms involved. Silver based adsorbents can operate efficiently at room temperature and atmospheric pressure, yet the mechanism by which adsorption takes place is not fully understood. Various types of adsorption of sulfur on surfaces have been reported in the literature, notably physisorption, strong chemisorption [139, 140], and the formation of sulfides with surface active sites [141, 142]. Sulfur adsorption can also occur via the π-bonds between the electron clouds of aromatic rings and the surface active sites when the rings are composed of heteroatoms [55, 68]. There are also reported cases of forming direct σ-bonds between sulfur and metals [130] and entrapping organosulfur compounds in "cage" like structures e.g. Metal Organic Framework (MOF) materials [57]. In addition, surface acid sites operate as the primary seats for many catalytic activities including hydrodesulfurization process [9], and can be a valid motivation for sulfur adsorption. Recently, the CM3-adsorption lab has postulated a novel adsorption

mechanism whereby the surface hydroxyl groups (Bronsted acid sites) form bonds with the π-electrons of the aromatic rings [100]. Characterization of the adsorbent materials with different probe molecules supported this hypothesis. However, it is essential to understand the pathways via which the metal oxides interact with the sulfur species at ambient conditions. Researchers have applied numerous analytical techniques to study the surface interactions. Among these analytical techniques, Infrared (IR) spectroscopy has been an excellent tool for qualitative measurement of adsorption and reaction mechanisms in the field of catalysis [89, 143]. Previously, researchers have identified various bonds between thiophene and adsorbents via IR [133]. It can be successfully employed to study the interactions between the adsorbate and adsorbent molecules and fully depict the corresponding bonds [144, 145]. Rigorous analytical studies including IR therefore should help in understanding adsorption phenomena and consequently assist in optimizing adsorbent formulation and adsorption process. IR study will also assist in tailoring the adsorbent formulation with respect to different fuel blends.

In this paper, desulfurization experiments and IR spectroscopy were used together to gather information about the sulfur adsorption mechanism on mixed oxide supported silver adsorbents. Nitrogen (N_2) physisorption was employed to characterize the pore structure. Desulfurization performances toward different commercial, logistic, and model fuels were also compared for investigating the adsorption affinity toward different sulfur species. Aromatic sulfur compounds (thiophene derivatives) and non-aromatic sulfur species (thiol and disulfide derivatives) were used to prepare model fuels. The effect of non-sulfur aromatic compounds on sulfur adsorption capacity was also gauged through desulfurization experiments. IR spectroscopy was employed to study the adsorption of

different sulfur species on TiO_2–Al_2O_3 and Ag/TiO_2–Al_2O_3 adsorbents. IR spectra of samples treated with sulfur aliphatics and aromatics were compared. The observations have been described in the results and discussion section.

V.2. Experimental Section

The preparation of TiO_2–Al_2O_3 and Ag/TiO_2–Al_2O_3 adsorbents has been described in section II.1. The Ti:Al weight ratio and Ag loading were constant all throughout this chapter (1:4.4 and 10 wt%, respectively). For the desulfurization experiments, dynamic breakthrough tests were carried out in order to assess the sulfur adsorption capacities of the adsorbents. The experiments were conducted using JP5, JP8, ORD, and model fuels. The real fuels used have been discussed in section II.2. The sulfur speciation in these fuels can be found in section III.3.2 [110]. The compositions of the model fuels used in this work are shown in Table V.1. These model fuels were used for investigating adsorbent selectivity and characterizing active adsorption sites.

Table V.1 Compositions of the model fuels used in fixed bed continuous adsorption (breakthrough) and infrared (IR) experiments.

Fuel	Sulfur conc. in n-octane (ppmw)	Sulfur compound	Benzene conc.(ppmw)
MF-1	3500	1-Butanethiol	-
MF-2		Diethyl Sulfide	-
MF-3		Thiophene	-
MF-4		Benzothiophene	-
MF-5		Benzothiophene	14678
MF-6		4,6-Dimethyldibenzothiophene	-
MF-7	-	-	14678

The experimental details of breakthrough tests, regeneration, and analysis can be found in section II.3.2 and section II.3. The bed weight, diameter, volume, and overall aspect ratio (bed length:bed diameter) were 10 g, 1 cm, 15–16 cm^3, and 22, respectively. The N_2 physisorption technique used for adsorbent characterization has been described in section II.5.

Adsorbent samples treated with sulfur probe molecules were analyzed via IR Spectroscopy. The experimental setup and the pretreatment procedures are described in section II.7. After every pretreatment, the sample was treated with different model fuels (Table V.2). MF-1 through MF-7 were used as adsorbate molecules. These were introduced to the sample in the cell by N_2 bubbling at room temperature. Every adsorbate treatment was followed by evacuation prior to IR analysis. Both the pretreatment and exposure to adsorbate steps were performed *in situ*.

Table V.2 Treatment steps with adsorbate molecules before IR analysis

Adsorbent	Adsorbate	N_2 flow rate (ml/min), temp. (°C), duration (min)	Evacuation after treatment (mTorr), duration (min)
10 wt% Ag/ TiO_2–Al_2O_3	n-Octane, MF-1 through MF-7*	10, 22, 20	100, 20
TiO_2–Al_2O_3			

*Please see Table V.1 for model fuel compositions

V.3. Results and Discussion

V.3.1. Adsorbent Characterization:

The pore structures of adsorbent materials are critical for liquid phase adsorption since the process involves diffusion of large sulfur heterocycles inside the small and tortuous pores. Macro and mesoporous materials with large pore sizes (>2 nm) have shown effective performances in adsorbing liquid organosulfur species, although these materials may not have very high surface areas. Previously microporous Y-zeolite (660 m^2/g) was used for liquid organosulfur adsorption but showed lower capacity than mesoporous alumina (267 m^2/g) [110]. Surface area is obviously another important factor for liquid phase desulfurization. The adsorbent capacity was increased for adsorbents with higher surface areas [70]. Therefore, pore structure and surface area should be synergistically optimized in order to attain the highest sulfur adsorption capacity. In this work, TiO_2–Al_2O_3 and Ag/TiO_2–Al_2O_3 were analyzed via N_2 physisorption to investigate the pore structures. Figure V.1 shows the N_2 isotherms of the two samples. Both TiO_2–Al_2O_3 and Ag/TiO_2–Al_2O_3 demonstrated type IV isotherms, indicating that the samples were mesoporous [146]. The corresponding surface areas, pore volumes, and average pore sizes are shown in Table V.3. The Ag/TiO_2–Al_2O_3 adsorbent had moderate surface area and the reduction in surface area after silver addition was ~13%.

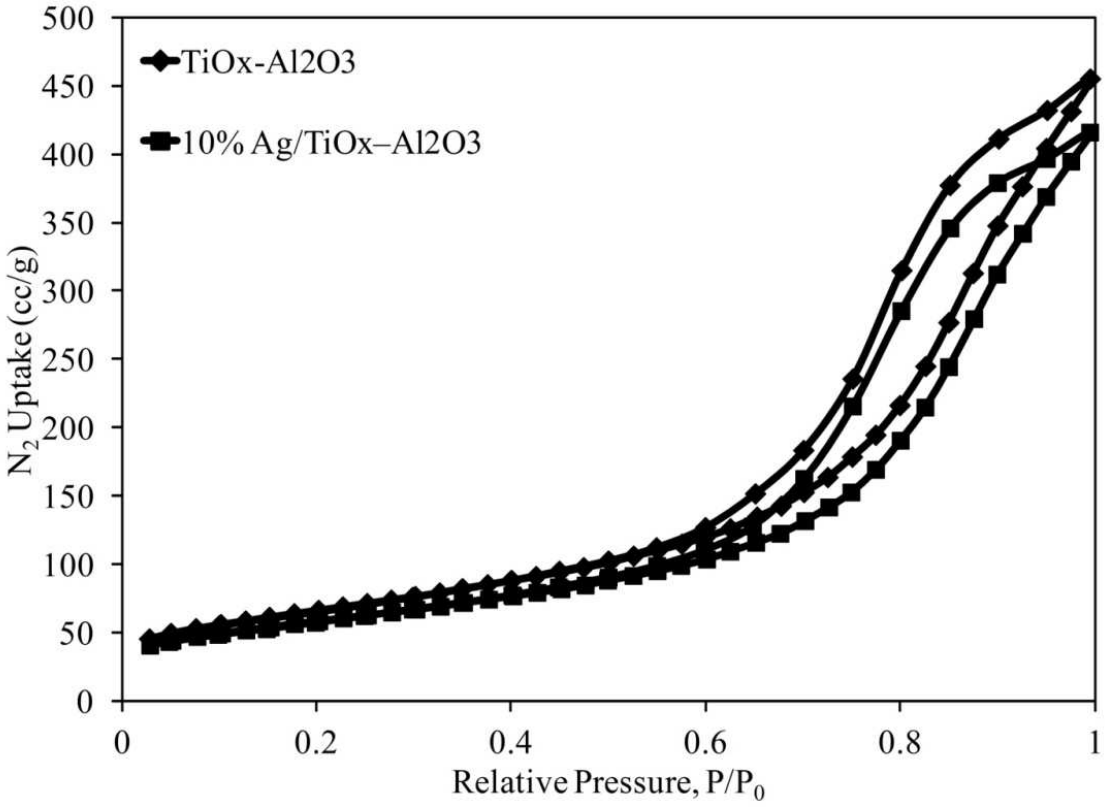

Figure V.1. Nitrogen isotherms of TiO_2–Al_2O_3 (Ti:Al = 1:4.4) and 10 wt% Ag/TiO_2–Al_2O_3 (Ti:Al = 1:4.4). Physisorption temperature: 77 K (–196°C)

Table V.3 Properties of the adsorbents used in the experiments.

Adsorbent	Surface Area (m^2/g)	Pore Volume (ml/g)	Avg. Pore Size (nm)
TiO_2–Al_2O_3	239.9	0.71	11.77
Ag/TiO_2–Al_2O_3	209.0	0.64	12.35

V.3.2. Desulfurization Performance toward Refined Hydrocarbon Fuels:

The $Ag/TiO_2–Al_2O_3$ adsorbent was tested for performance and sulfur selectivity using challenge JP5, JP8, and ORD fuels. Figure V.2 exhibits the breakthrough characteristics of the fuels and Table V.4 shows the corresponding sulfur adsorption capacities. The breakthrough capacities were higher than those reported previously [110] due to a higher value of overall aspect ratio (L/D~22) in this work. JP8 and ORD curves had secondary breakthroughs at the midway point, which indicated that the adsorbent had varied selectivities toward different sulfur species present in these fuels. In addition, the secondary breakthroughs might also be attributed to competitive adsorption among sulfur species [72]. Although the adsorbent had the higher capacity for JP5, it took the longest time to saturate for ORD due to its low initial sulfur content. The in-set figure in Figure V.2 shows the comparison of JP5, JP8, and ORD breakthrough curves in terms of the outlet to inlet sulfur concentration ratio (C/C_0) vs. cumulative weight of sulfur per adsorbent weight (mg S/g adsorbent). It can be seen that the extent of breakthrough for JP5 was the greatest when the initial sulfur concentrations were normalized. The low capacities at breakthrough for JP8 and ORD could be attributed to the structures of sulfur molecules. JP5 contains most of its sulfur compounds as methyl and dimethyl derivatives of BT while trimethylbenzothiophenes (TMBT's) constitute significant portion of the sulfur compounds present in JP8 and ORD [110]. The adsorbent selectivity for these compounds was the least, since the steric hindrances caused by three methyl groups were significant [110]. Thus, both JP8 and ORD breakthrough curves broke early as seen in the figure. Besides sulfur species, the presence of non-sulfur aromatics also reduced sulfur adsorption as the molecules can compete for the adsorption sites [72]. The aromatic

contents for all the real fuels used here were >15%, which also accounted for low breakthrough capacity. However, the saturation capacities were considerably higher than breakthrough capacities (Table V.4), indicating that the adsorption sites primarily occupied by non-sulfur aromatic compounds might have been subsequently replaced by sulfur species.

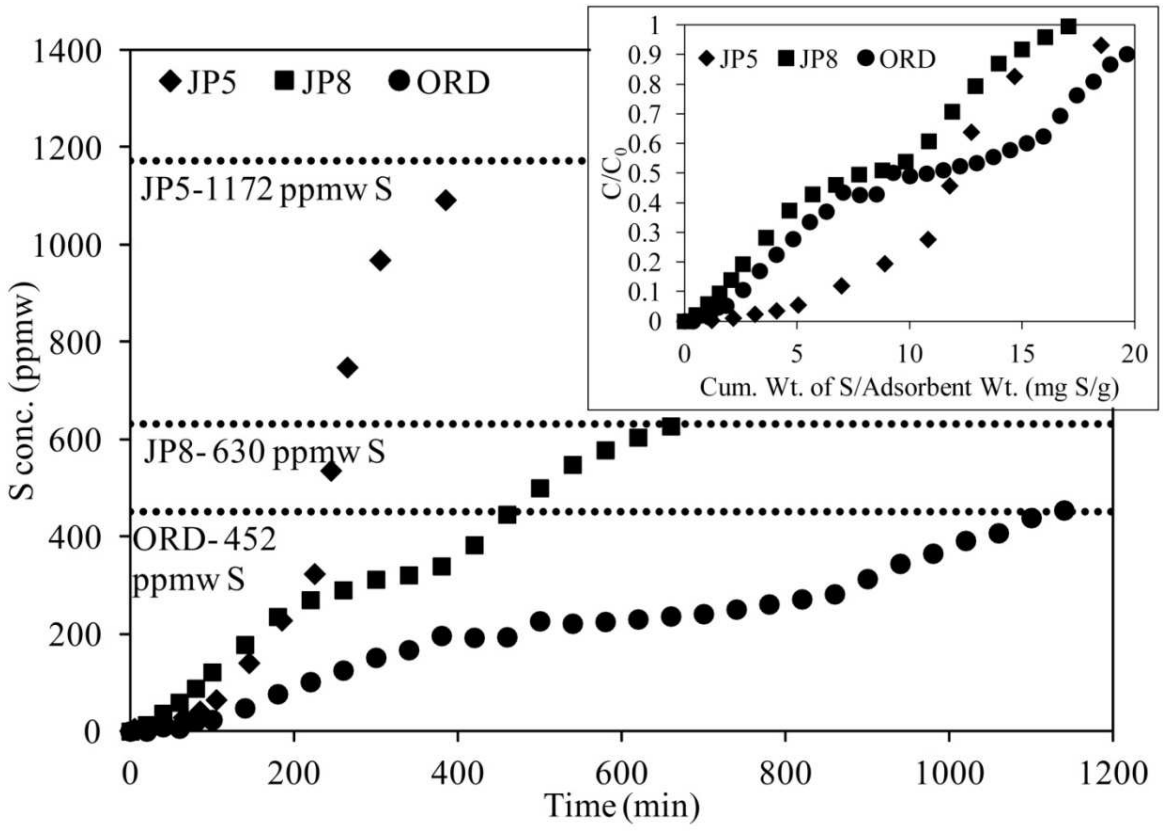

Figure V.2. Breakthrough performance comparison of 10 wt% $Ag/TiO_2–Al_2O_3$ (Ti:Al =1:4.4) adsorbent for desulfurizing JP5, JP8, and ORD (Bed wt.: 10 g, WHSV: ~2.5 h^{-1}). In-set figure: Breakthrough characteristics of JP5, JP8, and ORD using 10 wt% $Ag/TiO_2–Al_2O_3$ (Ti:Al =1:4.4) adsorbent in terms of C/C_0 vs. cumulative weight of S/adsorbent weight

Table V.4 Sulfur adsorption capacities of 10 wt% $Ag/TiO_2–Al_2O_3$ (Ti:Al = 1:4.4) for JP5, JP8, and ORD estimated from breakthrough experiments.

Challenge fuel	Sulfur conc. (ppmw)	Breakthrough time (min)	Breakthrough capacity at10ppm (mg S/g adsorbent)	Capacity at saturation (mg S/g adsorbent)
JP5	1172	38.7	1.84	11.83
JP8	630	15.0	0.38	8.01
ORD	452	73.4	1.36	10.91

V.3.3. Selectivity toward different Sulfur Compounds:

The adsorbent selectivity toward various types of organosulfur compounds was tested through breakthrough experiments of model fuels. The breakthrough graphs of MF-1 (1-C4T + C8), MF-2 (DES + C8), and MF-3 (T +C8) are shown in Figure V.3. All of these sulfur compounds had four carbon atoms. The 1-C4T molecule has a sulfur atom with a butyl group and a hydrogen atom on either side. The sulfur atom in DES molecule is situated in the middle bordered by two ethyl groups; while in T molecule, the sulfur atom participates in the formation of the aromatic ring. The sulfur adsorption capacities are shown in Table V.5. The adsorbent showed higher capacities for sulfur aliphatics than aromatics. The saturation capacity for 1-C4T was 104% and 94% higher than those for DES and T, respectively. This illustrated the effects of sulfur position in the molecules and the functionality of –SH groups. The position of S atom made the 1-C4T molecule

accessible to more active sites on the adsorbent surface. The functionality of the –SH group can assist in multilayer and self-assembled adsorption on silver materials [147, 148]. The adsorbent showed high breakthrough capacity toward DES as compared to T, although the saturation capacities for both sulfur species were very close to each other. The saturation time of the adsorbent using MF-3 was longer than MF-2, which indicated that the aromatic rings might assist in extending saturation time.

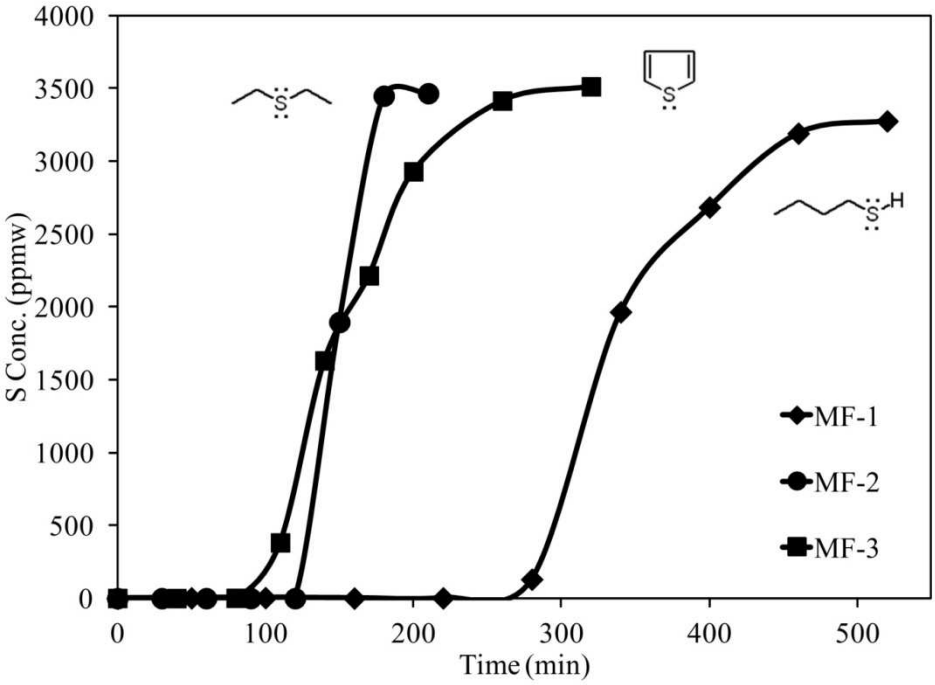

Figure V.3. Breakthrough performance comparison of 10 wt% Ag/TiO_2–Al_2O_3 (Ti:Al = 1:4.4) adsorbent for desulfurizing MF-1 (1-butanethiol + n-octane), MF-2 (diethyl sulfide + n-octane), and MF-3 (thiophene + n-octane) model fuels (Bed wt.: 10 g, WHSV: ~2.5 h^{-1}, S conc.: 3500 ppmw)

To investigate the effect of non sulfur aromatics, TiO_2–Al_2O_3 and Ag/TiO_2–Al_2O_3 adsorbents were tested in breakthrough experiments using MF-4 (BT + C8) and MF-5 (BT + benzene +C8). The breakthrough graphs and sulfur adsorption capacities are shown in Figure V.4 and Table V.5, respectively. For MF-4, the addition of 10 wt% Ag

on the TiO_2–Al_2O_3 support increased the capacities at breakthrough and saturation by 453% and 106%, respectively. MF-5 had similar benzene and BT concentration in C8 by weight. In presence of benzene, the loss of saturation capacities for TiO_2–Al_2O_3 and Ag/TiO_2–Al_2O_3 adsorbents were 7% and 18%, respectively. In other words, benzene occupied around 18% of the Ag/TiO_2–Al_2O_3 surface sites active for sulfur adsorption. These might be the sites responsible for π-bonding with the adsorbate molecules. The effect of benzene was higher for silver supported samples, suggesting that benzene mostly inhibited BT adsorption on silver sites. The low breakthrough capacity toward real fuels (JP5, JP8, and ORD) also reflected the effect of non-sulfur aromatics (aromatic content >15%). However, the capacities at breakthrough were considerably higher in experiments with model fuels, due to low non-sulfur aromatic content (3500 ppmw).

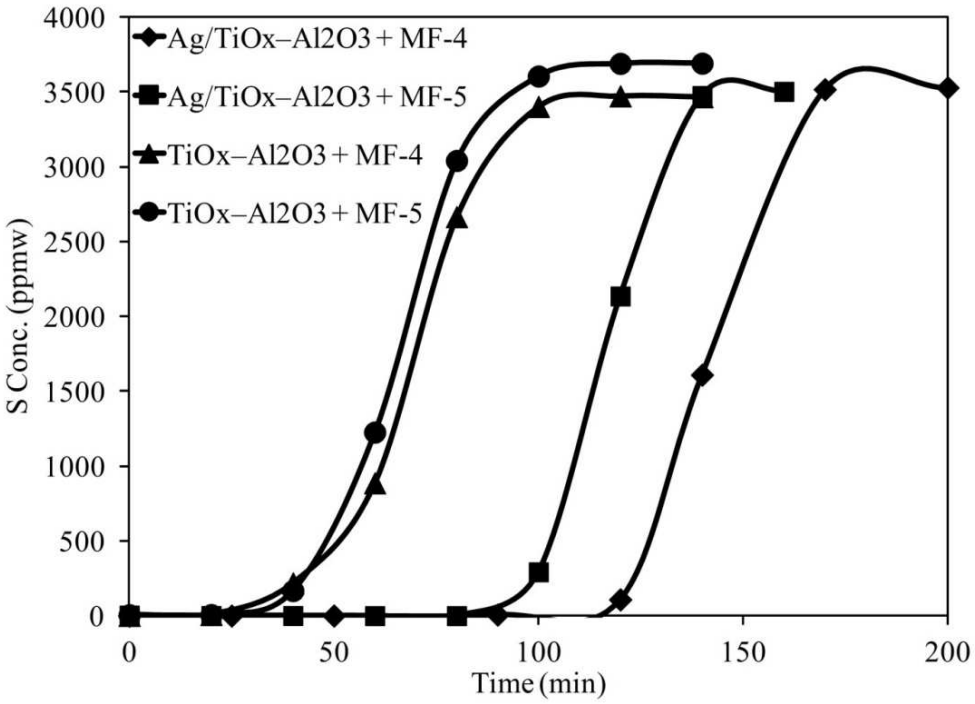

Figure V.4. Breakthrough performance comparison of TiO_2–Al_2O_3 (Ti:Al = 1:4.4) and 10 wt% Ag/TiO_2–Al_2O_3 (Ti:Al = 1:4.4) adsorbents for desulfurizing MF-4

(benzothiophene + n-octane) and MF-5 (benzothiophene + benzene + n-octane) model fuels (Bed wt.: 10 g, WHSV: ~2.5 h^{-1}, S conc.: 3500 ppmw)

Table V.5 Sulfur adsorption capacities of TiO_2–Al_2O_3 (Ti:Al = 1:4.4) and 10 wt% Ag/TiO_2–Al_2O_3 (Ti:Al = 1:4.4) for model fuels estimated from breakthrough experiments.

Adsorbents	Challenge fuel	Breakthrough time (min)	Breakthrough capacity at 10ppm (mg S/g adsorbent)	Capacity at saturation (mg S/g adsorbent)
Ag/TiO_2–Al_2O_3	MF-1 (1-butanethiol + n-octane)	250	30.97	37.80
	MF-2 (diethyl sulfide + n-octane)	122	15.11	18.50
	MF-3 (thiophene + n-octane)	102	12.64	19.49
	MF-4 (benzothiophene + n-octane)	116	14.37	17.63
	MF-5 (benzothiophene + benzene + n-octane)	91	11.27	14.39
TiO_2–Al_2O_3	MF-4 (benzothiophene + n-octane)	21	2.60	8.57
	MF-5 (benzothiophene + benzene + n-octane)	20	2.51	7.96

V.3.4. IR Spectroscopy:

V.3.4.1. Effect of thiophene adsorption:

IR spectroscopy was performed on TiO_2–Al_2O_3 and Ag/TiO_2–Al_2O_3 samples treated with sulfur molecules for determining the sulfur adsorption pathways. All samples were pretreated before analysis (Table V.2(a)). The treated sample spectra were compared and are shown in Figure V.5–V.8. Table V.6 illustrates the corresponding assignments of observed IR signatures. As all samples were subjected to evacuation before IR analysis, it was assumed that most of the physisorbed molecules were removed. Therefore, the adsorbent surface contained mostly chemisorbed species after evacuation. Figure V.5(a) and V.5(b) show the resulting IR spectra of calcined and pretreated TiO_2–Al_2O_3 and Ag/TiO_2–Al_2O_3 samples. Prior to the treatment, the calcined TiO_2–Al_2O_3 and Ag/TiO_2–Al_2O_3 sample spectra showed bands in the 3500–3750 cm^{-1} wavenumber region, which have been assigned to stretching vibrations of hydroxyl groups (–OH) [103, 119, 120]. The broad band represented –OH groups from silver oxide, titanium oxide [149], and alumina [89].

Model fuels containing sulfur compounds were used to treat the calcined and pretreated samples. Information regarding the model fuels and the treatment conditions are given in Table V.2(b). Figure V.5(e) shows the spectrum of Ag/TiO_2–Al_2O_3 treated with C8 alone (for reference). Two noticeable bands were observed at 1378 and 1641 cm^{-1} and these two bands were present in all treated adsorbent sample spectra (Figure V.5–V.8). However, their respective intensities were different. The 1378 cm^{-1} band has been ascribed to the $\delta(CH_3)_s$ bending vibrations of adsorbed octane or other aliphatic organic compounds [119]. The strong and broad band at 1641 cm^{-1} might be assigned to a

combined band resulting from water impurities in the fuels (–OH bending vibrations [122]) and the reacted products of model fuel components (–COO antisymmetric stretching vibrations or C=C stretching vibrations [122, 124]). In the 2800–3000 cm^{-1} wavenumber region, the bands representing –C–H stretching vibrations of CH_2 and CH_3 can be seen in the spectrum (Figure V.5(e)) at 2855, 2933, and 2969 cm^{-1} wavenumbers [119, 145, 150]. All these bands indicated that some of the octane molecules were adsorbed on adsorbent surfaces.

Figure V.5(c) and 5(d) show the IR spectra of MF-3 (T + C8) treated TiO_2–Al_2O_3 and Ag/TiO_2–Al_2O_3 samples. In all the IR spectra of sulfur treated samples, the bands at 3500–3750 cm^{-1} were diminished in intensity, indicating that the hydroxyl groups were interacting with the sulfur species. These were believed to be single surface hydroxyl groups where the oxygen atoms faced away from the plane of surface lattices [100]. A broad band was observed at 3100–3400 cm^{-1} for both the treated TiO_2–Al_2O_3 and Ag/TiO_2–Al_2O_3 samples, which has been assigned to be perturbed –OH stretching vibrations of surface hydroxyls interacting with T molecules [121, 135]. Panayotov and Yates had reported that hydrogen bonding would cause the bands representing –OH groups to shift to lower wavenumbers [136]. In our work, we observed a similar shift. The mode of adsorption was believed to be hydrogen bonding [121]. In the 2800–3100 cm^{-1} wavenumber region (Figure V.5(c) and V.6(d)), bands representing aliphatic –C–H stretching vibrations were observed [130, 133, 145]. The IR spectra did not reflect any presence of aromatic C–H stretching vibrations (3000–3100 cm^{-1}), which might indicate that the chemisorbed thiophenes were dissociated on the adsorbent surfaces and thus

produced aliphatic compounds. Other researchers had observed a similar phenomenon for work with acidic oxides at room temperatures [121, 135, 145].

In the 1200–1800 cm^{-1} wavenumber region (Figure V.5(c) and V.5(d)), numerous bands were observed, indicating dissociated thiophenes on the adsorbents. In the spectrum of MF-3 (T + C8) treated $Ag/TiO_2–Al_2O_3$, a strong and broad band was observed at 1641 cm^{-1}, which was similar to that in the C8 treated $Ag/TiO_2–Al_2O_3$ sample spectrum. The band was red shifted in the MF-3 treated $TiO_2–Al_2O_3$ sample spectrum. Figure V.5(c) and V.5(d) also demonstrated the 1378 cm^{-1} band, similar to Figure V.5(e). Another band appeared at 1465 cm^{-1} in both the spectra of MF-3 (T + C8) treated samples. This broad band represented $–CH_2$ bending + antisymmetric $–CH_3$ deformation of aliphatic compounds [122, 124]. Additional bands appeared at 1345 cm^{-1} (COO^- symmetric stretch of carboxylates/carboxylic acid salts [122]) in Figure V.5(c) and at 1305 cm^{-1} (wagging vibrations of methylene groups [124]) in Figure V.5(d). All these bands indicated dissociated thiophenes on the surface. These chemisorbed thiophenes underwent ring opening reactions to form aliphatic compounds. The probable products resulting from thiophene dissociation were either unsaturated thiol/sulfide like species [135] or carboxylates [145]. In the neat $TiO_2–Al_2O_3$ adsorbent, both Lewis (coordinatively unsaturated sites-CUS) and Bronsted (surface –OH groups) acid sites are present [74]. When silver is incorporated with $TiO_2–Al_2O_3$, it might occupy some of the CUS sites and might release additional Bronsted acid sites[100]. These acid sites can react with the sulfur molecules upon adsorption. Larrubia and his co-workers reported dissociation of sulfur heterocycles on the Lewis acid sites of Al_2O_3 surface [145]. The adsorbed sulfur molecules can also undergo C–S cleavage when attacked by protons [132]. The –OH

groups can yield hydrogen atoms to adsorbed thiophenes and might form saturated/partially saturated aliphatics [151]. Eventually, silver (I) oxides on the adsorbent might react with the sulfur atoms in the dissociated molecule to form silver (I) sulfide. The presence and absence of silver can affect surface acidity of the adsorbent and subsequently the nature of dissociated products, thereby changing the corresponding band intensities. The reduction of free –OH groups (3500–3750 cm^{-1}) and appearance of perturbed –OH groups (3100–3400 cm^{-1}) indicated that these hydroxyl groups were actively participating in adsorption and might be primarily responsible for ring opening reactions of thiophene [121, 135]. In this work, we could not collect specific information about the products due to the lack of pertaining data. Confirmed information regarding the nature of dissociated products and the surface acidity measurement of Ag–TiO_2 dispersed supports are currently in progress and will be reported in future.

The spectra in Figure V.5(c) and V.5(d) exhibited additional bands implying presence of intact thiophene molecules adsorbed on the surface. However, these bands were weak compared to those bands representing dissociated thiophenes. Therefore, only a small amount of the intact adsorbed molecules were observed among the chemisorbed species. Garcia et al. had reported that the dissociation rate of adsorbed thiophenes through surface –OH groups was slow and the ring opening reactions were observed after longer exposures [135]. In our case, the intact thiophene molecules might have demonstrated similar phenomenon. In the MF-3 treated TiO_2–Al_2O_3 sample spectrum, a shoulder at 1438 cm^{-1} was observed. This band has been assigned to be perturbed $\delta(C=C)_s$ stretching vibrations of T ring, blue shifted from its original wavenumber (generally at 1407–1409 cm^{-1} for gaseous T). This shift to higher frequencies resulted from the increased electron

density within the rings when T molecules were coordinated via the σ-interactions between S atoms and surface sites (e.g. cations) [130, 133]. In this case, the adsorbed T rings were oriented perpendicular to the plane of adsorbent surface. Besides this, the spectrum of treated TiO_2–Al_2O_3 sample also exhibited a band at 1400 cm^{-1} which has been assigned to the $\delta(C=C)_s$ stretching vibrations of T ring adsorbed on surface hydroxyl groups [152]. This further demonstrated the role of surface hydroxyls in sulfur adsorption. The band was absent in the spectrum of treated Ag/TiO_2–Al_2O_3 sample, the reason for which might be the incorporation of silver on these sites during impregnation stage. In the MF-3 treated Ag/TiO_2–Al_2O_3 sample spectrum, weak bands representing the $\delta(C=C)_s$ stretching vibrations of T rings were observed at 1409, 1438, and 1390 cm^{-1} wavenumbers [123]. The 1390 cm^{-1} band resulted from a red shift of the $\delta(C=C)_s$ stretching band after thiophene adsorption. This red shift usually indicates a decrease in the electron density of the thiophene rings when the adsorbed molecules are oriented parallel to the surface. Therefore, the shift observed in the spectrum indicated that some of the thiophene molecules were adsorbed onto the Ag/TiO_2–Al_2O_3 adsorbent via their π-electrons [133, 134]. This band was not observed in the MF-3 treated TiO_2–Al_2O_3 spectrum, indicating that silver oxide might be responsible for this interaction. The bands at 1390, 1400, 1409, and 1438 cm^{-1} indicated intact T molecules adsorbed on the surface.

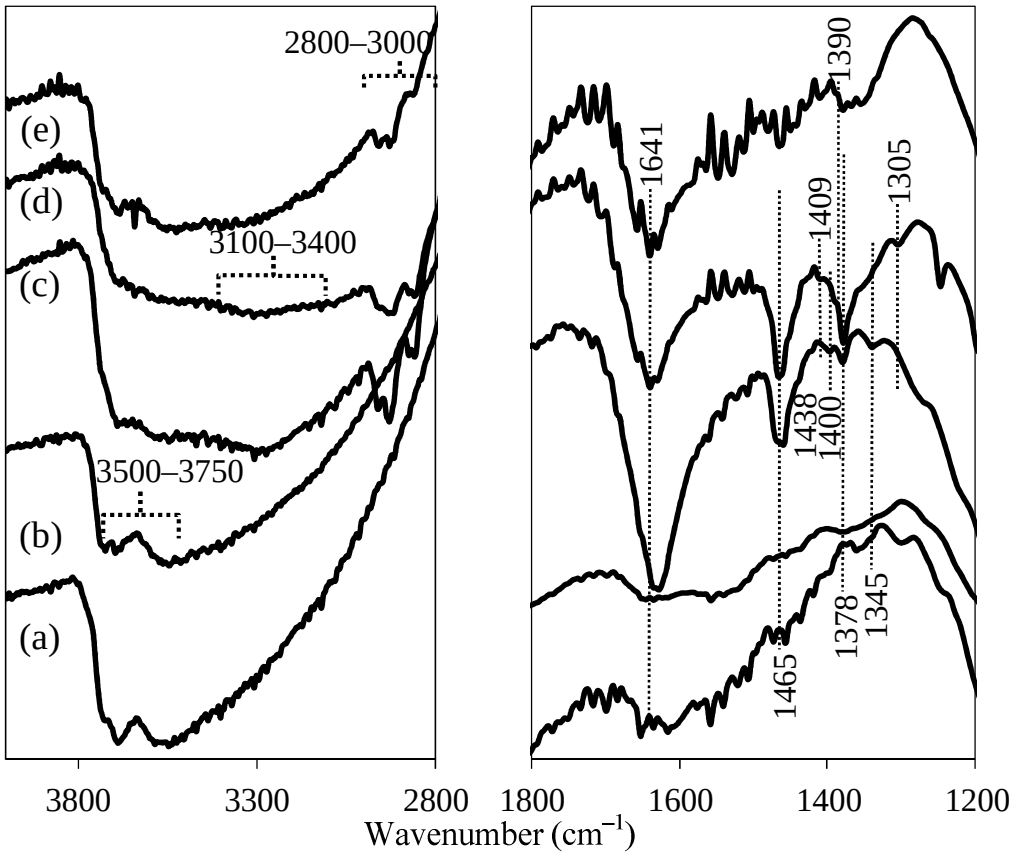

Figure V.5. *In situ* IR spectra (in transmission mode; Y-axis in transmittance-A.U.) of (a) calcined and pretreated TiO_2–Al_2O_3 (Ti:Al = 1:4.4) before treatment; (b) calcined and pretreated 10 wt% Ag/TiO_2–Al_2O_3 (Ti:Al = 1:4.4) before treatment; (c) TiO_2–Al_2O_3 (Ti:Al = 1:4.4) after treatment with MF-3 (thiophene + n-octane); (d) 10 wt% Ag/TiO_2–Al_2O_3 (Ti:Al = 1:4.4) after treatment with MF-3 (thiophene + n-octane); and (e) 10 wt% Ag/TiO_2–Al_2O_3 (Ti:Al = 1:4.4) after treatment with n-octane alone

V.3.4.2. Effect of aliphatic and aromatic sulfur species:

The IR spectra of calcined Ag/TiO_2–Al_2O_3 before and after individual treatments with MF-1 (1-C4T + C8), MF-2 (DES + C8), and MF-3 (T + C8) are shown in Figure V.6. The shift of hydroxyl groups from 3500–3750 cm^{-1} to 3100–3400 cm^{-1} was observed for MF-1 and MF-2 treated samples [119, 136]. Similar phenomenon was also observed for

MF-3 (T + C8) treated samples, as discussed before. In both Figure V.6(b) and V.6(c), bands were observed at 1641 and 1378 cm^{-1}, similar to Figure V.5(c), V.5(d), and V.5(e). These bands indicated that 1-C4T and DES molecules reacted with the surface sites as well. In the MF-1 (1-C4T + C8) treated sample spectrum (Figure V.6(b)), the adsorption of 1-C4T was evident from the bands at 1460 and 1296 cm^{-1}, representing the $\delta(-CH_2-)$ scissoring + $\delta(-CH_3)_{as}$ deformation and the $\delta(-CH_2-)$ wagging vibrations of methylene groups attached to sulfur atoms ($-CH_2-S-$), respectively [119, 123]. In 2007, Shimizu et al. had reported broad υ(S–H) bands at 2710 and 2600 cm^{-1} for samples treated with thiols [153]. The bands were absent in Figure V.6(b), implying that the sulfur molecule might have lost the hydrogen atom after reactive adsorption [147].

In the MF-2 (DES + C8) treated sample spectrum (Figure V.6(c)), the presence of adsorbed DES molecules was also confirmed via the bands at 1259 and 1460 cm^{-1} wavenumbers [119, 123, 154]. In this spectrum, the $\delta(-CH_2-S-)$ wagging vibration was observed at 1259 cm^{-1}, whereas the same vibration was observed at 1296 cm^{-1} in the 1-C4T treated sample spectra [119, 150]. The reason for this might be the decreased bonding strength between sulfur atoms and surface sites resulting from the change in position of S atoms in the molecules. There was an additional band at 1575 cm^{-1}, which has been associated with the vibrations of surface carboxylates (formiate or acetate or both) [150]. These carboxylates might have resulted from the reaction of DES molecules with surface attached hydroxyls, silver (I) oxide, or titanium oxide [119, 150].

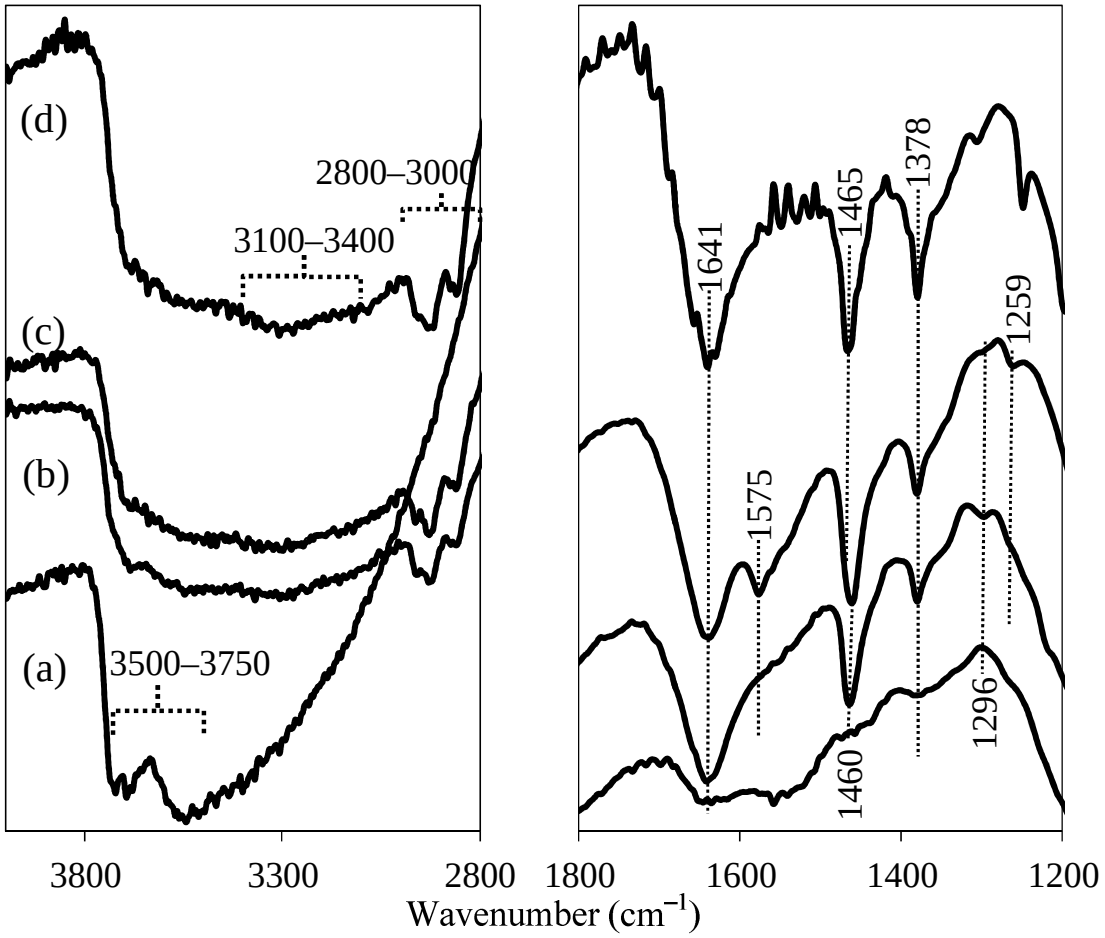

Figure V.6. *In situ* IR spectra (in transmission mode; Y-axis in transmittance-A.U.) of calcined and pretreated 10 wt% $Ag/TiO_2–Al_2O_3$ (Ti:Al = 1:4.4) (a) before treatment; (b) after treatment with MF-1 (1-butanethiol + n-octane); (c) after treatment with MF-2 (diethyl sulfide + n-octane); and (d) after treatment with MF-3 (thiophene + n-octane)

V.3.4.3. Effect of aromatic rings in sulfur species:

The $Ag/TiO_2–Al_2O_3$ adsorbent samples before treatment and after individual treatments with MF-3 (T + C8), MF-4 (BT + C8), and MF-6 (4,6-DMDBT + C8) treatments were analyzed via IR to observe the effect of aromatic rings in sulfur species (Figure V.7). The spectra in Figure V.7(b) and V.7(c) showed bands at 1378 and 1641 cm^{-1}, which were

similar to those in T treated sample spectrum. These bands indicated dissociated BT and 4,6-DMDBT on the adsorbent surface. However, the 1464 and 1641 cm^{-1} band intensities in the BT and 4,6-DMDBT treated sample spectra were lower than those in the T treated sample spectrum. The 1464 cm^{-1} band in Figure V.7(b) and V.7(c) was slightly red shifted as compared to that in Figure V.5(d), and might represent a combination of $–CH_2$ bending + antisymmetric $–CH_3$ deformation of aliphatic compounds and vibrations of aromatic ring [122, 124]. The MF-4 (BT + C8) and MF-6 (4,6-DMDBT +C8) treated sample spectra had bands at 1419 and 1438 cm^{-1} (perturbed $\delta(C=C)_s$ stretching vibrations of T ring), indicating presence of intact BT and 4,6-DMDBT molecules.

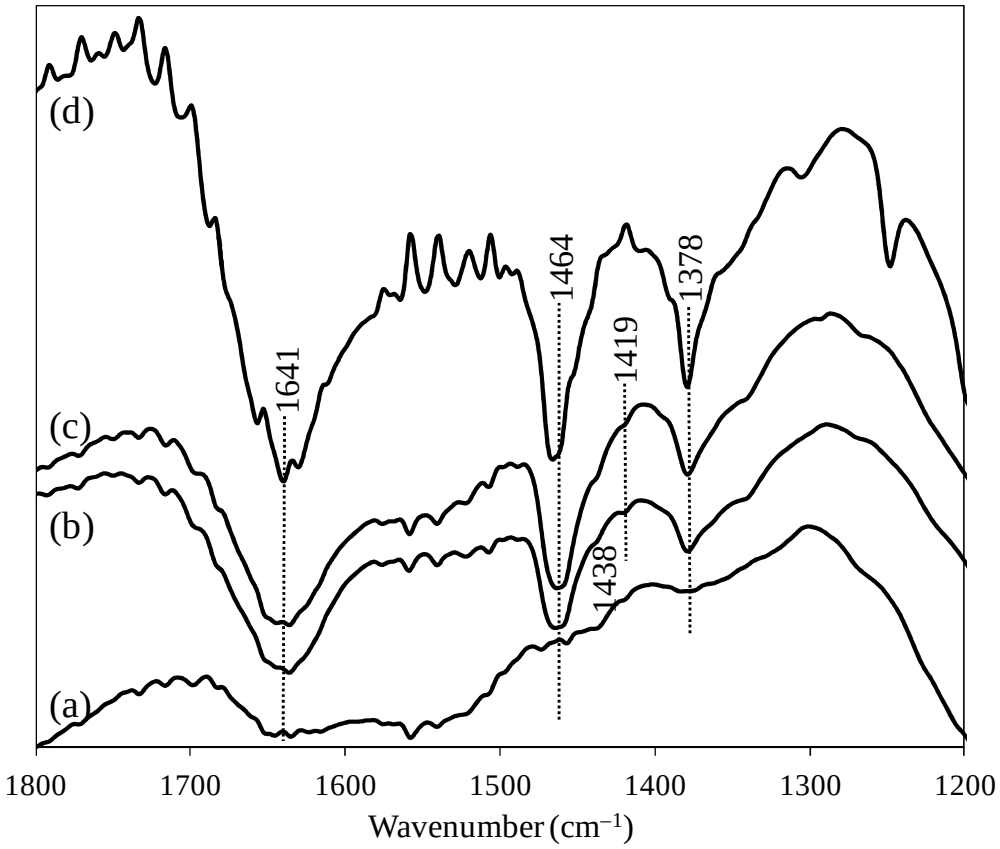

Figure V.7. *In situ* IR spectra (in transmission mode; Y-axis in transmittance-A.U.) of calcined and pretreated 10 wt% $Ag/TiO_2–Al_2O_3$ (Ti:Al = 1:4.4) (a) before treatment; (b)

after treatment with MF-6 (4,6-dimethyldibenzothiophene + n-octane); (c) after treatment with MF-4 (benzothiophene + n-octane); and (d) after treatment with MF-3 (thiophene + n-octane)

V.3.4.4. Effect of non-sulfur aromatics:

The effect of non sulfur aromatics on sulfur adsorption was investigated via IR and the resulting spectra of MF-4 (BT + C8), MF-5 (BT + benzene + C8), and MF-7 (benzene + C8) treated adsorbent samples are shown in Figure V.8. All the treated sample spectra exhibited bands at 1641 and 1378 cm^{-1}, which indicated dissociated products of BT, and possibly benzene. The MF-7 treated sample spectrum (Figure V.8(d)) showed a strong band at 1471 cm^{-1}, which has been ascribed to the perturbed δ(C=C) stretching vibrations of benzene rings [134, 155]. The band wavenumber was 15 cm^{-1} lower than that for the fundamental ring of gaseous benzene [123]. This implied that benzene was adsorbed on the adsorbent via π-interactions [134]. The intensity of the band showing intact benzene (1471 cm^{-1}) was higher than those of the other bands (e.g. 1378 and ~1641 cm^{-1}). Therefore, there was a significant amount of adsorbed benzene in intact form. In Figure V.8(b) and V.8(c), the shift of the band from 1464 (MF-4 treated sample) to 1470 cm^{-1} (MF-5 treated sample) was observed. This indicated that benzene competed and occupied the adsorption sites, thereby decreasing BT adsorption. This was supported by the results from breakthrough tests (section 3.3).

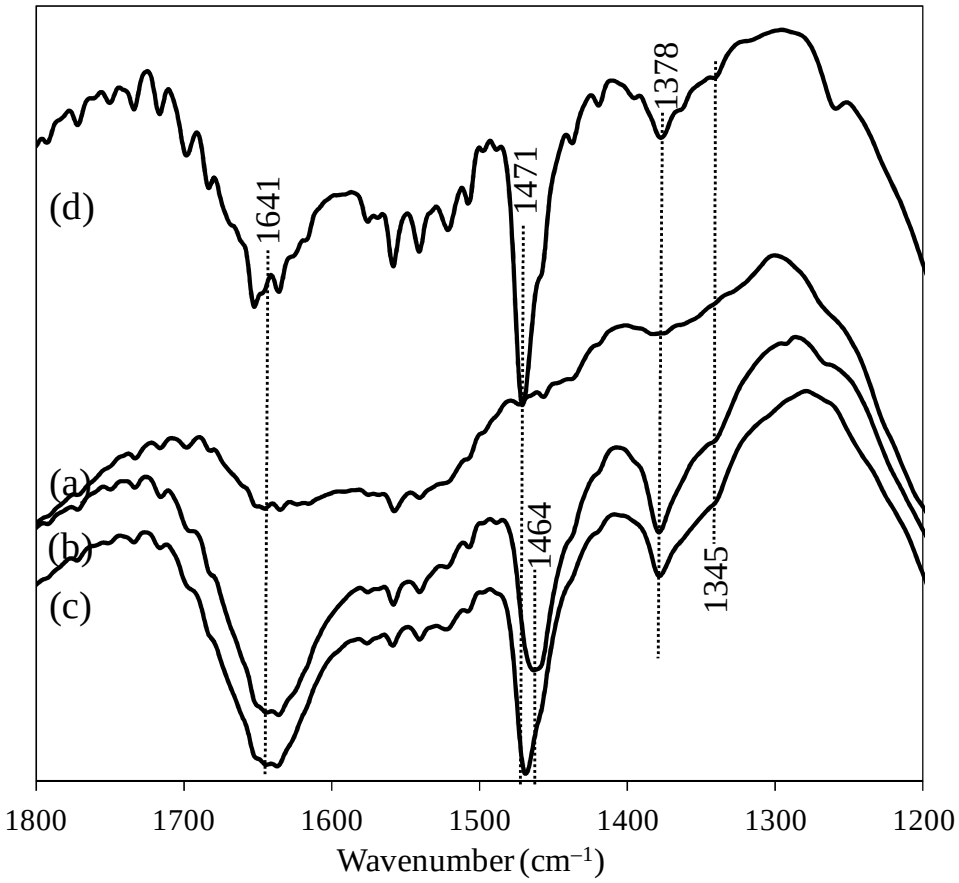

Figure V.8. *In situ* IR spectra (in transmission mode; Y-axis in transmittance-A.U.) of calcined and pretreated 10 wt% $Ag/TiO_2–Al_2O_3$ (Ti:Al = 1:4.4) (a) before treatment; (b) after treatment with MF-4 (benzothiophene + n-octane); (c) after treatment with MF-5 (benzothiophene + benzene + n-octane); (d) after treatment with MF-7 (benzene + n-octane)

Table V.6 IR bands and their respected assignments for calcined and pretreated adsorbents before and after treatment with different adsorbate molecules (The "×" symbols indicate observed bands for untreated and treated samples)

Wave-number	Assignments	T1 *	T2 *	T3 *	T4 *	T5 *	T6 *	T7 *	T8 *	T9 *	T10*
1259	$\delta(-CH_2-S-)$ wagging vibrations [119, 150]				×						
1296	$\delta(-CH_2-S-)$ wagging vibrations [119]			×							
1305	$\delta(-CH_2-)$ wagging vibrations of methylene groups [124]					×					
1345	COO^- symmetric stretch [122]						×	×	×		×
1378	$\delta(CH_3)_s$ bending vibrations [119]		×	×	×	×	×	×	×	×	×
1390	Perturbed $\delta(C=C)_s$ stretching vibrations of T ring [133, 134]					×					
1400	$\delta(C=C)_s$ stretching vibrations of T adsorbed on surface –OH groups [152]										×
1409	$\delta(C=C)_s$ stretching vibrations of T ring [123]					×					×
1419	$\delta(C=C)_s$ stretching vibrations [123]						×		×		
1438	Perturbed $\delta(C=C)_s$ stretching vibrations [130, 133]					×	×	×	×		×
1460	$\delta(-CH_2-)$ scissoring + $\delta(-CH_3)_{as}$ deformation [119, 123]			×	×						
1464	$-CH_2-$ bending + antisymmetric $-CH_3$ deformation of aliphatic compounds; or (C=C) vibrations of aromatic compounds with benzene rings [122, 124]						×		×		
1465	$-CH_2-$ bending + antisymmetric $-CH_3$ deformation of aliphatic compounds [122, 124]					×					×
1470	$-CH_2-$ bending + antisymmetric $-CH_3$ deformation of aliphatic compounds; or (C=C) vibrations of aromatic compounds with benzene rings [122, 124]							×			
1471	(C=C) vibrations of aromatic compounds with benzene rings [123, 134, 155]									×	
1575	Surface carboxylates (formiate/acetate) [150]				×						
2800–3000	–C–H stretching vibrations of aliphatic compounds [119, 133, 145, 150]		×	×	×	×	×	×	×	×	×
3100–3400	–OH stretching vibrations of perturbed surface hydroxyls [121, 135, 136]		×	×	×	×	×	×	×	×	×
3500–3750	–OH stretching vibrations [89, 103, 119]	×									

* T1: $Ag/TiO_2-Al_2O_3$, No treatment

T2: $Ag/TiO_2–Al_2O_3$+ n-octane

T3: $Ag/TiO_2–Al_2O_3$+ MF-1 (1-butanethiol + n-octane)

T4: $Ag/TiO_2–Al_2O_3$+ MF-2 (diethyl sulfide + n-octane)

T5: $Ag/TiO_2–Al_2O_3$+ MF-3 (thiophene + n-octane)

T6: $Ag/TiO_2–Al_2O_3$+ MF-4 (benzothiophene + n-octane)

T7: $Ag/TiO_2–Al_2O_3$+ MF-5 (benzothiophene + benzene + n-octane)

T8: $Ag/TiO_2–Al_2O_3$+ MF-6 (4,6-dimethyldibenzothiophene + n-octane)

T9: $Ag/TiO_2–Al_2O_3$+ MF-7 (benzene + n-octane)

T10: $TiO_2–Al_2O_3$ + MF-3 (thiophene + n-octane)

V.4. Conclusions

Organosulfur adsorption pathways onto $Ag/TiO_2–Al_2O_3$ adsorbent were investigated using breakthrough experiments and IR spectroscopy. In the breakthrough tests at ambient conditions, the mesoporous $Ag/TiO_2–Al_2O_3$ adsorbent (10 wt% Ag, Ti:Al = 1:4.4 by weight) had saturation capacities of 11.83, 8.01, and 10.9 mg S/g adsorbent for challenge JP5, JP8, and ORD (initial sulfur contents of 1172, 630, and 452 ppmw, respectively). The breakthrough capacities for 1-C4T and DES sulfur species were higher than that for T. IR spectra of adsorbents samples treated with sulfur aromatics revealed significant amount of dissociated products on the mixed oxide supported silver adsorbent. The surface acid sites, primarily surface hydroxyl groups were responsible for executing ring opening reactions of chemisorbed thiophene derivatives (T, BT, and 4,6-DMDBT) and for producing aliphatic like species. The reactive adsorption of aliphatic 1-C4T and DES on the acidic material was also evident from IR analysis. The presence of non-sulfur aromatics (e.g. benzene) reduced the sulfur adsorption capacity by competing and

occupying the sulfur adsorption sites. The adsorption sites added by silver incorporation were primarily affected by the presence of aromatic compounds, possibly due to the competitive adsorption via π-interactions. This was confirmed by both breakthrough experiments and IR spectroscopy. The sulfur affinity of silver along with the surface acidity of TiO_2–Al_2O_3 supports enabled enhanced organosulfur adsorption and made the adsorbent efficient in desulfurizing diversified compositions of hydrocarbon fuels. This work also provided insights on the sulfur adsorption and reaction mechanisms using acidic metal oxides at ambient conditions. Further investigations will be focused on the characterization of silver based adsorbents to determine the surface acidity and molecular simulations for estimating adsorption energies.

VI. Density Functional Theory Study of Organosulfur Selective Adsorption on $Ag–TiO_2$ Adsorbents

Abstract:

$Ag–TiO_2$ adsorbents have pronounced capacity for selective removal of organosulfur compounds from complex fuel mixtures. Computational calculations were performed to investigate the nature of this pronounced selectivity as well as to study the adsorbent structure. A cluster model was developed for this study. Geometry optimization, frequency analysis and single-point energy calculations were carried out using density functional theory (B3LYP/6-31G(d)(ECP=SDD(Ag,Ti))//B3LYP/LANL2DZ). The computed adsorption energies included dispersion terms (GD3) and were corrected for basis set superposition errors (BSSE). Silver spontaneously incorporated to anatase-TiO_2 clusters, and with greater preference in the presence of –OH groups. Adsorption energies were calculated for sulfur containing species (thiophene, benzothiophene, dibenzothiophene, 4,6-dimethyldibenzopthiophene) and non-sulfur aromatics (quinoline, benzofuran, naphthalene, benzene) typically present in fuel mixtures. Calculated adsorption energies are consistent with the selective binding of organosulfur compounds through the Ag atom of the $AgTi_6O_8(OH)_8$ cluster rather than the –OH groups of the titania analog. The adsorption orientation of organosulfur compounds was π-preferred. Heterocycles with more aromatic rings were adsorbed more strongly. Organonitrogen compounds (i.e., quinoline) showed the strongest adsorption. Results from equilibrium

saturation adsorption experiments were also compared with DFT calculations and the trends and selective separation factors were shown to be in good agreement.

VI.1. Introduction

Desulfurization of logistic and commercial hydrocarbon fuels is an essential step in fuel processing for both environmental concerns [156, 157] and fuel cell applications [102, 108]. To produce ultra low sulfur fuels, adsorptive desulfurization is being investigated as a viable supplement to the conventional hydrodesulfurization (HDS) process [27, 69, 108]. Adsorptive desulfurization is promising for its low energy requirements and scalability to small size [156]. The adsorbents used in the process must have high selectivity toward refractory sulfur heterocycles [27]. Supported and unsupported silver–titania adsorbents have demonstrated regenerable organosulfur adsorption capacities from hydrocarbon fuels such as jet fuels and diesels [69, 110, 158]. Supported Ag–TiO_2 adsorbents were able to selectively remove sulfur down to parts per billion (ppbw) levels [110] and were effective even when the ratio of non-sulfur to sulfur aromatics was more than 25000:1. These adsorbents have shown efficacy in removing organosulfur compounds, nonetheless very little is known about the role and structure of Ag in the adsorbent and/or the selective nature of the adsorption mechanism. The affinity of Ag toward organosulfur compounds depends on the position of Ag in a support matrix and on Ag particle sizes. Therefore, it is important to understand how Ag is incorporated into the surfaces of high surface area TiO_2 supports and the significance of defect sites and surface –OH groups.

Sulfur selectivity is a vital criterion for an effective adsorbent. It is known that petroleum-based fuels are a mixture of various organic compounds ranging from simple

straight chain hydrocarbons to complex aromatic molecules with various functional groups. In addition to organosulfur compounds, typical fuel mixtures have much higher concentrations of other aromatic hydrocarbons and organonitrogen and organooxygen compounds. These compounds will compete with organosulfur compounds for active sites. Therefore an effective adsorbent should have high organosulfur affinity and selectivity.

In order to develop a fundamental understanding of sulfur selectivity, a comparison of experimental adsorptive desulfurization performance and computational investigation is warranted. Adsorption energy is an ideal indicator in the sulfur selectivity study [159, 160]. It can differentiate the strength of various adsorption sites. For estimating adsorption energy, density functional theory (DFT) is a very popular method. DFT is a quantum mechanical technique for calculating optimized geometries and energies. It is an efficient tool, especially for transition metals, and can be used with an Effective Core Potentials (ECP) representation of the core electrons [68]. Researchers have previously reported DFT studies of adsorption on anatase-TiO_2 [160, 161] and rutile-TiO_2 [162]. DFT calculations were also used to investigate optical properties [163] and photocatalytic activities [164] of Ag–TiO_2 materials. Other researchers have employed DFT techniques in investigating thiophene adsorption on π-complexation adsorbents [45, 55, 68] and thiophene incorporation during HDS reactions [165]. A similar adsorption modeling of Ag–TiO_2 adsorbents with DFT would be beneficial for a better design of selective organosulfur adsorbents.

Here we present a DFT study to investigate the sulfur selectivity of Ag–TiO_2 to provide an accurate description of the adsorption phenomena. In addition, we also investigate the

adsorption energies of organosulfur compounds to the surface hydroxyl groups on the TiO_2 cluster and compare these with experimental equilibrium saturation capacities. Separation factor values of Ag–TiO_2 are also presented in order to test its ability as an effective commercial adsorbent.

VI.2. Experimental and Computational Methodologies:

VI.2.1. Adsorption experiments:

Equilibrium saturation experiments were carried out for calculating saturation capacities. The Ag/TiO_2–Al_2O_3 (Ti:Al = 1:4.4 by weight, 10 wt% Ag loading) adsorbent was used for this study. The adsorbent preparation steps have been mentioned in section II.1. For saturation experiments, the adsorbent was treated with model fuel consisting of different sulfur (T, BT, DBT, 4,6-DMDBT) compounds in n-octane (C8). The sulfur compounds were dissolved into C8 individually where the concentration was 1000 ppmw S in each case. The fuels have been discussed in detail in section II.2. In every saturation test, the fuel to adsorbent ratio was 20 ml/g. The experimental procedures and the capacity calculation methods are described in section II.3.1. For analyzing sulfur concentration, the fuels were measured in an Antek 9000S total sulfur analyzer.

VI.2.2. DFT calculations:

Geometry optimizations, frequency analysis, and single-point energy calculations were undertaken using DFT methods. All the calculations were carried out using the Gaussian 09 software package on computers located at the Alabama Supercomputer (ASC) Facility. The models were constructed using Gaussview (version 5.0) and Molden at Auburn University. Geometry optimizations were performed at the B3LYP level with

LANL2DZ basis sets. B3LYP is a hybrid DFT method [166]. It is the combination of Becke gradient corrected exchange functional and Lee-Yang-Parr correlation functional [166, 167] that can effectively provide parameters for metal-ligand interactions. LANL2DZ is a double-ζ basis set with ECP [168]. ECP are used to represent the core electrons for post third row atoms. It can substantially reduce computation time with almost no effect on the results since the core electrons are assumed to have a minor effect on adsorption. After optimization, the geometries were subjected to frequency analysis using B3LYP/LANL2DZ. Frequency analysis was carried out to verify whether the geometries were at true minima on the potential energy surface. This was followed by single-point energy calculations using B3LYP. For energy calculations, the 6-31G(d) basis set was used for all non-metal atoms; whereas the Stuttgart effective core potential (SDD) was used to replace the core electrons of all metal atoms (Ti and Ag). Therefore, the single-point energies were calculated at the B3LYP/[6-31G(d)+SDD] level on structures optimized at the B3LYP/LANL2DZ level. An empirical dispersion term "GD3" was added in the single-point energy calculations in order to include dispersion effects. The dispersion term employs structure (coordination number) dependent dispersion coefficients that are based on first principles calculations. It provides more reliable binding energies and is particularly useful for systems with metals [169]. The natural population analysis (NPA) charges were also calculated and discussed.

VI.2.3. Binding and adsorption energy:

Binding energies were calculated to study the Ag incorporation and –OH generation mechanism on the TiO_2 clusters. Adsorption energies were calculated for various sulfur and non-sulfur aromatics. Thiophene (T), benzothiophene (BT), dibenzothiophene

(DBT), and 4,6-dimethyldibenzothiophene (4,6-DMDBT) were used as sulfur aromatics whereas benzene (C6) and naphthalene (C10) were used as non-sulfur aromatics. To compare the organosulfur compounds with the organonitrogen and organooxygen compounds, quinoline and benzofuran were employed. The following equation was employed for calculating the adsorption energy (E_{ads}):

$$E_{adsorption} = E_{adsorbent\text{-}adsorbate} - (E_{adsorbent} + E_{adsorbate})$$

Where, $E_{adsorbent\text{-}adsorbate}$, $E_{adsorbent}$ and $E_{adsorbate}$ are the energies of adsorbent-adsorbate system, free adsorbent, and free adsorbate, respectively. A more negative value of E_{ads} corresponds to a stronger adsorption. Solvent effects were not taken into account since the adsorption usually takes place in a non-aqueous environment where the effect of polarity and polarizability is negligible. Since these were non-covalent interactions, the E_{ads} values were corrected for Basis Set Superposition Errors (BSSE). The counterpoise correction (CP) [170] method was employed to calculate the BSSE for adsorbent-adsorbate interactions [171]. In our work, the range of BSSE was between 12–26 kJ/mol. Since the CP method overestimates the BSSE, the final energies were calculated by taking an average of the BSSE corrected and uncorrected adsorption energies [172]. The details regarding BSSE corrections can be found elsewhere [172]. The BSSE correction was not included in the Ag and H_2O binding energy calculations. Zero-point corrections of the energies were not calculated since our objective was to qualitatively investigate the adsorbent selectivity through the adsorption energies.

VI.2.4. Separation factor:

Separation factors (α_{21}) were calculated from adsorption energies [45]. The following formula was used to determine α_{21}:

$$\alpha_{21} = \frac{X_2/X_1}{Y_2/Y_1}$$

where X and Y are mole fractions in the adsorbed and solution phases, respectively. In the current work, subscripts 1 and 2 corresponded to non-sulfur aromatics (benzene) and organosulfur/organonitrogen/organooxygen compounds, respectively. For the lowest estimate of α_{21}, Henry's law was assumed for the isotherms of adsorbate compounds. The Henry constant is approximately proportional to $e^{-E/RT}$, where E is the adsorption bond energy. This was assumed since non-sulfur aromatics are usually at higher concentrations in the fuels; therefore X_1 is much smaller than that estimated from Henry's law. Low concentrations of the solute and high concentrations of the solvent were also assumed in α_{21} calculations.

VI.3. Results and Discussion:

VI.3.1. Effect on different sulfur compounds on equilibrium saturation capacity:

Desulfurization experiments were carried out to investigate the effect of various sulfur heterocycles on sulfur adsorption capacity and to compare with the computational results. Figure VI.1 shows the saturation capacities of neat and Ag supported TiO_2 adsorbents for model fuels with T, BT, DBT, and 4,6-DMDBT. In terms of saturation capacity, the order from high to low was DBT>4,6-DMDBT>BT>T. The addition of benzene rings resulted in higher adsorption capacity. This has been attributed to the π-electron cloud of benzene rings which might have assisted in raising the negative charge density of adsorbate molecules and consequently increasing adsorption energy. Therefore, the increase in aromaticity had a beneficial effect on adsorption. The selectivity order of Ag–TiO_2 adsorbent makes it ideal as a polishing agent since the thiophenic molecules are more

refractory to HDS process. However, the adsorption capacity for 4,6-DMDBT was lower than DBT since the attached methyl groups created a steric hindrance to adsorption onto silver [17]. The trend was also consistent with the continuous adsorption experiments [72].

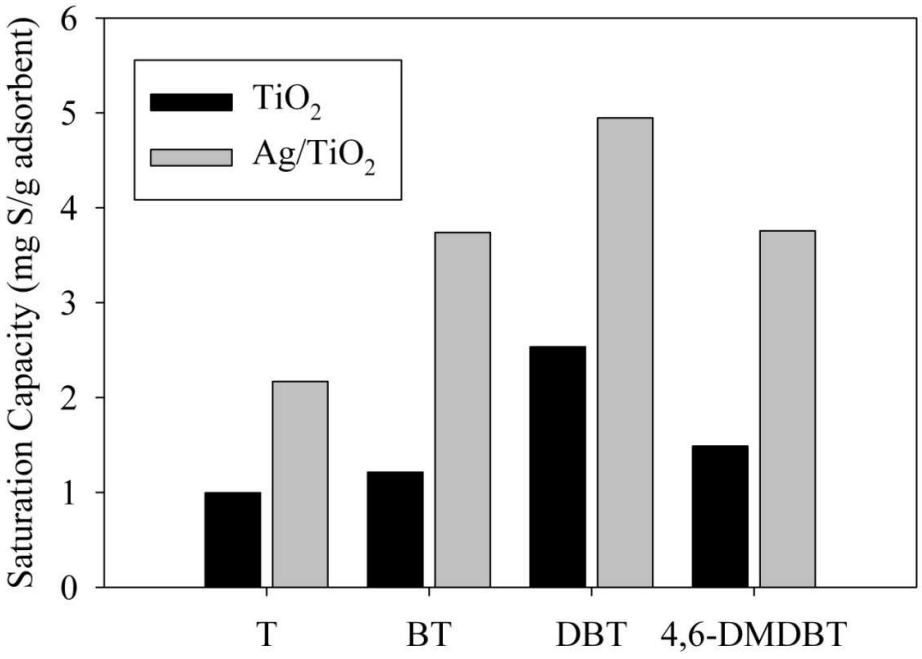

Figure VI.1. Equilibrium saturation capacities acquired from saturation experiments (adsorbents: TiO_2 and 4 wt% Ag–TiO_2, duration: 48 hours, fuel to adsorbent ratio: 20 ml/g, initial sulfur concentration in model fuel: 1000 ppmw S)

VI.3.2. Model construction for DFT calculations:

We constructed different models in order to simulate supported and unsupported TiO_2 and Ag–TiO_2 based on the adsorbent characterization results reported previously (chapter IV) [137] In both unsupported and supported Ag–TiO_2, the anatase phase of TiO_2 was shown to have higher capacity and the ability to effectively disperse Ag (chapter IV) [137]. The oxidation state of Ag was measured to be +1, as seen from electronic spin

resonance (ESR) and x-ray absorption spectroscopy (EXAFS) studies [71, 137]. EXAFS studies further revealed that the Ag–O coordination number was 4 and the Ag–O bond distance was 2.32 Å [137]. Ag–Ag or Ag–Ti interactions were not seen within 3 Å. The supported Ag–TiO_2 adsorbent was analyzed via X-ray diffraction (XRD), where the diffractograms did not show any Ag or Ag oxide peaks. It indicated that silver was present as nanosized or even smaller sized particles (chapter IV). We also carried out infrared (IR) studies on the neat and Ag supported adsorbents and found –OH signatures in both (chapter IV). Changes in –OH bands were also observed in the IR spectra of adsorbents after Ag impregnation (chapter IV). Therefore, the –OH groups are closely associated with Ag.

Based on these observations, the neat and silver supported titania clusters were constructed. The overall size of each cluster was below 10 Å. The clusters were relaxed and were assumed to be free of contaminants. It was assumed that the Al_2O_3 and SiO_2 supports used in the supported Ag–TiO_2 adsorbents [110] would have minimal effect on organosulfur adsorption and therefore were not included in the DFT calculations. For representing anatase TiO_2 without any defect site, a small cluster consisting of six Ti atoms was constructed ($Ti_6O_9(OH)_6$). Additional hydroxyl groups were included to neutralize the edge effects. T[70]o construct the Ag supported cluster, $Ti_6O_9(OH)_6$ was incorporated with a neutral Ag atom. One Ag atom was placed between four oxygen atoms ($AgTi_6O_9(OH)_6$). The geometrically optimized neat and Ag supported TiO_2 clusters (without any defects) are shown in Figure VI.2. All the structures had neutral charge with singlet multiplicity, except for the Ag supported clusters which had neutral charge with doublet multiplicity. Ag^0 was employed in the cluster construction instead of Ag^+ since

metallic Ag usually results from the thermal decomposition of $AgNO_3$ (Ag precursor for $Ag–TiO_2$ adsorbent). This was also confirmed from the EXAFS studies [137]. The Ti coordination number in these clusters was 4. Four coordinated Ti are more active than five or six coordinated Ti [173], and are usually more available at the surface than in the bulk and Ag incorporation is a surface phenomenon in our case. The effect of Ag impregnation on the titania cluster was evaluated by calculating the binding energy. The following mechanism was assumed for Ag incorporation:

$$Ti_6O_9(OH)_6 + Ag \xrightarrow{E_{b_0}} AgTi_6O_9(OH)_6$$

$$\text{where, } E_{b_0} = E_{AgTi_6O_9(OH)_6} - (E_{Ti_6O_9(OH)_6} + E_{Ag})$$

Here E_{b_0} represents the binding energy of Ag incorporation. The structure energies were acquired by means of calculating the single-point energies of the geometrically optimized structures, as described in section 2.2. The value of E_{r_0} was calculated to be –24.6 kJ/mol. The negative value indicated that the incorporation reaction was exothermic.

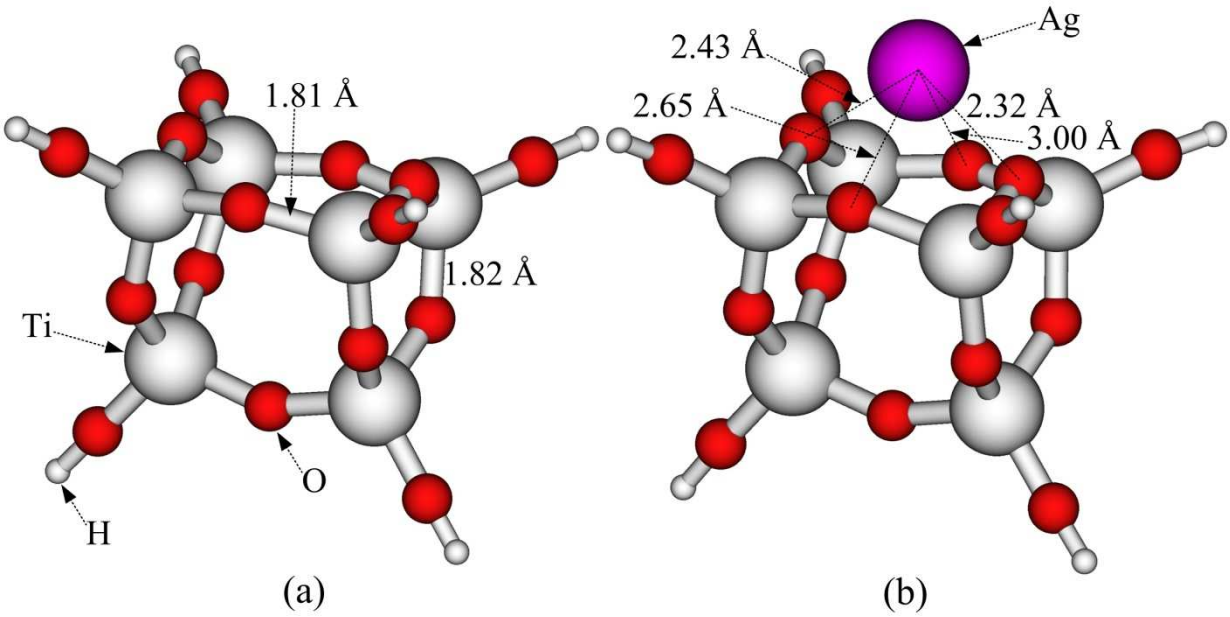

Figure VI.2. Geometrically optimized structures of (a) $Ti_6O_9(OH)_6$ and (b) $AgTi_6O_9(OH)_6$ (with no –OH group)

The clusters discussed earlier contained TiO_2 with no defect site or –OH group. Here, –OH groups were introduced to the $Ti_6O_9(OH)_6$ cluster to investigate the consequent effect in Ag incorporation and organosulfur adsorption. This was carried out by interacting the cluster with H_2O. It is well known that anatase TiO_2 can dissociate H_2O to form –OH groups upon adsorption [174]. After H_2O adsorption, new –OH groups were formed ($Ti_6O_8(OH)_8$). The optimized clusters with bridged –OH groups are shown in Figure VI.3. Some of the bond distances are also shown in Figure VI.3. Silver was impregnated on the hydroxylated cluster through a similar procedure as before. The overall water/silver incorporation steps can be shown as follows:

$$Ti_6O_9(OH)_6 + H_2O \xrightarrow{E_{b_1}} Ti_6O_8(OH)_8 \text{ (Two bridged –OH)}$$

$$Ti_6O_8(OH)_8 + Ag \xrightarrow{E_{b_2}} AgTi_6O_8(OH)_8$$

where, $E_{b_1} = E_{Ti_6O_8(OH)_8} - (E_{Ti_6O_9(OH)_6} + E_{H_2O})$

$$E_{b_2} = E_{AgTi_6O_8(OH)_8} - (E_{Ti_6O_8(OH)_8} + E_{Ag})$$

Here E_{b_1} and E_{b_2} represent the H_2O and Ag binding energies, respectively. The E_{b_1} and E_{b_2} values were calculated to be -72.6 and -69.9 kJ/mol, respectively. The values indicated that the incorporation mechanism was likely to be spontaneous. In addition, Ag incorporation with a hydroxylated titania cluster resulted in an almost three times increase in negative binding energy as compared to a non-hydroxylated cluster. Therefore, –OH groups greatly facilitated Ag incorporation. It should be noted that the present results did not take into account solvent effects. Nevertheless, the results qualitatively indicated that Ag impregnation results in the formation of a highly active adsorbent. The Ti–O calculated distances of the bridged hydroxyls were 2.02 Å, somewhat longer than typical Ti–O bonds in anatase (ca. 1.93-1.97 Å [175]), while the other calculated Ti-O distances were about 1.81 Å which were shorter than observed in anatase. The position of Ag in $AgTi_6O_8(OH)_8$ was almost similar to that in $AgTi_6O_9(OH)_6$. The Ag–O bond distances were between 2.33–3.01 Å, which were close to the experimental bond distance of 2.32 Å [137]. In $AgTi_6O_8(OH)_8$, the Ti–O bond distances of bridged hydroxyl groups increased to 2.19 and 2.13 Å.

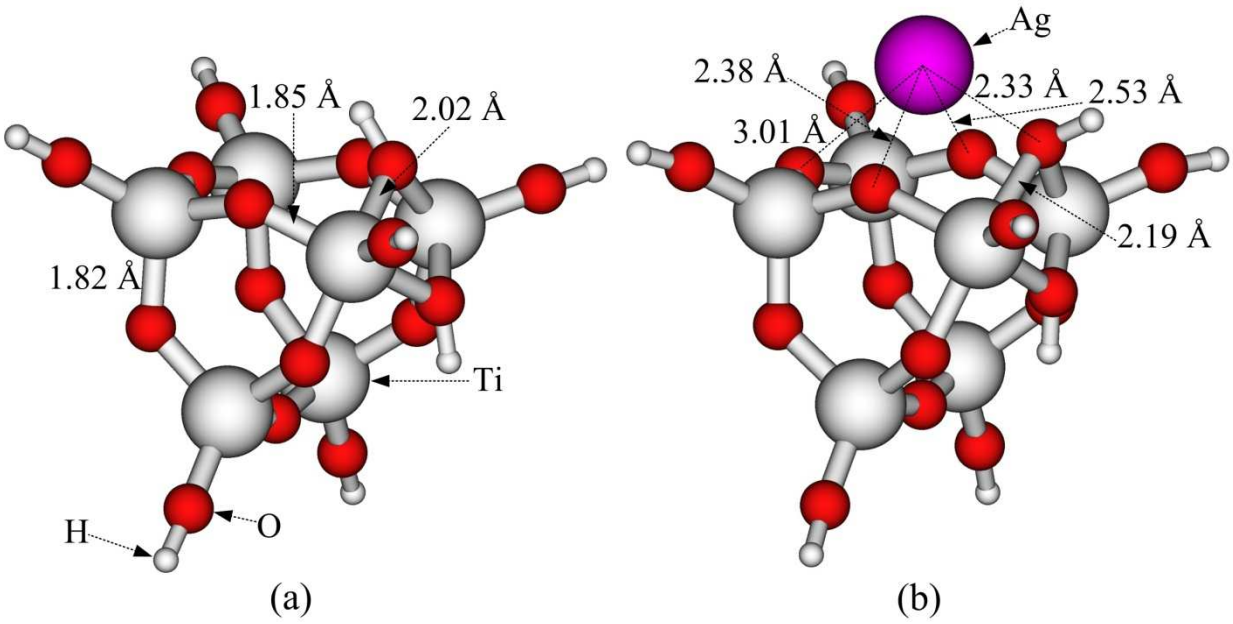

Figure VI.3. Geometrically optimized structures of (a) $Ti_6O_8(OH)_8$ and (b) $AgTi_6O_8(OH)_8$ with two bridged –OH groups

In the structures discussed earlier, two bridged –OH groups were formed after H_2O incorporation. Calculations were carried out for the structures where two single –OH groups were formed after H_2O incorporation. The $Ti_6O_8(OH)_8$ (with two single –OH groups) and the corresponding $AgTi_6O_8(OH)_8$ structures are shown in Figure VI.4. The binding energies were calculated for the following mechanisms.

$$Ti_6O_9(OH)_6 + H_2O \xrightarrow{E_{b_1}'} Ti_6O_8(OH)_8 \text{ (Two single –OH)}$$

$$Ti_6O_8(OH)_8 + Ag \xrightarrow{E_{b_2}'} AgTi_6O_8(OH)_8$$

where, $E_{b_1}' = E_{Ti_6O_8(OH)_8} - (E_{Ti_6O_9(OH)_6} + E_{H_2O})$

$E_{b_2}' = E_{AgTi_6O_8(OH)_8} - (E_{Ti_6O_8(OH)_8} + E_{Ag})$

The values of E_{b_1}' and E_{b_2}' were calculated to be -38.1 and -66.1 kJ/mol, respectively. Although both binding energies were negative, these were less negative than those with

bridged –OH groups. Therefore, the Ag–TiO_2 structures with bridged –OH groups were observed to be more stable. Optimization was also carried out for a structure consisting of one bridged and one single –OH groups. However, the bridged –OH group was transformed to single –OH group after optimization.

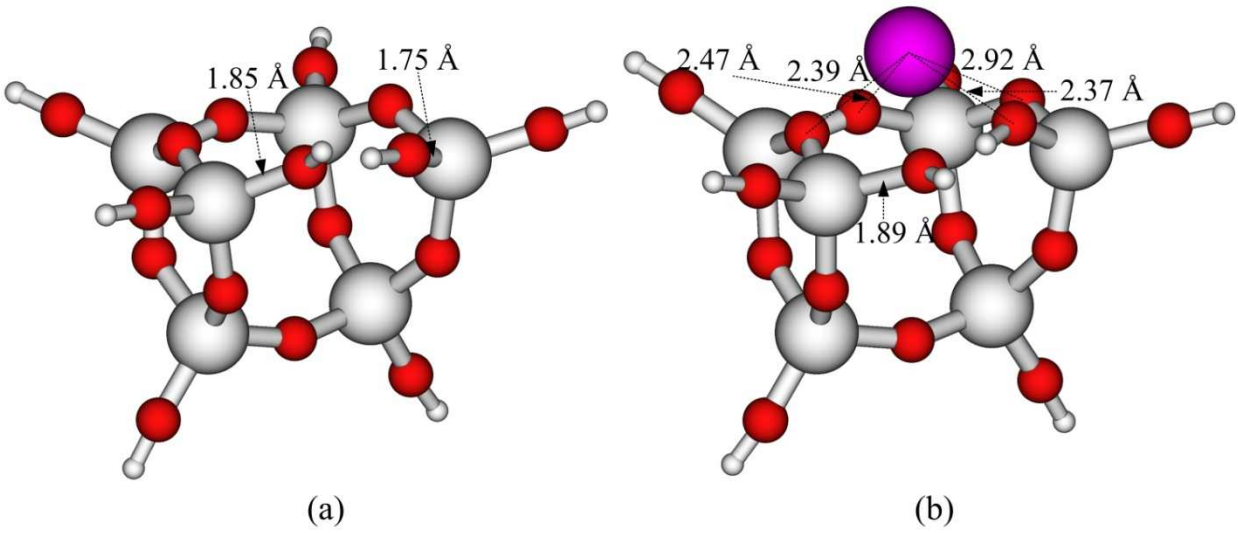

Figure VI.4. Geometrically optimized structures of (a) $Ti_6O_8(OH)_8$ and (b) $AgTi_6O_8(OH)_8$; each with two single –OH groups

VI.3.3. Adsorption energy calculation and selectivity comparison:

VI.3.3.1. Difference between neat and silver supported clusters:

The E_{ads} of T and BT on neat and silver supported clusters were calculated and are summarized in Table VI.1. Both uncorrected and average BSSE corrected E_{ads} values are included. The optimized structures of T and BT adsorbed on both $Ti_6O_8(OH)_8$ and $AgTi_6O_8(OH)_8$ (each with bridged –OH groups) are shown in Figure VI.5 and Figure VI.6. The orientation of each was such so that the organosulfur molecules would adsorb through the S atoms (with a –OH group for $Ti_6O_8(OH)_8$ and with the Ag for $AgTi_6O_8(OH)_8$). For both T and BT, we can see that $AgTi_6O_8(OH)_8$ had more negative

adsorption energies than $Ti_6O_8(OH)_8$, further confirming the sulfur affinity of silver. This was also in accord with the sulfur adsorption capacities of neat and silver supported TiO_2 and TiO_2–Al_2O_3 (chapter IV). However, the hydroxyl groups can act as secondary adsorption sites for sulfur heterocycles. In a desulfurization process, organosulfur compounds can be adsorbed on the –OH groups once all active Ag sites are occupied. This can also be supported by the curved breakthrough characteristics of the adsorbent for commercial and logistic fuels [158]. The Ag–O bond distances were changed after sulfur adsorption, as shown in the figures.

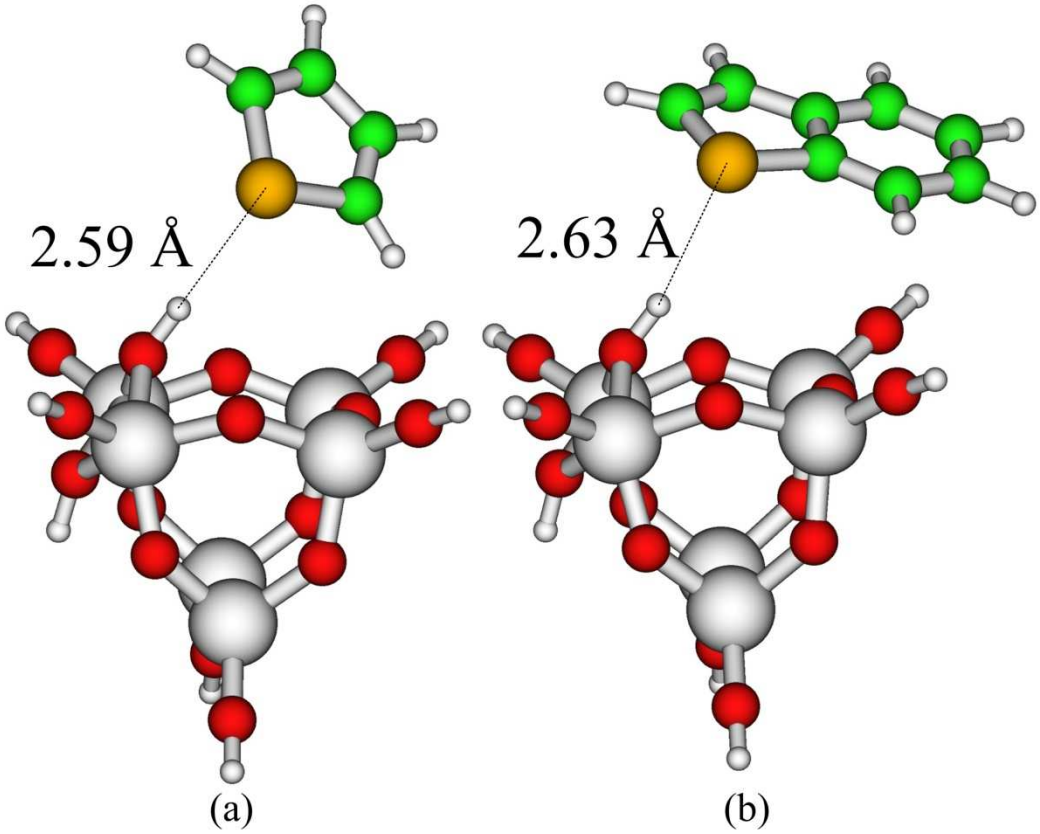

Figure VI.5. Geometrically optimized structures of (a) thiophene adsorbed on $Ti_6O_8(OH)_8$ (with bridged OH groups and (b) benzothiophene adsorbed on $Ti_6O_8(OH)_8$

(with bridged OH groups). Avg. BSSE corrected energy: (a) -34.1 kJ/mol; (b) -54.4 kJ/mol

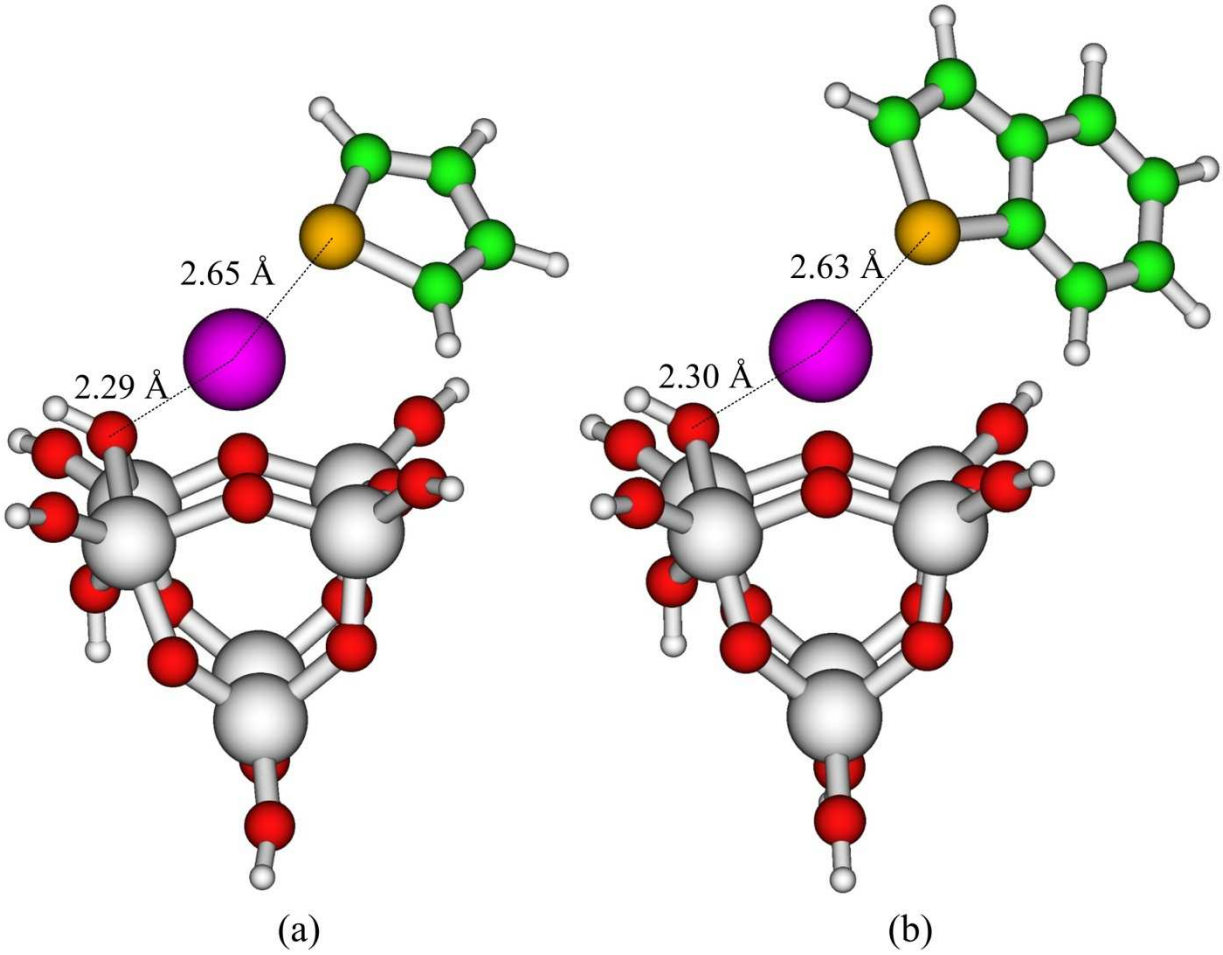

Figure VI.6. Geometrically optimized structures of (a) thiophene adsorbed on $AgTi_6O_8(OH)_8$ (S–Ag interaction) and (b) benzothiophene adsorbed on $AgTi_6O_8(OH)_8$ (S–Ag interaction); the clusters consisted of bridged –OH groups. Avg. BSSE corrected energy: (a) –98.0 kJ/mol; (b) -104.7 kJ/mol

The E_{ads} of T adsorption on the $Ti_6O_8(OH)_8$ and $AgTi_6O_8(OH)_8$ clusters with single –OH groups were also calculated using DFT methods. The adsorption orientations were S–H

for T–$Ti_6O_8(OH)_8$ and S–Ag for T–$AgTi_6O_8(OH)_8$. The optimized structures are shown in Figure VI.7 and the calculated adsorption energies are summarized in Table VI.1. T adsorption on clusters with single –OH groups were weak, as compared to that on clusters with bridged –OH groups. Therefore, the clusters with bridged –OH groups were more stable as well as had stronger affinity for organosulfur compounds. These clusters were therefore used in further studies.

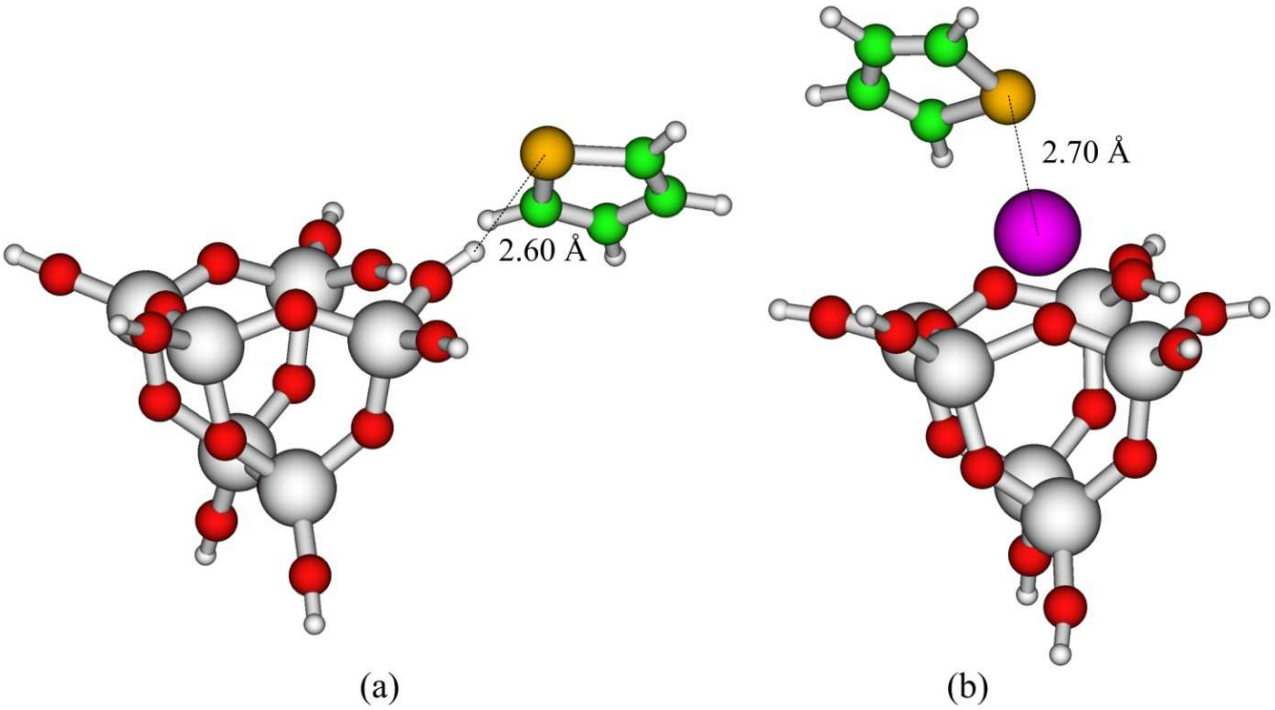

Figure VI.7. Geometrically optimized structures of (a) thiophene adsorbed on $Ti_6O_8(OH)_8$ (S–H interaction) and (b) thiophene adsorbed on $AgTi_6O_8(OH)_8$ (S–Ag interaction); the clusters consisted of single –OH groups. Avg. BSSE corrected energy: (a) -27.1 kJ/mol; (b) -77.4 kJ/mol

VI.3.3.2. Difference in π–Ag and S–Ag bonding:

To distinguish between the π–Ag and S–Ag interactions, T and BT were each adsorbed on $AgTi_6O_8(OH)_8$ through two initial orientations: one with the S atom close to Ag, and

the other one with the ring close to Ag. Multiple trials were carried out to determine the π–Ag and S–Ag orientations which would result in the strongest adsorptions. The corresponding energies are summarized in Table VI.1 and the optimized structures are shown in Figure VI.6 and Figure VI.8. The results indicated that the π–Ag interactions were stronger than S–Ag. This result supported our previous observations in infrared studies demonstrating π-bond between Ag and T (chapter IV). The bond distances between Ag and organosulfur molecules were also smaller for π–Ag than those for S–Ag. We also attempted to interact T and BT with $Ti_6O_8(OH)_8$ through π–H. However, the organosulfur molecules reoriented to S–H after geometry optimization.

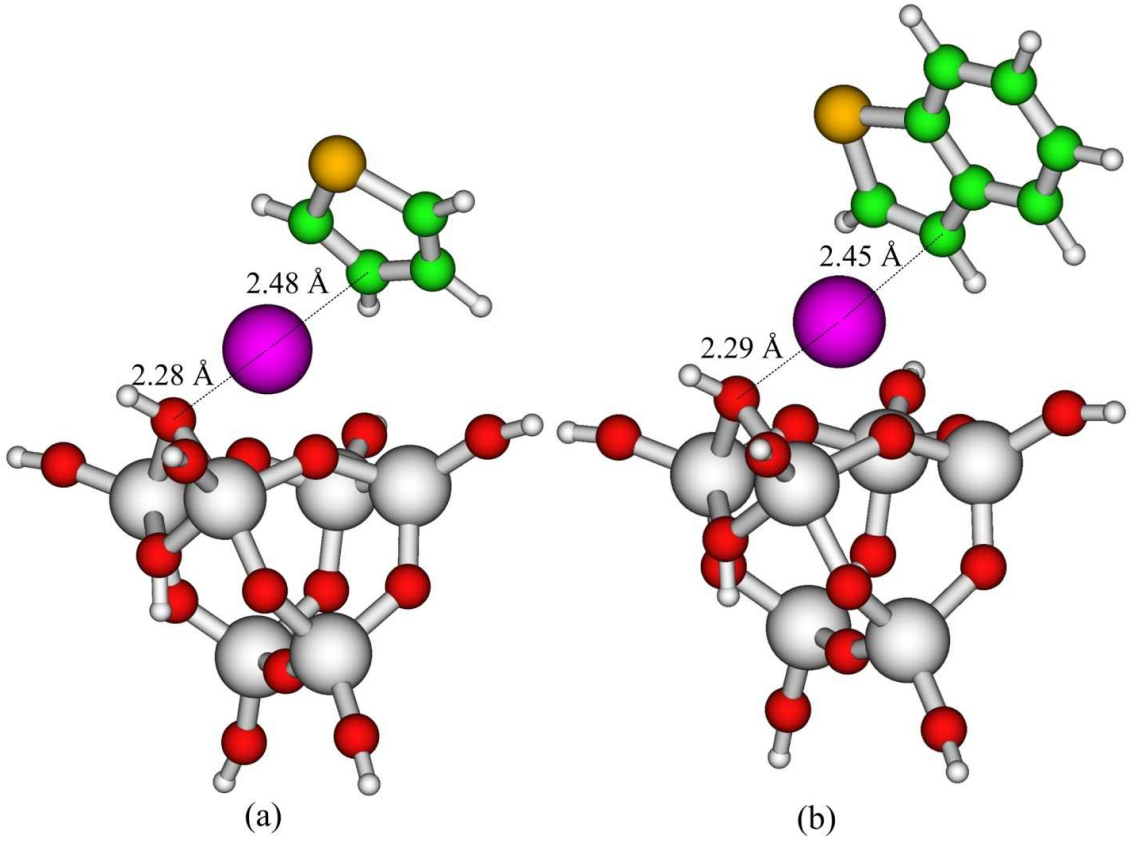

Figure VI.8. Geometrically optimized structures of (a) thiophene adsorbed on $AgTi_6O_8(OH)_8$ (π–Ag) and (b) benzothiophene adsorbed on $AgTi_6O_8(OH)_8$ (π–Ag); the

clusters consisted of bridged –OH groups. Avg. BSSE corrected energy: (a) -111.1 kJ/mol; (b) -117.9 kJ/mol

VI.3.3.3. Effect of benzene rings and methyl groups:

We compared the E_{ads} of various sulfur heterocycles adsorbed on $AgTi_6O_8(OH)_8$ in order to study the effect of benzene rings and methyl groups. Figure VI.8, Figure VI.9, and Table VI.1 illustrate the corresponding structures and the E_{ads} values of T, BT, DBT, and 4,6-DMDBT adsorbed on $AgTi_6O_8(OH)_8$. Both π–Ag and S–Ag orientations were studied and the corresponding E_{ads} values are included in the table. The S–Ag oriented 4,6-DMDBT could not be calculated because the steric effect was significant. For DBT adsorbed onto $AgTi_6O_8(OH)_8$, π-interaction was the preferred mode of adsorption as well. From the table, it can be restated that the adsorbent had stronger adsorption toward sulfur heterocycles with more benzene rings. However, as a slight counterexample, the adsorption energy for 4,6-DMDBT was weaker than that for DBT. From more negative to less negative, the E_{ads} values followed the order: DBT>4,6-DMDBT>BT>T. This indicated that the adsorbent had the strongest affinity for DBT among these molecules. The order was in accord with that from the saturation experimental results done here. However, the E_{ads} of 4,6-DMDBT adsorption was close to that of DBT adsorption in the calculations, whereas the adsorbent capacity for 4,6-DMDBT was close to that for BT in the experiments. During saturation tests, 4,6-DMDBT might have more diffusion resistance into the adsorbent mesopores because of its structure and thus the adsorbent might have a reduced capacity.

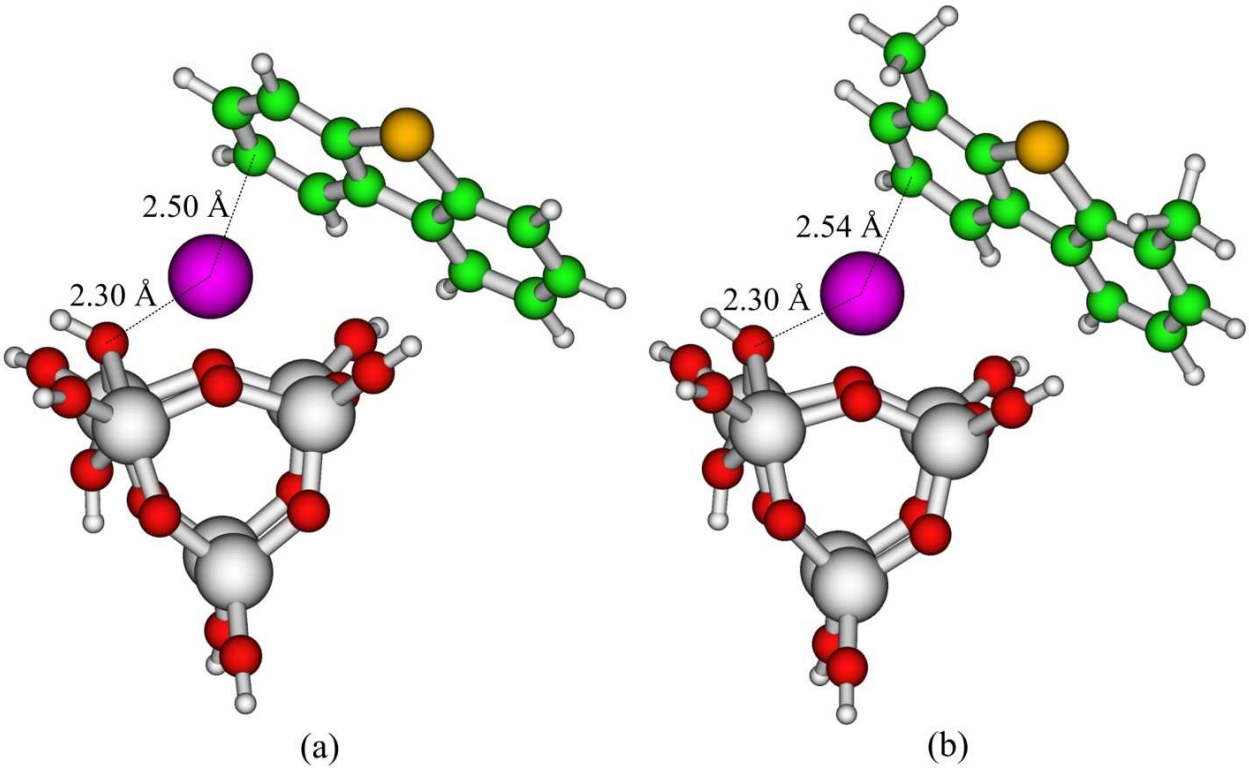

Figure VI.9. Geometrically optimized structures of (a) dibenzothiophene adsorbed on $AgTi_6O_8(OH)_8$ (π–Ag) and (b) 4,6-dimethyldibenzothiophene adsorbed on $AgTi_6O_8(OH)_8$ (π–Ag); the clusters consisted of bridged –OH groups. Avg. BSSE corrected energy: (a) -126.2 kJ/mol; (b) -123.8 kJ/mol

VI.3.3.4. Effect of non-sulfur aromatics:

To investigate the effect of non-sulfur aromatics on sulfur adsorption, we performed DFT calculations regarding benzene and naphthalene adsorption on $AgTi_6O_8(OH)_8$. The optimized clusters and the corresponding E_{ads} values are included in Figure VI.10 and Table VI.1, respectively. Since the molecules have no functional groups other than C, interactions though π electrons were predominant. Benzene and naphthalene adsorption on $AgTi_6O_8(OH)_8$ were weaker than T and BT adsorption. The presence of S increases the electron density, thereby enhancing the adsorption affinity. It also indicated that silver has very high selectivity toward sulfur aromatics over non-sulfur aromatics. Therefore,

sulfur heterocycles can be preferentially adsorbed onto the silver surface over aromatic hydrocarbons, as supported by the computational calculations. Because of this, $AgTi_6O_8(OH)_8$ has high selectivity even when the concentration ratio of non-sulfur aromatics to sulfur aromatics in hydrocarbon fuels is more than 25000:1 [110]. Naphthalene had more negative adsorption energy than benzene due to the added benzene rings. This was also reported by other researchers [176]. The adsorption energies were consistent with the experimental heats of adsorption data [177].

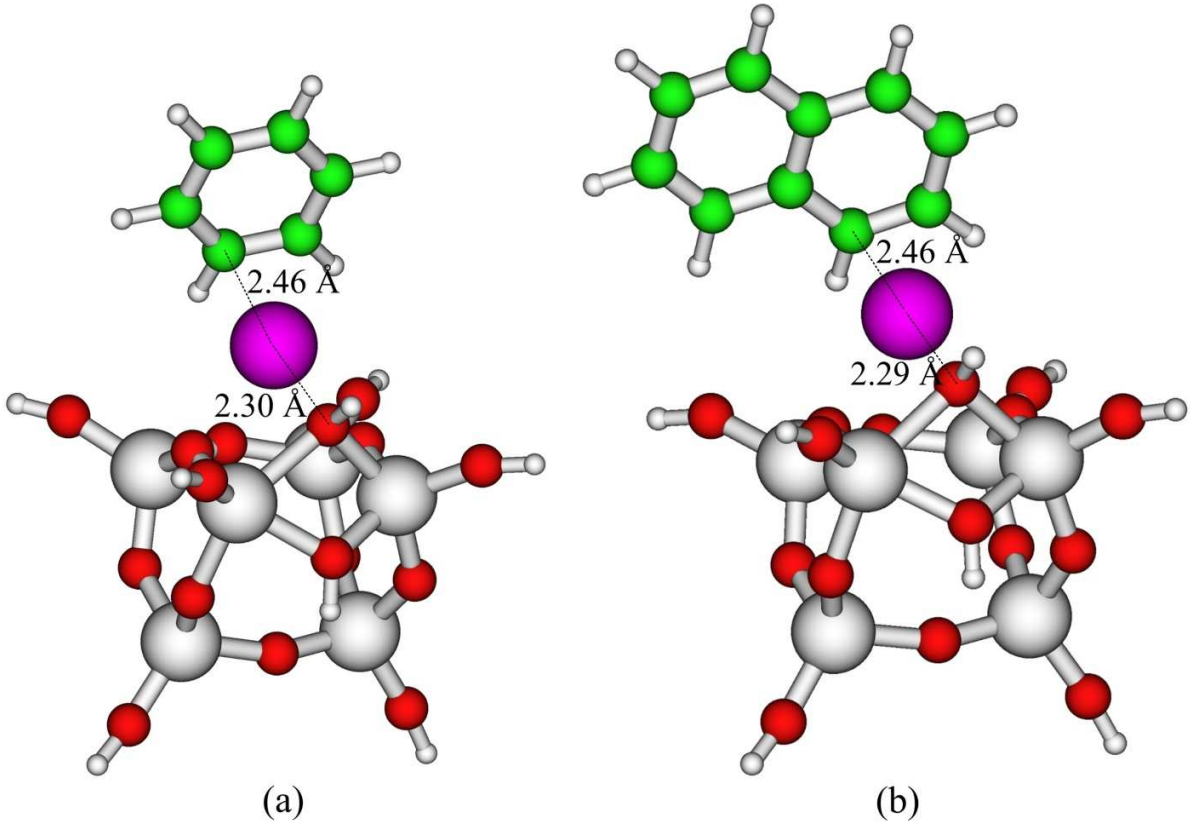

Figure VI.10. Geometrically optimized structures of (a) benzene adsorbed on $AgTi_6O_8(OH)_8$ (π–Ag) and (b) naphthalene adsorbed on $AgTi_6O_8(OH)_8$ (π–Ag); the clusters consisted of bridged –OH groups. Avg. BSSE corrected energy: (a) -101.4 kJ/mol; (b) -115.5 kJ/mol

VI.3.3.5. Effect of different hetero atoms:

In the previous section, we observed that the adsorption energy was less negative for aromatic hydrocarbons whereas it was more negative for the molecules containing sulfur. Therefore, the adsorbent had higher selectivity toward organosulfur compounds. To study its selectivity toward organonitrogen and organooxygen compounds, E_{ads} were calculated for quinoline and benzofuran adsorbed on $AgTi_6O_8(OH)_8$ and were compared with that for BT adsorption (Figure VI.6, Figure VI.8, Figure VI.11, and Table VI.1). Quinoline and benzofuran had N and O as the functional groups, respectively. For E_{ads} calculation, S–Ag, N–Ag, and O–Ag interactions were considered for BT, quinoline, and benzofuran, respectively. For each molecule, π–Ag interaction was considered as well. Figure VI.11 shows quinoline and benzofuran adsorbed on $AgTi_6O_8(OH)_8$ though orientations that resulted in the stronger adsorptions. We can see from the figure that quinoline was adsorbed perpendicular to the adsorbent surface, indicating σ-bonding. Similar bonding was observed in the case of benzofuran adsorbed through O–Ag orientation. From the DFT studies, the order in terms of E_{ads} values from more negative to less negative was: quinoline (N–Ag)>benzothiophene (S–Ag)>benzofuran (O–Ag) or N>S>O. This was similar to the basicity order of the functional groups. These results supported the conclusions from the desulfurization experiments reported previously [100]. The π-interacted adsorbate molecules were also studied and the corresponding E_{ads} values are included in Table VI.1. π-bonding was preferred for BT and benzofuran but not for quinoline. The highest occupied molecular orbital (HOMO) is π-type for both quinoline and benzofuran (8.62 [178] and 8.8 [179] eV, respectively). However, the first σ orbital is much higher for quinoline compared to benzofuran which means quinoline is a much

better donor species. Relative to the calculated HOMO energy (B3LYP/6-31G(d)), the first σ molecular orbital of quinoline was only 0.6 eV lower, while for benzofuran, the first σ molecular orbital was 3.2 eV below the HOMO. Thus, it can be rationalized that the π-interactions are very similar for quinoline and benzofuran, while the σ-interaction is much stronger for quinoline. The π-interaction was 8.9 kJ/mol stronger for quinoline compared to benzofuran (-109.4 vs. -100.5 kJ/mol), and was consistent with a π ionization potential (IP) higher by 0.2 eV (better donor), while the σ-interaction was 63.1 kJ/mol stronger (-141.4 vs. -78.3 kJ/mol) consistent with a much higher σ IP (better donor). The computational calculations indicated that organonitrogen compounds are highly detrimental to desulfurization through this route. These compounds compete for the active sites with organosulfur species [68]. Alternatively, the Ag–TiO_2 adsorbent can also act as a good denitrogenation adsorbent. In the optimized structures, the Ag–N bond distance was the shortest.

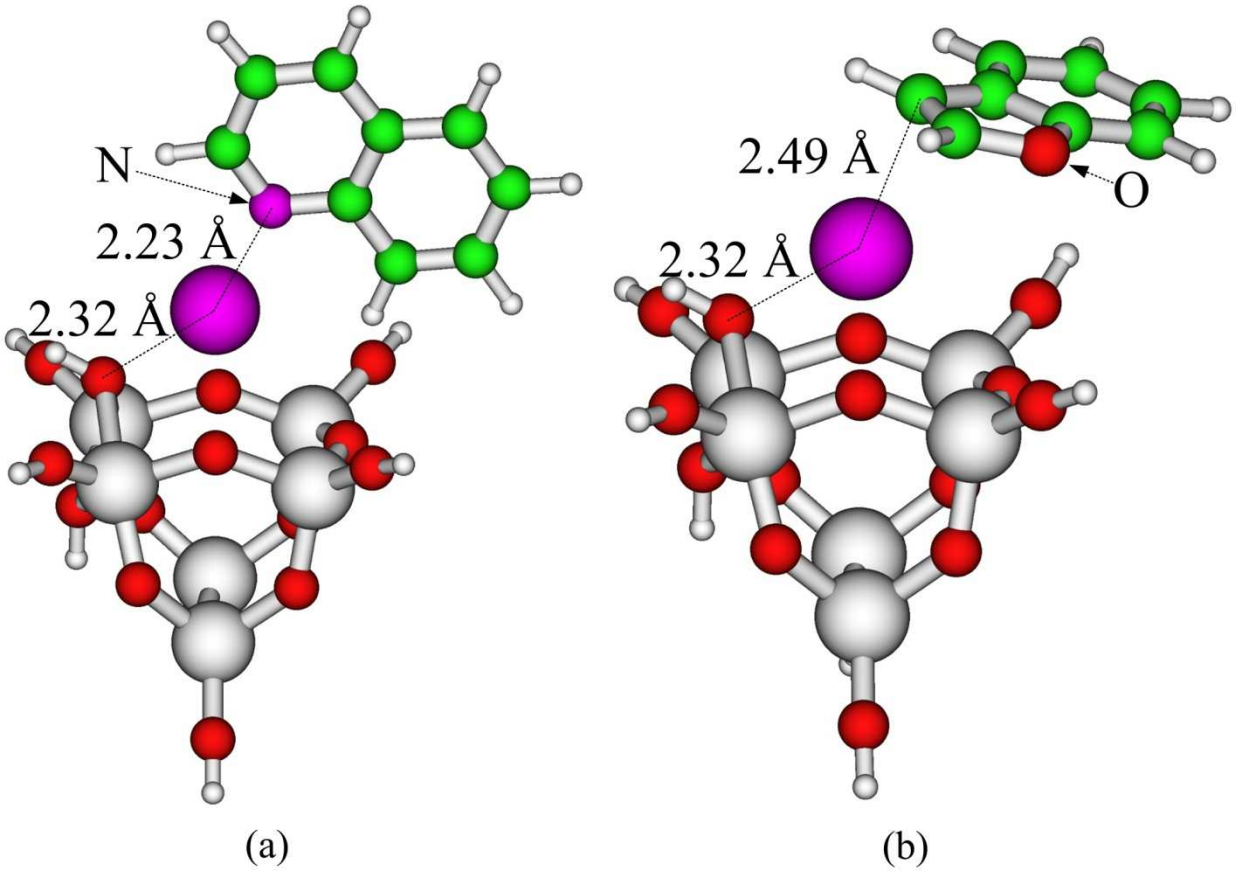

Figure VI.11. Geometrically optimized structures of (a) quinoline adsorbed on $AgTi_6O_8(OH)_8$ (N–Ag orientation) and (b) benzofuran adsorbed on $AgTi_6O_8(OH)_8$ (π–Ag orientation); the clusters consisted of bridged –OH groups. Avg. BSSE corrected energy: (a) -141.4 kJ/mol; (b) -100.5 kJ/mol

Table VI.1 Adsorption energies (uncorrected and average BSSE corrected) of sulfur and non-sulfur aromatics adsorption on $Ti_6O_8(OH)_8$ and $AgTi_6O_8(OH)_8$

Structure	**Adsorbate**	**Orientation**	**E_{ads} (kJ/mol)**	
			Uncorrected	**Avg. BSSE Corrected**
$Ti_6O_8(OH)_8$ (With single –OH groups)	Thiophene	S–H	-30.8	-27.1
$AgTi_6O_8(OH)_8$ (With single –OH groups)		S–Ag	-85.4	-77.4
$Ti_6O_8(OH)_8$ (with bridged –OH groups)	Thiophene	S–H	-40.1	-34.1
	Benzothiophene	S–H	-62.8	-54.4
$AgTi_6O_8(OH)_8$ (with bridged –OH groups)	Thiophene	S–Ag	-105.9	-98.0
		π–Ag	-121.0	-111.1
	Benzothiophene	S–Ag	-113.8	-104.7
		π–Ag	-127.7	-117.9
	Dibenzothiophene	S–Ag	-129.0	-117.3
		π–Ag	-139.2	-126.2
	4,6-dimethyl dibenzothiophene	π–Ag	-136.7	-123.8
	Benzene	π–Ag	-111.2	-101.4
	Naphthalene	π–Ag	-125.8	-115.5
	Quinoline	N–Ag	-153.3	-141.4
		π–Ag	-120.1	-109.4
	Benzofuran	O–Ag	-89.2	-78.3
		π–Ag	-113.1	-100.5

VI.3.4. NPA charges:

The NPA charges of Ag and S in the adsorbate-adsorbent clusters were calculated and are presented in Table VI.2. The charges of Ag before adsorption were consistent with the experimental data, where the +1 oxidation state of Ag were observed to be the active form in Ag–TiO_2 adsorbent [71]. Silver charges were decreased after adsorption; whereas S charges were increased for π-interacted molecules and decreased for S-interacted molecules. The S charges were seen to be positive in all adsorbate-adsorbent clusters whereas the C atoms had negative charges. Apart from S, both N and O functional groups in quinoline and benzofuran, respectively, had negative charges. After adsorption, the charges of N and O were reduced during σ-interaction, and were increased during π-interaction.

Table VI.2 The NPA charges (calculated via B3LYP/6-31G(d) method) of Ag and S/N/O from optimized adsorbate, adsorbent, and adsorbate-adsorbent structures

Cluster	Adsorbate	Orientation	Charge (e^-)			
			Ag	Ag	S/N/O	S/N/O
$Ti_6O_8(OH)_8$ (with	Thiophene	S–H	-	-	0.38	0.34
$AgTi_6O_8(OH)_8$ (with		S–Ag	0.73	0.61		0.35
$Ti_6O_8(OH)_8$ (with bridged –OH groups)	Thiophene	(S–H)	-	-		0.35
	Benzothiophene	(S–H)	-	-	0.36	0.34
$AgTi_6O_8(OH)_8$ (with bridged –OH groups)	Thiophene	(S–Ag)	0.72	0.61	0.38	0.34
		(π–Ag)		0.66		0.43
	Benzothiophene	(S–Ag)		0.60	0.36	0.34
		(π–Ag)		0.67		0.40
	Dibenzothiophene	(S–Ag)		0.59	0.35	0.34
		(π–Ag)		0.67		0.38
	4,6-dimethyl	(π–Ag)		0.66	0.33	0.34
	Benzene	(π–Ag)		0.67	-	-
	Naphthalene	(π–Ag)		0.68	-	-
	Quinoline	(N–Ag)		0.64	-0.45	-0.54
		(π–Ag)		0.68		-0.43
	Benzofuran	(O–Ag)		0.69	-0.48	-0.53
		(π–Ag)		0.65		-0.46

VI.3.5. Separation factor:

Separation factor is employed in adsorption/absorption processes to determine the quality of separating a particular component from a mixture [45]. It is essential in hydrocarbon fuel desulfurization since every fuel contains numerous compounds which can interfere

with the process. This factor can adequately describe the adsorbent ability to selectively remove sulfur derivatives from the fuels. The α values of various sulfur, nitrogen, and oxygen aromatics over benzene are given in Table VI.3. The E_{ads} values of species adsorbed through preferred orientations (N–Ag for quinoline, π–Ag for the rest) were employed for separation factor calculation. Benzene represented the non-sulfur aromatic content of hydrocarbon fuels. As seen from the table, all α values except $\alpha_{Benzofuran/C6}$ were greater than 2, indicating that the adsorbent can be a good separation agent commercially [45]. Therefore, Ag–TiO_2 is a feasible adsorbent for removing all the aforesaid sulfur heterocycles. The value of $\alpha_{Thiophene/Benzene}$ was 50, indicating high selectivity toward T over C6. The values were consistent with experimental separation factors reported by other researchers [177].

Table VI.3 Separation factors of all sulfur heterocycles as compared to benzene.

Separation Factor	**Adsorption on $AgTi_6O_8(OH)_8$**
$\alpha_{Thiophene/Benzene}$ (π–Ag)	50
$\alpha_{Benzothiophene/Benzene}$ (π–Ag)	794
$\alpha_{Dibenzothiophene/Benzene}$ (π–Ag)	22466
$\alpha_{4,6\text{-}dimethyldibenzothiophene/Benzene}$ (π–Ag)	8648
$\alpha_{Quinoline/Benzene}$ (N–Ag)	1.0×10^7
$\alpha_{Benzofuran/Benzene}$ (π–Ag)	0.7

VI.4. Conclusions:

In this work, a computational study was carried out using DFT methods to investigate the sulfur selectivity of Ag–TiO_2. We also studied the adsorbent activation steps and found

out that the Ag–TiO_2 structures (both hydroxylated and non-hydroxylated) were stable. Silver incorporation with TiO_2 was likely to be spontaneous and the presence of –OH facilitated the process. The –OH groups contributed not only in Ag incorporation, but also acted as secondary adsorption sites. Bridged –OH groups were more stable and demonstrated stronger affinity toward organosulfur compounds than single –OH groups. Ag–TiO_2 clusters had much stronger adsorption affinities than neat TiO_2 clusters. For all sulfur and most of the non-sulfur heterocycles, π-interaction was the preferred mode of adsorption. For $AgTi_6O_8(OH)_8$ cluster with bridged –OH groups, the order of adsorbate molecules in terms of the adsorption energies from more negative to less negative was: quinoline (N–Ag)>DBT (π–Ag)>4,6-DMDBT (π–Ag)>BT (π–Ag)>C10 (π–Ag)>T (π–Ag)>C6 (π–Ag)>benzofuran (π–Ag). This was also in agreement with the results from saturation experiments. The effect of aromaticity was found significant as organosulfur species with more aromatic rings tended to adsorb more strongly onto silver. This has been attributed to the π-electron cloud contributing more to the negative charge density. Functional groups in heterocycles had considerable effect on adsorption energy, and the presence of functional groups such as S and N significantly enhanced heterocycle adsorption on the adsorbent. The separation factors of Ag–TiO_2 were promising and reflected its ability to adsorb sulfur aromatics even in the presence of 25000 times higher concentration of non-sulfur aromatics. The adsorption energy of silver-titania calculated in this work can be utilized in the adsorbent formulation for maximizing adsorbent activity and in the design of other adsorption processes.

VII. Conclusions and Recommendations for Future works

VII.1. Conclusions:

The summary of findings from each study has been discussed at the end of each chapter. I present here the summary of the overall research work presented in this dissertation and its broader contribution.

1. An adsorbent formulation was developed and optimized based on silver supported on novel anatase-titania dispersed supports.
2. The formulation was effective in desulfurizing a wide variety of logistic and commercial fuels (~10 mg S/g sorbent).
3. The adsorbent was the first of its kind to produce ultra clean hydrocarbon fuels (<0.1 ppmw S) for PEM fuel cell applications.
4. The adsorbent demonstrated promising sulfur adsorption capacities for both aliphatic and aromatic sulfur compounds.
5. Mesoporous supports were found to be the most appropriate for room temperature adsorptive desulfurization of liquid fuels.
6. A variety of characterization methods such as XRD, Raman, UV-DRS, N_2 physisorption, O_2 chemisorption, NH_3 adsorption, and IR spectroscopy were employed to evaluate the adsorbent and the adsorption mechanism.
7. An *in situ* apparatus for infrared measurement was designed and built for investigating adsorbent activation and sulfur adsorption mechanism.

8. DFT studies were performed for the first time on the organosulfur adsorption on titania supported silver oxides.
9. The sulfur adsorption mechanism was found to be unique, which consisted of multiple adsorption sites (Ag and –OH groups). The mechanisms were confirmed by both experiment.

The mixed oxide supported silver adsorbent is the only oxide formulation for liquid fuel desulfurization. Inexpensive formulation, activation free operation, regeneration in air, low pressure drop, and the absence of any auxiliary units or reducing gases make the adsorbent highly feasible for application in an on-board desulfurizer unit. The formulation developed in the current work has promising sulfur adsorption capacities for both logistic and commercial fuels. The adsorbent was also designed to effectively desulfurize hydrocarbon fuels down to fuel cell application range. This work also highlighted the versatility of the formulation by introducing multiple adsorption sites on the adsorbent for the first time. The individual capacities of silver and hydroxyl groups; and their synergistic effects were the significant findings of this work. The adsorption process and the formulation was also designed and optimized to ensure maximum performance. The resulting formulation is both effective and viable for a continuous operation in an upstream desulfurizer unit for any type of fuel cells and is also capable of handling a wide variety of hydrocarbon fuel blends. The overall study is important not only for desulfurization and fuel cell applications, but also for other liquid phase adsorption and fuel cleaning processes (e.g. Denitrogenation and olefin-paraffin separation).

VII.2. Recommendations for future work

VII.2.1. Development of new materials

The $Ag/TiO_2–Al_2O_3$ and $Ag/TiO_2–SiO_2$ adsorbents have shown good performances in desulfurizing hydrocarbon fuels. However, to make the formulation more feasible, efforts should be given in increasing its capacity. Currently 1 g of $Ag/TiO_2–Al_2O_3$ can desulfurize around 10–15 ml of ULSD down to ppbw level. The formulation can be further developed to desulfurize more volume of fuel per adsorbent weight basis. The adsorbent formulation can be further optimized for achieving maximum performance.

One way to explore its effectiveness is to disperse $Ag–TiO_2$ on various supports. So far I have discussed $Ag–TiO_2$ supported on only Al_2O_3 and SiO_2 supports since they are the simplest, cheapest, and most widely used supports. Similar dispersion can be made over other supports such as zeolites, ZrO_2, MgO, SBA-15, ZSM-5 etc. The resulting formulations can exert in higher sulfur adsorption capacity and greater efficiency in ppbw level desulfurization. However, the mass transfer limitation and the supports with appropriate pore structure should be taken into consideration. In this dissertation, I have mentioned the preparation of mixed oxides via incipient wetness impregnation and co-precipitation. However, there are other methods available for preparing such materials; such as atomic layer deposition, ion exchange, deposition precipitation etc. These methods might result in more active TiO_2 dispersed supports and therefore should be tested.

In our earlier discussion, we have mentioned that silver is active for sulfur adsorption in +1 oxidation state. However, in practical case, the amount of Ag which are present in +1 form as well as exposed are very less (only around 21 wt% for $Ag/TiO_2–Al_2O_3$).

Therefore, efforts should be given to increase the presence of more Ag with +1 oxidation state. This is to remind the readers here that we use $AgNO_3$ as Ag precursor in the preparation techniques. Ag is in +1 oxidation state; therefore $AgNO_3$ can be an excellent adsorbent. Other researchers have also reported its effectiveness as adsorbents [68]. $AgNO_3$ supported on mixed oxides might be a stronger adsorbent for sulfur adsorption. However, the material is not thermally regenerable. Therefore, other methods of regeneration should be tested so that it can be successfully applied in a continuous operation.

VII.2.2. Characterization of the Ti and Ag phase via spectroscopy

Silver supported on mixed oxide supports has resulted in higher sulfur adsorption capacity because of the presence of more silver oxides. Due to the increase in surface area and titania active sites, more silver could be loaded in reducible form. However, to determine the optimized silver loading for a particular mixed oxide, more sophisticated spectroscopic techniques should be used. Among different spectroscopic techniques, x-ray absorption spectroscopy (EXAFS) can be successfully employed to deduce the amount of Ag–O and the optimized loading of Ag which could yield the highest fraction of silver (I) oxide. Ag–TiO_2 can be dispersed onto other supports and the formulations can be consequently optimized via EXAFS in terms of silver loading. EXAFS can also be useful by investigating the Ag K edge to look into the Ag–O pattern. By examining the Ag K edge of Ag–TiO_2 adsorbents dispersed on different supports, the disorderliness of silver (I) oxide can be estimated. This can lead to the development of adsorbents with highly dispersed silver since higher disorderliness would be commensurate to greater dispersion. The quantification of Ag supported on TiO_2 and on primary support can also

be estimated by looking into the Ag edge. This study could be used to investigate different surface treatment methods for yielding the highest Ag fraction on TiO_2 sites. Besides Ag loading, the Ti–O bond length can also be examined using EXAFS by looking into the Ti K edge. The effect of Ag impregnation on anatase structure disruption can be discerned. This would complement the results found from Raman spectroscopy which revealed changes in anatase Ti–O bonds after Ag impregnation. Other than EXAFS, x-ray photoelectron spectroscopy (XPS) can be used to detect the silver particle size.

VII.2.3. Photocatalytic Activity of $Ag/TiO_2–Al_2O_3$ in Liquid Fuel Desulfurization

Silver and titania are known to be excellent photocatalysts employed in many applications such as oxidation, decomposition, and disinfection [62, 180-182]. These materials under ultraviolet (UV) or visible (Vis) light become active even at room temperature and atmospheric pressure. UV-vis irradiation can excite the electrons of TiO_2, creating electron-hole pairs. This can promote defect mediated dissociation of water to generate hydroxyl groups [183]. Silver itself can act as an electron receptor, inhibiting the recombination of electron-hole pair [184]. Silver can also lower down the band gap of titania when they are combined [181]. The individual photocatalytic characteristics of Ag and TiO_2 have shown positive effects on desulfurizing organosulfur species [182]. Titania can oxidize sulfur aliphatics and thiophenes in presence of H_2O, O_2 and/or H_2O_2 [136, 150]. The individual photocatalytic activities of Ag and TiO_2 warrant an investigation of the synergistic effect of combined silver-titanium oxide material and also its probable implementation in liquid fuel desulfurization. The $Ag/TiO_2–Al_2O_3$ adsorbent has shown promising sulfur adsorption capacities from liquid fuel. Its

desulfurization capacity might be improved still further via photo-irradiation. UV-irradiation on $Ag/TiO_2–Al_2O_3$ in presence of H_2O and O_2 might increase sulfur adsorption capacity through enhancing –OH concentration (Bronsted acid sites) on the surface. In addition, UV-excited TiO_2 surfaces might oxidize the sulfur compounds using O_2. Silver under photo-irradiation might assist TiO_2 in oxidizing organosulfur species. Therefore, the photocatalytic properties of $Ag/TiO_2–Al_2O_3$ and its effect on liquid phase desulfurization should be investigated.

To investigate the photocatalytic characteristics of $Ag/TiO_2–Al_2O_3$, desulfurization experiments should be carried out under UV light. Low P Hg or Xe-Hg lamps can be used as light sources. Most of the researchers have employed visible lights ($\lambda \geq 400$ nm) for photo-oxidation using TiO_2 [180, 182]. However, TiO_2 has demonstrated higher activity when exposed to radiation at UV-C range ($\lambda \sim 254$ nm) [181]. Therefore, we can use UV-C light sources. For activation or as reactants, we can use air/O_2 with H_2O mixture (RH ~70%). The experiments should be performed at room temperature and atmospheric pressure. A probable setup for UV-irradiated desulfurization experiments is shown in Figure IV.4.The experiment should be a packed bed-continuous process, although batch operations can also be carried out. For characterizing the photocatalytic materials and for estimating band gaps, UV-DRS can be employed.

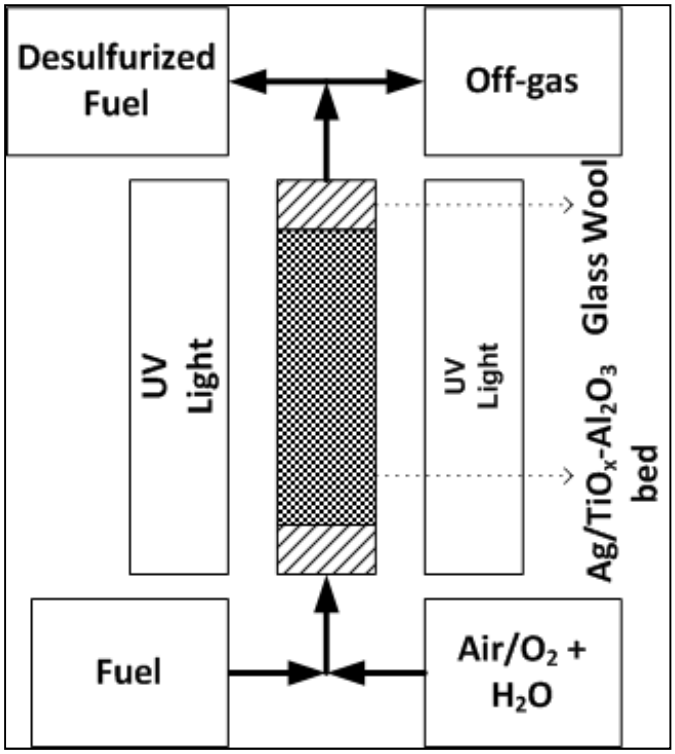

Figure VII.1. Experimental setup for UV-irradiated fixed bed desulfurization test

VII.2.4. Design of desulfurization unit

So far most of the efforts have been given to the adsorbent development. The next steps after adsorbent formulation are the process design for a practical sulfur adsorber. The process conditions should be thoroughly optimized in terms of particle sizes, flow rates, adsorber aspect ratio with a view to the fuel production at the outlet. The adsorber should be adequately customized for achieving sharper breakthrough since this is more desirable in a practical process. Higher aspect ratio, smaller particle sizes, and the use of diluents in the adsorbent beds may facilitate in achieving sharper breakthrough. The adsorption and regeneration process should also be integrated for a continuous operation. After proper design, scale up of the process should be undertaken for a practical process. The process can be incorporated with a refinery or a fuel cell operation via process simulation software.

VII.2.5. Oxidative desulfurization

Oxidative desulfurization can also be an alternative method to conventional HDS process, as described earlier (section I.2.2). It has advantages of being a catalytic process, of not requiring H_2, and of mild operating conditions. In addition, the process has high selectivity toward more refractory sulfur compounds. Therefore, it should have higher reactivity toward 4,6-DMDBT like compounds and higher desulfurizing capability for fuels who contains these compounds (e.g. ULSD). If O_2 or air is used as oxidants, the process can also be feasible and less complicated. These gases also have an edge in terms of green chemistry.

References

[1] K.G. Knudsen, B.H. Cooper, H. Topsoe, Applied Catalysis a-General 189 (1999) 205-215.

[2] C. Song, X.L. Ma, Applied Catalysis B-Environmental 41 (2003) 207-238.

[3] A.J. Hernandez-Maldonado, F.H. Yang, G. Qi, R.T. Yang, Applied Catalysis B-Environmental 56 (2005) 111-126.

[4] S.A. Nair, Desulfurization of Hydrocarbon Fuels at Ambient Conditions Using Supported Silver Oxide-Titania Sorbents, Chemical Engineering, Auburn University, Auburn, Alabama, USA, 2010, p. 146.

[5] Diesel fuels technical review, Chevron Corporation, 2007.

[6] C.S. Song, Catalysis Today 86 (2003) 211-263.

[7] B. Pawelec, R.M. Navarro, J.M. Campos-Martin, J.L.G. Fierro, Catalysis Science & Technology 1 (2011) 23-42.

[8] A. Stanislaus, A. Marafi, M.S. Rana, Catalysis Today 153 (2010) 1-68.

[9] I.V. Babich, J.A. Moulijn, Fuel 82 (2003) 607-631.

[10] M. Specht, F. Staiss, A. Bandi, T. Weimer, International Journal of Hydrogen Energy 23 (1998) 387-396.

[11] D. Shekhawat, J.J. Spivey, D.A. Berry, Fuel cells: technologies for fuel processing, Elsevier, Spain, 2011.

[12] C.S. Song, Catalysis Today 77 (2002) 17-49.

[13] S. Velu, X.L. Ma, C.S. Song, M. Namazian, S. Sethuraman, G. Venkataraman, Energy & Fuels 19 (2005) 1116-1125.

[14] A. Samokhvalov, B.J. Tatarchuk, Catalysis Reviews-Science and Engineering 52 (2010) 381-410.

[15] S.K. Bej, S.K. Maity, U.T. Turaga, Energy & Fuels 18 (2004) 1227-1237.

[16] O.L. Holbrook, in: R.A. Meyers (Ed.), Handbook of Petroleum Refining Processes, 2nd ed., McGraw-Hill, New York, 1997, pp. 11-29.

[17] B.C. Gates, H. Topsoe, Polyhedron 16 (1997) 3213-3217.

[18] S. Inoue, T. Takatsuka, Y. Wada, S. Hirohama, T. Ushida, Fuel 79 (2000) 843-849.

[19] K.G. Knudsen, H. Topsoe, R. Egeberg, Hydrotreating catalysis. From molecular understanding of reaction pathways and support interactions to improved industrial solutions, 22nd Annual Meeting, North American Catalysis Society, Detroit, MI, USA, June 5-10, 2011.

[20] C. Sentorun-Shalaby, S.K. Saha, X.L. Ma, C.S. Song, Applied Catalysis B-Environmental 101 (2011) 718-726.

[21] A. Cybulski, J.A. Moulijn, Structured Catalysts and Reactors, 2nd ed., Taylor & Francis, Boca Raton, FL, 2006.

[22] D.R. Cahela, B.J. Tatarchuk, Catalysis Today 69 (2001) 33-39.

[23] B.K. Chang, Y. Lu, B.J. Tatarchuk, Chemical Engineering Journal 115 (2006) 195-202.

[24] R.S. Peninger, J.C. Demeter, E.A. Schwarz, K.L. Rock, The European Refinery Technology Conference, Rome, Italy, November 13-15, 2000.

[25] M. Seredych, J. Lison, U. Jans, T.J. Bandosz, Carbon 47 (2009) 2491-2500.

[26] A. Chica, K. Strohmaier, E. Iglesia, Langmuir 20 (2004) 10982-10991.

[27] R.T. Yang, A.J. Hernandez-Maldonado, F.H. Yang, Science 301 (2003) 79-81.

[28] A. Deshpande, A. Bassi, A. Prakash, Energy & Fuels 19 (2005) 28-34.

[29] S. Murata, K. Murata, K. Kidena, M. Nomura, Energy & Fuels 18 (2004) 116-121.

[30] M.J. Grossman, M.K. Lee, R.C. Prince, K.K. Garrett, G.N. George, I.J. Pickering, Applied and Environmental Microbiology 65 (1999) 3264-3264.

[31] H. Mei, B.W. Mei, T.F. Yen, Fuel 82 (2003) 405-414.

[32] P. Forte, Process for the Removal of Sulfur from Petroleum Fractions, in: U. Patent (Ed.), US patent, UOP, Des Plaines, Illinois, USA, 1996.

[33] L.D. Gao, Q.S. Xue, Y. Liu, Y. Lu, Aiche Journal 55 (2009) 3214-3220.

[34] G. Capozzi, J. Drabowicz, P. Kiellbasinski, S. Menichetti, M. Mikolajczyk, C. Nativi, K. Schank, N. Schott, U. Zoller, Syntheses of sulphones, sulphoxides and cyclic sulphides, John Wiley and sons, England, 1994.

[35] V. Prasad, K.E. Jeong, H.J. Chae, C.U. Kim, S.Y. Jeong, Catalysis Communications 9 (2008) 1966-1969.

[36] J. Chang, A.J. Wang, J. Liu, X. Li, Y.K. Hu, Catalysis Today 149 (2010) 122-126.

[37] A. Chica, A. Corma, M.E. Domine, Journal of Catalysis 242 (2006) 299-308.

[38] Y. Lu, Y. Wang, L.D. Gao, J.C. Chen, J.P. Mao, Q.S. Xue, Y. Liu, H.H. Wu, G.H. Gao, M.Y. He, Chemsuschem 1 (2008) 302-306.

[39] R. Sundararaman, X.L. Ma, C.S. Song, Industrial & Engineering Chemistry Research 49 (2010) 5561-5568.

[40] R.E. Levy, A.S. Rappas, S.J. DeCanio, V.P. Nero, NPRA 2001 Annual Meeting, New Orleans, USA, March 18-20, 2001.

[41] B.L. McFarland, D.J. Boron, W. Deever, J.A. Meyer, A.R. Johnson, R.M. Atlas, Critical Reviews in Microbiology 24 (1998) 99-147.

[42] R.B. Qi, Y.J. Wang, J. Chen, J.D. Li, S.L. Zhu, Separation and Purification Technology 57 (2007) 170-175.

[43] P.T. Burnett, G.A. Huff, V.R. Pradhan, M. Hodges, J.A. Glassett, S.G. McDaniel, P. Hurst, The European Refinery Technology Conference, Rome, Italy, November 13-15, 2000.

[44] G.J. Greenwood, D. Kidd, L. Reed, NRPA 2000 Annual Meeting, San-Antonio, Texas, USA, March 26-28, 2000.

[45] Y.H. Wang, F.H. Yang, R.T. Yang, J.M. Heinzel, A.D. Nickens, Industrial & Engineering Chemistry Research 45 (2006) 7649-7655.

[46] A.J. Hernandez-Maldonado, G.S. Qi, R.T. Yang, Applied Catalysis B-Environmental 61 (2005) 212-218.

[47] J.H. Kim, X.L. Ma, A.N. Zhou, C.S. Song, Catalysis Today 111 (2006) 74-83.

[48] S.G. McKinley, R.J. Angelici, Chemical Communications (2003) 2620-2621.

[49] V.M. Bhandari, C.H. Ko, J.G. Park, S.S. Han, S.H. Cho, J.N. Kim, Chemical Engineering Science 61 (2006) 2599-2608.

[50] G. Weber, J.P. Bellat, F. Benoit, C. Paulin, S. Limborg-Noetinger, M. Thomas, Adsorption-Journal of the International Adsorption Society 11 (2005) 183-188.

[51] W. Min, Korean Journal of Chemical Engineering 19 (2002) 601-606.

[52] S.P. Hernandez, D. Fino, N. Russo, Chemical Engineering Science 65 (2010) 603-609.

[53] X.L. Ma, M. Sprague, C.S. Song, Industrial & Engineering Chemistry Research 44 (2005) 5768-5775.

[54] M.V. Landau, M. Herskowitz, R. Agnihotri, J.E. Kegerreis, Industrial & Engineering Chemistry Research 47 (2008) 6904-6916.

[55] A.J. Hernandez-Maldonado, R.T. Yang, Catalysis Reviews-Science and Engineering 46 (2004) 111-150.

[56] Y. Toida, K. Nakamura, K. Matsumoto, Journal of the Japan Petroleum Institute 53 (2010) 342-350.

[57] K.A. Cychosz, A.G. Wong-Foy, A.J. Matzger, Journal of the American Chemical Society 130 (2008) 6938-6939.

[58] S. Achmann, G. Hagen, M. Hammerle, I. Malkowsky, C. Kiener, R. Moos, Chemical Engineering & Technology 33 (2010) 275-280.

[59] S. Haji, C. Erkey, Industrial & Engineering Chemistry Research 42 (2003) 6933-6937.

[60] A.N. Zhou, X.L. Ma, C.S. Song, Applied Catalysis B-Environmental 87 (2009) 190-199.

[61] R.P. Wang, X.W. Guo, X.S. Wang, J.Q. Hao, Catalysis Today 93-5 (2004) 217-222.

[62] M.P. Reddy, A. Venugopal, M. Subrahmanyam, Water Research 41 (2007) 379-386.

[63] M. Richter, U. Bentrup, R. Eckelt, M. Schneider, M.M. Pohl, R. Fricke, Applied Catalysis B-Environmental 51 (2004) 261-274.

[64] W.L. Dai, C. Yong, L.P. Ren, X.L. Yang, J.H. Xu, H.X. Li, H.Y. He, K.N. Fan, Journal of Catalysis 228 (2004) 80-91.

[65] T. Nanba, S.M. Asukawa, J. Uchisawa, A. Obuchi, Journal of Catalysis 259 (2008) 250-259.

[66] A.J. Hernandez-Maldonado, R.T. Yang, Industrial & Engineering Chemistry Research 42 (2003) 123-129.

[67] S. Satokawa, Y. Kobayashi, H. Fujiki, Applied Catalysis B-Environmental 56 (2005) 51-56.

[68] H. Chen, Y.H. Wang, F.H. Yang, R.T. Yang, Chemical Engineering Science 64 (2009) 5240-5246.

[69] B. Tatarchuk, H. Yang, S. Nair, Processes for removing sulfur from a hydrocarbon stream utilizing silver-based sorbents, US8425763 B2, US Patent Application, 2013.

[70] S. Nair, B.J. Tatarchuk, Fuel 89 (2010) 3218-3225.

[71] A. Samokhvalov, S. Nair, E.C. Duin, B.J. Tatarchuk, Applied Surface Science 256 (2010) 3647-3652.

[72] S. Nair, B.J. Tatarchuk, Adsorption-Journal of the International Adsorption Society 17 (2011) 663-673.

[73] J. Ramirez, G. Macias, L. Cedeno, A. Gutierrez-Alejandre, R. Cuevas, P. Castillo, Catalysis Today 98 (2004) 19-30.

[74] G.S. Walker, E. Williams, A.K. Bhattacharya, Journal of Materials Science 32 (1997) 5583-5592.

[75] M.S. Rana, S.K. Maity, J. Ancheyta, G.M. Dhar, T. Rao, Applied Catalysis a-General 253 (2003) 165-176.

[76] S. Kamaruddin, D. Stephan, Catalysis Today 161 (2011) 53-58.

[77] J. Keranen, C. Guimon, E. Liskola, A. Auroux, L. Niinisto, Catalysis Today 78 (2003) 149-157.

[78] J.R. Grzechowiak, I. Wereszczako-Zielinska, K. Mrozinska, Catalysis Today 119 (2007) 23-30.

[79] J. Ramirez, P. Rayo, A. Gutierrez-Alejandre, J. Ancheyta, M.S. Rana, Catalysis Today 109 (2005) 54-60.

[80] L.C. Chen, F.R. Tsai, C.M. Huang, Journal of Photochemistry and Photobiology a-Chemistry 170 (2005) 7-14.

[81] J.B. Peri, Journal of Physical Chemistry 70 (1966) 3168-3179.

[82] B. Braconnier, C.A. Paez, S. Lambert, C. Alie, C. Henrist, D. Poelman, J.P. Pirard, R. Cloots, B. Heinrichs, Microporous and Mesoporous Materials 122 (2009) 247-254.

[83] G.M. Dhar, B.N. Srinivas, M.S. Rana, M. Kumar, S.K. Maity, Catalysis Today 86 (2003) 45-60.

[84] S. Yoshinaka, K. Segawa, Catalysis Today 45 (1998) 293-298.

[85] J.H. Li, Y.Q. Zhu, R. Ke, J.M. Hao, Applied Catalysis B-Environmental 80 (2008) 202-213.

[86] Q. Liu, Y. Cao, W.L. Dai, J.F. Deng, Catalysis Letters 55 (1998) 87-91.

[87] T. Klimova, O. Gutierrez, L. Lizama, J. Amezcua, Microporous and Mesoporous Materials 133 (2010) 91-99.

[88] R. Castillo, B. Koch, P. Ruiz, B. Delmon, Journal of Materials Chemistry 4 (1994) 903-906.

[89] C. Pophal, F. Kameda, K. Hoshino, S. Yoshinaka, K. Segawa, Catalysis Today 39 (1997) 21-32.

[90] W.P. Hsu, R.C. Yu, E. Matijevic, Journal of Colloid and Interface Science 156 (1993) 56-65.

[91] A.W. Czanderna, Journal of Physical Chemistry 68 (1964) 2765-2771.

[92] D.E. Strohmayer, G.L. Geoffroy, M.A. Vannice, Applied Catalysis 7 (1983) 189-198.

[93] Y.E. Sung, W.Y. Lee, H.K. Rhee, H.I. Lee, Korean Journal of Chemical Engineering 6 (1989) 300-305.

[94] K.L. Yeung, A. Gavriilidis, A. Varma, M.M. Bhasin, Journal of Catalysis 174 (1998) 1-12.

[95] X.E. Verykios, F.P. Stein, R.W. Coughlin, Journal of Catalysis 66 (1980) 368-382.

[96] W.W. Smeltzer, E.L. Tollefson, A. Cambron, Canadian Journal of Chemistry-Revue Canadienne De Chimie 34 (1956) 1046-1060.

[97] P. Dhage, A. Samokhvalov, M.L. McKee, E.C. Duin, B.J. Tatarchuk, Surface and interface analysis 45 (2013) 865-872.

[98] L. Liao, C.W. Ingram, Applied Catalysis a-General 433 (2012) 18-25.

[99] R. Chauhan, A. Kumar, R.P. Chaudhary, Research on Chemical Intermediates 38 (2012) 1443-1453.

[100] S. Nair, A.H.M.S. Hussain, B.J. Tatarchuk, Fuel 105 (2013) 695-704.

[101] D.M. Ginosar, K. Coates, D.N. Thompson, Industrial & Engineering Chemistry Research 41 (2002) 6537-6545.

[102] D.T. Tran, Z.W. Dunbar, D. Chu, International Journal of Hydrogen Energy 37 (2012) 10430-10434.

[103] M.S. Lee, G.D. Lee, S.S. Hong, Journal of Industrial and Engineering Chemistry 9 (2003) 412-418.

[104] O. van Rheinberg, K. Lucka, H. Kohne, Journal of Power Sources 196 (2011) 8983-8993.

[105] Y.H. Wang, R.T. Yang, J.M. Heinzel, Industrial & Engineering Chemistry Research 48 (2009) 142-147.

[106] L.G. Lin, A.D. Wang, L.H. Zhang, M.M. Dong, Y.Z. Zhang, Journal of Power Sources 220 (2012) 138-146.

[107] A. Ates, G. Azimi, K.-H. Choi, W.H. Green, M.T. Timko, Applied Catalysis B: Environmental 147 (2014) 144-155.

[108] X.H. Xu, S.Y. Zhang, P.W. Li, Y.S. Shen, Fuel 117 (2014) 499-508.

[109] E.R. Webster, A. Park, M.B. Stratton, V.C. Park, A.M. Mosier, R.S. Shine, L. Benz, Energy & Fuels 27 (2013) 6575-6580.

[110] A.H.M.S. Hussain, B.J. Tatarchuk, Fuel 107 (2013) 465-473.

[111] P. Iengo, M. Di Serio, A. Sorrentino, V. Solinas, E. Santacesaria, Applied Catalysis a-General 167 (1998) 85-101.

[112] K. Kobayakawa, Y. Nakazawa, M. Ikeda, Y. Sato, A. Fujishima, Berichte Der Bunsen-Gesellschaft-Physical Chemistry Chemical Physics 94 (1990) 1439-1443.

[113] X.T. Gao, S.R. Bare, J.L.G. Fierro, M.A. Banares, I.E. Wachs, Journal of Physical Chemistry B 102 (1998) 5653-5666.

[114] M. Wu, B.F. Yang, Y. Lv, Z.P. Fu, J.A. Xu, T. Guo, Y.X. Zhao, Applied Surface Science 256 (2010) 7125-7130.

[115] G. Liu, Y. Liu, G. Yang, S.Y. Li, Y.H. Zu, W.X. Zhang, M.J. Jia, Journal of Physical Chemistry C 113 (2009) 9345-9351.

[116] J.Y. Shi, J. Chen, Z.C. Feng, T. Chen, Y.X. Lian, X.L. Wang, C. Li, Journal of Physical Chemistry C 111 (2007) 693-699.

[117] S. Krejcikova, L. Matejova, K. Koci, L. Obalova, Z. Matej, L. Capek, O. Solcova, Applied Catalysis B-Environmental 111 (2012) 119-125.

[118] F.E. Kiviat, L. Petrakis, Journal of Physical Chemistry 77 (1973) 1232-1239.

[119] T.L. Thompson, D.A. Panayotov, J.T. Yates, Journal of Physical Chemistry B 108 (2004) 16825-16833.

[120] S. Yamazoe, T. Okumura, Y. Hitomi, T. Shishido, T. Tanaka, Journal of Physical Chemistry C 111 (2007) 11077-11085.

[121] S.Y. Yu, J. Garcia-Martinez, W. Li, G.D. Meitzner, E. Iglesia, Physical Chemistry Chemical Physics 4 (2002) 1241-1251.

[122] H.F. Shurvell, Spectra–Structure Correlations in the Mid- and Far-infrared, John Wiley & Sons, Chichester, England, 2002.

[123] T. Shimanouchi, Tables of Molecular Vibrational Frequencies, National Institute of Standards and Technology, Gaithersburg, MD, USA, 1972.

[124] B. Stuart, Infrared Spectroscopy: Fundamentals and Applications, John Wiley & Sons, Ltd., Chichester, England, 2004.

[125] K. Hadjiivanov, O. Saur, J. Lamotte, J.C. Lavalley, Zeitschrift Fur Physikalische Chemie-International Journal of Research in Physical Chemistry & Chemical Physics 187 (1994) 281-300.

[126] K. Hadjiivanov, Applied Surface Science 135 (1998) 331-338.

[127] L. Ferretto, A. Glisenti, Chemistry of Materials 15 (2003) 1181-1188.

[128] J. Macht, C.D. Baertsch, M. May-Lozano, S.L. Soled, Y. Wang, E. Iglesia, Journal of Catalysis 227 (2004) 479-491.

[129] T.J. Dines, C.H. Rochester, A.M. Ward, Journal of the Chemical Society-Faraday Transactions 87 (1991) 643-651.

[130] X.L. Tang, L. Shi, Langmuir 27 (2011) 11999-12007.

[131] C.G. Armistead, J.A. Hockey, Transactions of the Faraday Society 63 (1967) 2549-2556.

[132] D. Liu, Z. Li, Q. Sun, X. Kong, A. Zhao, Z.X. Wang, Fuel 92 (2012) 77-83.

[133] H.G. Wang, L.J. Song, H. Jiang, J. Xu, L.L. Jin, X.T. Zhang, Z.L. Sun, Fuel Processing Technology 90 (2009) 835-838.

[134] F.P. Tian, W.C. Wu, Z.X. Jiang, C.H. Liang, Y.X. Yang, P.L. Ying, X.P. Sun, T.X. Cai, C. Li, Journal of Colloid and Interface Science 301 (2006) 395-401.

[135] C.L. Garcia, J.A. Lercher, Journal of Physical Chemistry 96 (1992) 2669-2675.

[136] D. Panayotov, J.T. Yates, Journal of Physical Chemistry B 107 (2003) 10560-10564.

[137] J.M. Heinzel, Identification of Adsorption Mechanisms of Sulfur Heterocycles via Surface Analysis of Selected Metal-Doped Adsorbent Materials for Logistics Fuels Desulfurization, Chemical Engineering, Auburn University, Auburn University, Auburn, Alabama, USA, 2013, p. 178.

[138] R.D. Giles, J.A. Harrison, H.R. Thirsk, Journal of Electroanalytical Chemistry 22 (1969) 375-388.

[139] G. Rovida, F. Pratesi, Surface Science 104 (1981) 609-624.

[140] J. Benard, J. Oudar, Cabanebr.F, Surface Science 3 (1965) 359-372.

[141] V.A. Lavrenko, A.I. Malyshevskaya, L.I. Kuznetsova, V.F. Litvinenko, V.N. Pavlikov, Powder Metallurgy and Metal Ceramics 45 (2006) 476-480.

[142] S. Satokawa, K. Shimizu, A. Satsuma, Zeoraito 24 (2007) 60-66.

[143] J. Ryczkowski, Catalysis Today 68 (2001) 263-381.

[144] T.L. Tarbuck, K.R. McCrea, J.W. Logan, J.L. Heiser, M.E. Bussell, Journal of Physical Chemistry B 102 (1998) 7845-7857.

[145] M.A. Larrubia, A. Gutierrez-Alejandre, J. Ramirez, G. Busca, Applied Catalysis a-General 224 (2002) 167-178.

[146] S.I. Pyun, C.K. Rhee, Electrochimica Acta 49 (2004) 4171-4180.

[147] G. Berhault, M. Lacroix, M. Breysse, F. Mauge, J.C. Lavalley, L.L. Qu, Journal of Catalysis 170 (1997) 37-45.

[148] A. Ulman, An Introduction to Ultrathin Organic Films : From Langmuir–Blodgett to Self-Assembly, Academic Press, Boston, 1991.

[149] S.J. Lee, S.W. Han, M. Yoon, K. Kim, Vibrational Spectroscopy 24 (2000) 265-275.

[150] D.V. Kozlov, A.V. Vorontsov, P.G. Smirniotis, E.N. Savinov, Applied Catalysis B-Environmental 42 (2003) 77-87.

[151] A.S. Sultanov, U.B. Khakimov, G.S. Talipov, J.M. Shchekochinin, Reaction Kinetics and Catalysis Letters 2 (1975) 243-250.

[152] W.C. Wu, Z.L. Wu, Z.C. Feng, P.L. Ying, C. Li, Physical Chemistry Chemical Physics 6 (2004) 5596-5602.

[153] K.I. Shimizu, S.I. Komai, T. Kojima, S. Satokawa, A. Satsuma, Journal of Physical Chemistry C 111 (2007) 3480-3485.

[154] J.Y. Gui, D.A. Stern, D.G. Frank, F. Lu, D.C. Zapien, A.T. Hubbard, Langmuir 7 (1991) 955-963.

[155] C.L. Angell, M.V. Howell, Journal of Colloid and Interface Science 28 (1968) 279-287.

[156] D. Shekhawat, J.J. Spivey, D.A. Berry, Fuel cells: technologies for fuel processing, Elsevier, Spain, 2011.

[157] J.C. Garcia-Martinez, C.O. Castillo-Araiza, J.A.D. Heredia, E. Trejo, A. Montesinos, Chemical Engineering Journal 210 (2012) 53-62.

[158] A.H.M.S. Hussain, H.Y. Yang, B.J. Tatarchuk, Energy & Fuels 27 (2013) 4353-4362.

[159] F.H. Yang, A.J. Hernandez-Maldonado, R.T. Yang, Separation Science and Technology 39 (2004) 1717-1732.

[160] J.H. Guo, S. Watanabe, M.J. Janik, X.L. Ma, C.S. Song, Catalysis Today 149 (2010) 218-223.

[161] A. Ignatchenko, D.G. Nealon, R. Dushane, K. Humphries, Journal of Molecular Catalysis a-Chemical 256 (2006) 57-74.

[162] L. Yang, D. Tunega, L. Xu, N. Govind, R. Sun, R. Taylor, H. Lischka, W.A. DeJong, W.L. Hase, Journal of Physical Chemistry C 117 (2013) 17613-17622.

[163] M. Khan, J.N. Xu, N. Chen, W.B. Cao, Asadullah, Z. Usman, D.F. Khan, Research on Chemical Intermediates 39 (2013) 1633-1644.

[164] Y.T. Zhu, W. Wei, Y. Dai, B.B. Huang, Applied Surface Science 258 (2012) 4806-4812.

[165] G. Liu, J.A. Rodriguez, J. Hrbek, B.T. Long, D.A. Chen, Journal of Molecular Catalysis a-Chemical 202 (2003) 215-227.

[166] C.J. Cramer, Essentials of Computational Chemistry: Theories and Models, 2nd ed., Wiley, Chichester, UK, 2004.

[167] W. Koch, M.C. Holthausen, A Chemist's Guide to Density Functional Theory, 2nd ed., Wiley-VCH, Weinheim, Germany, 2001.

[168] T.V. Russo, R.L. Martin, P.J. Hay, A.K. Rappe, Journal of Chemical Physics 102 (1995) 9315-9321.

[169] S. Grimme, J. Antony, S. Ehrlich, H. Krieg, Journal of Chemical Physics 132 (2010) 1-19.

[170] L.M. Mentel, E.J. Baerends, Journal of Chemical Theory and Computation 10 (2014) 252-267.

[171] S.F. Boys, F. Bernardi, Molecular Physics 19 (1970) 553-566.

[172] L.A. Burns, M.S. Marshall, C.D. Sherril, Journal of Chemical Theory and Computation (2013).

[173] K. Hadjiivanov, E. Vasileva, M. Kantcheva, D. Klissurski, Materials Chemistry and Physics 28 (1991) 367-377.

[174] A. Selloni, Nature Materials 7 (2008) 613-615.

[175] S. Hamad, C.R.A. Catlow, S.M. Woodley, S. Lago, J.A. Mejias, Journal of Physical Chemistry B 109 (2005) 15741-15748.

[176] A. Jayaraman, F.H. Yang, R.T. Yang, Energy & Fuels 20 (2006) 909-914.

[177] A. Takahashi, F.H. Yang, R.T. Yang, Industrial & Engineering Chemistry Research 41 (2002) 2487-2496.

[178] M.J.S. Dewar, S.D. Worley, Journal of Chemical Physics 51 (1969) 263-267.

[179] S.-Y. Tang, J.C. McGowan, M. Singh, P. Galatsis, B.E. Ellis, R.K. Boyd, S.A. Brown, Canadian Journal of Chemistry 57 (1979) 1995-2003.

[180] J.W. Lu, F.L. Su, Z.Q. Huang, C.X. Zhang, Y. Liu, X.B. Ma, J.L. Gong, Rsc Advances 3 (2013) 720-724.

[181] J. Menesi, R. Kekesi, A. Oszko, V. Zollmer, T. Seemann, A. Richardt, I. Dekany, Catalysis Today 144 (2009) 160-165.

[182] A. Samokhvalov, Catalysis Reviews-Science and Engineering 54 (2012) 281-343.

[183] Y.J. Zang, R. Farnood, Topics in Catalysis 37 (2006) 91-96.

[184] D.J. Wang, G.L. Xue, Y.Z. Zhen, F. Fu, D.S. Li, Journal of Materials Chemistry 22 (2012) 4751-4758.